Subthalamic nucleus bursting dynamics and prediction of motor measures using machine learning



Saed Bassam Kamel Khawaldeh

St. Hugh's College

University of Oxford

A thesis submitted for the degree of

Doctor of Philosophy

Trinity 2021

Supervised by Prof. Peter Brown and Prof. Mark Woolrich

Declaration

I, Saed Bassam Kamel Khawaldeh, confirm that the work submitted is my own and that appropriate credit has been given where reference has been made to the work of others.

Signed:……

Date:……..……

Acknowledgements

Firstly, I would like to express my deep gratitude to Prof. Peter Brown and Prof. Mark Woolrich. Their ever-positive attitude, deep insights, and invaluable feedback has helped me to cultivate this work, encouraged me to grow as a researcher, and ultimately aided me to understand the computational and clinical techniques.

I would like to thank the Medical Research Council (MRC), the Nuffield Department of Clinical Neurosciences (NDCN), the Islamic Development Bank (IsDB), and the Inception Institute for Artificial Intelligence (IIAI) for their financial support, which enabled me to pursue the DPhil studies.

Finally, I am very grateful to my family, colleagues, and friends who have encouraged and supported me every step of the way.

Abstract

Whilst exaggerated bursts of beta frequency band oscillatory synchronization in the subthalamic nucleus (STN) have been associated with motor impairment in Parkinson's disease (PD), a plausible mechanism linking the two phenomena has been lacking. Here I test the hypotheses that increased beta synchronization might compromise information coding capacity in basal ganglia (BG) networks, that beta activity is just one of several dynamic states in the STN local field potential (LFP) in PD, and that together these different states predict motor impairment with high fidelity. To this end, STN LFP activity was recorded in two experiments; the first in 18 PD patients as they executed cued upper and lower limb movements, and the second in 32 PD patients at rest following an overnight withdrawal of anti-parkinsonian medication, and after administration of levodopa.

In the first study, I used the accuracy of LFP-based limb-movement classification as an index of the information held by the STN. Machine learning (ML) using naïve Bayes showed that the intended movements could be predicted from the STN LFP recordings well ahead of their execution. The presence of bursts of LFP activity in the beta band significantly compromised the prediction of the limb to be moved, which denotes that exaggerated beta band synchronisation may restrict the capacity of the BG system to encode physiologically relevant information about intended actions.

In the second study, an unsupervised ML method based on hidden Markov modelling, was used to identify the nature and timing of transient states of distinct spectral content (e.g. theta, alpha, beta) in resting STN LFP recordings. This showed that levodopa reduced the occurrence rate and

duration of low beta states, and the greater the reductions, the greater the improvement in motor impairment. However, additional LFP states were distinguished in the theta, alpha and high beta bands, and these behaved in an opposite manner. In addition, levodopa favoured the transition of low beta states to the other spectral states. When all LFP states and corresponding features were considered in a multivariate model it was possible to predict over 50% of the variance in patients' hemibody impairment OFF medication, and in the change in hemibody impairment following levodopa.

These findings are important as they suggest that LFP activity may potentially be decoded to enable effector selection, in addition to force control in restorative brain-machine interface applications. Moreover, multiple spectral states in the STN LFP have a bearing on motor impairment, and that levodopa-induced shifts in the balance between these states can predict clinical change with high fidelity. This is important in suggesting that some states might be upregulated to improve parkinsonism and in suggesting how LFP feedback can be made more informative in closed-loop deep brain stimulation systems.

Publications incorporated into thesis

1. **Khawaldeh, Saed**, Gerd Tinkhauser, Flavie Torrecillos, Shenghong He, Thomas Foltynie, Patricia Limousin, Ludvic Zrinzo, Ashwini Oswal, Andrew J. Quinn, Diego Vidaurre, Huiling, Vladimir Litvak, Andrea A. Kühn, Mark Woolrich* and Peter Brown*. "*Balance between competing spectral states in the Subthalamic nucleus is linked to motor impairment in Parkinson's Disease.*" Brain (2021). (*Authors contributed equally to the work) (***Link***).

2. **Khawaldeh, Saed**, Gerd Tinkhauser, Syed Ahmar Shah, Katrin Peterman, Ines Debove, T.A. Khoa Nguyen, Andreas Nowacki, Lenard Lachenmayer, Michael Schuepbach, Claudio Pollo, Paul Krack, Mark Woolrich and Peter Brown. "*Subthalamic nucleus activity dynamics and limb movement prediction in Parkinson's disease*." Brain 143.2 (2020): 582-596 (***Link***).

Other publications during the PhD:

1. Shah, Ashesh, Khoa Nygyuen, Katrin Peterman, **Saed Khawaldeh**, Ines Debove, Syed Ahmar Shah, Flavie Torrecillos, Huiling Tan, Alek Pogosyan, Lennard Lachenmayer, Joan Michelis, Peter Brown, Claudio Pollo, Paul Krack, Andreas Nowacki, and Gerd Tinkhauser. "*Combining multimodal biomarkers to guide deep brain stimulation programming in Parkinson's disease*." Brain Stimulation (Under review).

2. He, Shenghong, Alceste Deli, Petra Fischer, Christoph Wiest, Yongzhi Huang, Sean Martin, **Saed Khawaldeh**, Tipu Aziz, Alexander Green, Peter

Brown, and Huiling Tan. “*Gait-phase modulates alpha and beta oscillations in the pedunculopontine nucleus*.” Journal of Neuroscience (In press) (***Link***).

3. Tinkhauser, Gerd, Ahmar Syed Shah, Petra Fischer, Katrin Peterman, Ines Debove, Khoa Nygyuen, Andreas Nowacki, Flavie Torrecillos, **Saed Khawaldeh**, Huiling Tan, Alek Pogosyan, Michael Schuepbach, Claudio Pollo and Peter Brown. “*Electrophysiological differences between Upper and Lower Limb movements in the human subthalamic nucleus*.” Clinical Neurophysiology 130.5 (2019): 727-738 (***Link***).

4. He, Shenghong, Jean Debarros, **Saed Khawaldeh**, Alek Pogosyan, Abteen Mostofi, Fahd Baig, Erlick Pereira, Peter Brown, and Huiling Tan. "*Closed-loop DBS triggered by real-time movement and tremor decoding based on thalamic LFPs for essential tremor*.” 42nd Annual International Conferences of the IEEE Engineering in Medicine and Biology Society 2020 (***Link***).

Table of contents

Acknowledgements ..... **iii**
Abstract ..... **iv**
Publications incorporated into thesis ..... **vi**
Table of contents ..... **viii**
List of tables ..... **xi**
List of tables ..... **xi**
List of figures ..... **xii**
List of abbreviations ..... **xiv**
Chapter 1 General introduction **2**
1.1 An overview of Parkinson's disease 2
1.2 Basal ganglia and recent theories of motor impairment in Parkinson's disease 4
1.3 Neuromodulation using deep brain stimulation 7
1.4 Closed-loop DBS 9
1.5 Thesis objectives 11
Chapter 2 General materials and methods **15**
2.1 Ethics 15
2.2 Physiological recordings 15
2.2.1 Electromyography and accelerometery recordings 15
2.2.2 Local field potential recordings 17
2.3 Data processing 19
2.4 Machine learning 21
2.4.1 Feature extraction 21
2.4.2 Naïve Bayes classifier 24
2.4.3 Hidden Markov modelling 25
2.4.4 Multivariate regression 28
2.5. Statistical analyses 29
Chapter 3 Bursting activity dynamics and movement prediction **32**
3.1 Introduction 32
3.2 Material and methods 34
3.2.1 Patients and surgery 34
3.2.2 Postoperative localization of directional contacts 38
3.2.3 Local field potential recordings and limb assessments 40

3.2.4 Signal processing 41
3.2.5 Feature extraction and selection 42
3.2.6 Burst detection 44
3.2.7 Decoding algorithm 46
3.2.8 Statistical analyses 46
3.3 Results 47
3.3.1 Subthalamic activity contains information predictive of forthcoming movement 47
3.3.2 Bursts of 8-30Hz subthalamic activity compromise the prediction of forthcoming movement 51
3.3.3 Spectral features over a wide frequency range contribute to limb prediction 57
3.4 Discussion 60
3.4.1 Experimental considerations 61
3.4.2 Potential applications and limitations 64
3.5 Summarized findings 66
Chapter 4 Balance between competing states and motor impairment 68
4.1 Introduction 68
4.2 Material and methods 70
4.2.1 Patients and surgery 70
4.2.2 Experiment and recordings 71
4.2.3 Clinical assessment 72
4.2.4 Signal processing and determination of bursts 73
4.2.5 Time-Delay Embedded Hidden Markov Model for Burst Detection 76
4.2.6 Data analysis and statistics 77
4.3 Results 82
4.3.1 Medication-induced changes in STN LFP states 82
4.3.2 Medication-induced changes in STN LFP states correlate with motor impairment 89
4.3.3 Medication-induced changes across STN LFP states predict motor impairment 91
4.3.4 Both low beta and other spectral states contribute to prediction of change in motor impairment with levodopa 98
4.3.5 Multivariate correlations between STN LFP states and motor impairment OFF medication 101
4.4 Discussion 107

4.4.1 Experimental considerations 109
4.4.2 Implications for therapy 112
4.5 Summarized findings 114
Chapter 5 General discussion 116
5.1 Machine learning for clinical applications 117
5.2 Involvement of beta activity in motor impairment 118
5.3 Involvement of non-beta activity in motor impairment 119
5.4 Why should bursts of different frequency have contrasting properties? 120
5.5 Potential improvement in closed-loop deep brain stimulation 122
5.6 Thesis limitations 123
5.7 Conclusion 126
References 129

List of tables

Table 3.1 Clinical details. 35
Table 4.1 Clinical details. 71

List of figures

Figure 3.1 Experimental setup and analysis pipeline. 37

Figure 3.2 Localization of all the directional contacts in all 18 subjects included in the study. 39

Figure 3.3 Burst detection process.. 45

Figure 3.4 Classification AUC across various task periods.. 49

Figure 3.5 Burst characteristics during the pre-cue period in the fixed-limb experiment... 52

Figure 3.6 Classification AUC during the pre-cue period for different burst conditions [alpha (8–12 Hz), beta (13–30 Hz), and non-burst]. 55

Figure 3.7 Feature importance for prediction during different task periods in fixed-limb blocks for raw LFP before classification into burst conditions.. 57

Figure 3.8 Feature importance during the pre-cue period for the burst conditions: non-bursts, alpha bursts, and beta bursts.....59

Figure 4.1 Data recorded during OFF (A) and ON (B) medications.....74

Figure 4.2 Example of HMM model with 8 states and 7 lags showing the process of assigning states to frequency bands. 75

Figure 4.3 Flow chart summarizing analysis pipeline.. 80

Figure 4.4 Box-and-whisker plots of change (ON-OFF) in the rate of theta (4-7 Hz), alpha (8–12 Hz), low beta (13–21 Hz) and high beta (22-35 Hz) states identified by the combination of different HMM models.. 84

Figure 4.5 Box-and-whisker plots of medication-linked change in transition probability between various state bands (theta, alpha, low beta, high beta, and background) for different HMM models... 85

Figure 4.6 Box-and-whisker plots of change (ON-OFF) in number of theta, alpha, low beta and high beta states relative to the total number of states identified by the combination of different HMM models. 86

Figure 4.7 Box-and-whisker plots of medication-induced change (ON-OFF medication) in fractional occupancy (A), life time (B) and interval time (C) for different HMM models.. 88

Figure 4.8 Correlation between medication-induced change (ON-OFF medication) in bursting and % change (ON-OFF medication) in contralateral hemibody UPDRS score including tremor items. 90

Figure 4.9 LFP HMM state prediction of change in contralateral hemibody UPDRS score including tremor items upon treatment with levodopa.. 92

Figure 4.10 Normalised ridge regression coefficients for the features used to predict change in contralateral hemibody UPDRS score ON medication across different HMM models. 94

Figure 4.11 LFP HMM state prediction of change in contralateral bradykinesia-rigidity without tremor items upon treatment with levodopa. 95

Figure 4.12 LFP HMM state prediction of change in contralateral bradykinesia-rigidity without tremor items upon treatment with levodopa.. 96

Figure 4.13 Normalised ridge regression coefficients for the features used to predict change in contralateral hemibody tremor score across different HMM models.. 97

Figure 4.14 LFP HMM state prediction of change in contralateral hemibody UPDRS score upon treatment with levodopa using different feature sets... 99

Figure 4.15 Box-and-whisker plots of LFP HMM state prediction of change in contralateral hemibody UPDRS score including tremor items upon treatment with levodopa after including states and bands amplitude information (A) and both amplitude and gamma features (B). 101

Figure 4.16 Box-and-whisker plot of coefficient of determination (r^2) between predicted and actual contralateral hemibody UPDRS score, including tremor items, OFF medication.. 102

Figure 4.17 Box-and-whisker plots of LFP HMM state prediction of contralateral bradykinesia-rigidity (A) and contralateral tremor (B) OFF levodopa. 103

Figure 4.18 Normalised ridge regression coefficients for the features used to predict contralateral hemibody UPDRS scores including tremor items during OFF medication across different HMM models... 104

Figure 4.19 Scatterplot of normalised ridge regression coefficients for the features used to predict change in contralateral hemibody UPDRS score including tremor items ON medication and for the features used to predict contralateral hemibody UPDRS scores including tremor items during OFF medication 105

Figure 4.20 Box-and-whisker plots of LFP HMM state prediction of contralateral hemibody UPDRS score including tremor items after including states and bands amplitude information (A) and both amplitude and gamma features (B) OFF levadopa.. 106

List of abbreviations

ANOVA	Analysis of variance
AUC	Area under the receiver operator characteristic curve
BCI	Brain computer interface
BG	Basal ganglia
CI	Confidence interval
CT	Computed tomography
DBS	Deep brain stimulation
EEG	Electroencephalography
EMG	Electromyography
FDR	False discovery rate
GPi	Globus pallidus interna
HMM	Hidden Markov modelling
LFP	Local field potential
MAR	Multivariate autoregressive
ML	Machine learning
MRI	Magnetic resonance imaging
MEG	Magnetoencephalography
PD	Parkinson’s disease

SD Standard deviation

SEM Standard error of the mean

SNr Substantia nigra pars reticulate

STN Subthalamic nucleus

TDE Time delay embedded

TMS Transcranial magnetic stimulation

UPDRS Unified Parkinson's Disease Rating Scale

Chapter 1

General introduction

1.1 An overview of Parkinson's disease

There are many neurological disorders which require clinical treatment by physicians or healthcare professionals. Parkinson disease (PD) is one such neurological disease and the second most common neurological disorder. It is a progressive disease that becomes more prevalent with advancing age and gradually strips away motor abilities causing patients to have slow gait, rigid limbs, bradykinesia, tremor, shuffling and a lack of postural balance (Gelb et al., 1999; Tolosa et al., 2006; Jankovic, 2008; Sveinbjornsdottir, 2016; Poewe et al., 2017). PD starts unilaterally and it is caused by loss of dopaminergic input to the basal ganglia, -a group of nuclei linked to the thalamus in the base of the cerebrum.

PD patients exhibit a broad impairment of flexible motor control whereby normally a dynamic competition between motor strategies is based on accumulated information. This can be described by various models such as the internal forward model and through external cues driving adaption (Diedrichsen et al., 2010). As a result, patients struggle with rhythmic inter-limb coordination when performing bimanual or bipedal exercise including gait (Almeida et al., 2002; Hausdorff et al., 2003; Ponsen et al., 2006; Moore et al., 2008; Vercruysse et al., 2012), find it challenging to synchronize to external sensory cues (Hwang et al., 2014; Bienkiewicz and Craig, 2015), and often have deficits in action-switching (Lewis et al., 2000; Byblow et al., 2002) and inhibition (Gauggel et al., 2004; Obeso et al., 2011). These various control

functions are dependent on processing of proprioceptive and external sensory information to tune or stop the ongoing movement strategy.

Gait is the pattern of walking, i.e. while walking the body is normally upright, neither leaning forwards nor backwards, with even steps and the arms swinging at sides. Holding the upright position above the centre of gravity leads to good body balance. PD affects patients' gait by causing abnormal gait pattern generation or posture, perceptual malfunction, problems with movement automaticity or frontal executive dysfunction (Bloem et al., 2004; Spildooren et al., 2010; Heremans et al., 2013). These drive various PD gait-related impairments which include freezing of gait. Another impairment that PD patients develop is deficient interval timing in sensorimotor synchronization tasks which is caused by dysregulated dopamine (Merchant et al., 2008; Greenland et al., 2019). This can be reduced by dopaminergic medication which improves dopaminergic signalling. The interval timing effect developed in PD seems to be similar to that developed in other diseases including schizophrenia, Huntington's disease, and multiple system atrophy (Beste et al., 2007; Allman and Meck, 2012; Högl et al., 2014).

Parkinson's has no cure; however symptoms can be efficaciously managed using pharmacological treatment (i.e. levodopa and dopamine agonists) (Hammond et al., 2007; Kühn et al., 2009), and in advanced cases using surgical interventions (i.e. deep brain stimulation) (Brown et al., 2001; Priori et al., 2004; Kühn et al., 2008a). The most common drug used to treat PD is levodopa which is a precursor of dopamine. Levodopa can be associated with motor side effect of dyskinesias, which are uncontrollable and involuntary movements involving one limb or the entire body. This side effect gradually

gets worse over years (Bezard et al., 2001; Mosharov et al., 2015). As PD progresses, medication efficacy is reduced, causing unpredictable variations in motor symptoms (McColl et al., 2002; Aquino et al., 2015), which lead to a need for more advanced treatments such as deep brain stimulation (DBS) surgery. DBS mostly targets the subthalamic nucleus (STN) in the basal ganglia (BG) for stimulation. Stimulation is delivered at a regular high frequency (~130 Hz) in clinically available devices, and is a well-established and effective treatment (Rodriguez-Oroz et al., 2005; Deuschl et al., 2006; Benabid et al., 2009).

1.2 Basal ganglia and recent theories of motor impairment in Parkinson's disease

The BG play central roles in action selection (Mink, 1996; Redgrave et al., 1999, 2007), time estimation (Jones and Jahanshahi, 2014), the regulation of movement kinematics (Redgrave et al., 1999; Desmurget and Turner, 2010; Dudman and Krakauer, 2016), and motor learning (Turner and Desmurget, 2010).

Studies of the BG show that there are three main processing pathways; the direct, the indirect and the hyperdirect pathway (Nambu et al., 2002; Milardi et al., 2015). The direct and the indirect pathways receive inputs from the cortex and the thalamus through the striatum (Smith et al., 1998). Cortical input to the hyperdirect pathway travels directly to the STN bypassing the striatum. The two main output structures are the globus pallidus interna (GPi) and the substantia nigra pars reticulata (SNr) projecting to the thalamus (Rinvik, 1975), which then projects to motor cortex (Chevalier et al., 1984,

1985). The GPi/SNr also project to the brainstem, including a direct pathway to the superior colliculus, which projects then back to the striatum and the STN via a tecto-thalamic route (Redgrave et al., 2010; Alloway et al., 2017). The STN also sends direct projections to the thalamus (O'Connor, 1998; Lanciego et al., 2012), and di-synaptically projects to the cerebellum through the pontine nuclei (Bostan et al., 2010).

When dopamine receptors in the striatum are not sufficiently stimulated, parts of the BG become either under- or over-stimulated. More specifically, the STN becomes overactive, stimulating the GPi (Haslinger et al., 2005). When the GPi is overstimulated, it has a greater inhibitory effect on the thalamus, which in turn decreases excitatory thalamus output to the cerebral cortex and causes akinesia (Niktarash et al., 2004). However, this classical view of basal ganglia dysfunction in PD has been challenged through the highlighting of several paradoxes (Marsden and Obeso, 1994). Chief among these is the fact that both akinesia and hyperkinesia can be treated by surgical interventions involving the STN (Brown and Eusebio, 2008). This has led to the abnormal patterning hypothesis of basal ganglia dysfunction, whereby it is not the change in net firing rate that drives motor impairments but rather a change in the pattern of neuronal activity (Brown, 2003), irrespective of the net firing rate. In this way surgical interventions involving the STN can ameliorate different abnormal patterns of activity and therefore ameliorate both akinesia and hyperkinesia which are each associated with different patterns of abnormal activity. The key activity associated with PD is an increase in the synchronisation of BG neurons which manifests as an exaggerated beta band oscillatory activity in the LFPs of the BG, especially the STN, of PD patients OFF medication (Levy et al., 2002; Brown, 2003; Kühn et al., 2005;

Weinberger et al., 2006; Moshel et al., 2013; Miller et al., 2009; Tan et al., 2014; Torrecillos et al., 2015; Deffains et al., 2016; Fischer et al., 2016). This beta band synchronisation may play a central role in driving motor impairment in PD as captured by several computational models (Feng et al., 2007; Guo et al., 2008; van Albada et al., 2009; Moran et al., 2011; Marreiros et al.,; Müller and Robinson, 2018).

A reduction in STN beta activity occurs during movement initiation and execution and is followed by a beta rebound (Cassidy et al., 2002; Kühn et al., 2004; Hebb et al., 2012; Khawaldeh et al., 2020; Tinkhauser et al., 2020) which suggests that beta activity may be anti-kinetic. The power of STN beta activity is reduced by dopaminergic medications and by stimulating the STN with DBS (Brown et al., 2001; Priori et al., 2004; Kühn et al., 2008b; Eusebio et al., 2011; Neumann et al., 2016; Khawaldeh et al., 2021). There is a correlation between motor impairment and beta activity, and between improvement in motor impairment and change in beta activity as a result of drug or DBS therapy (Kühn et al., 2006, 2008a; Ray et al., 2008; Neumann et al., 2016; Oswal et al., 2016; Steiner et al., 2017). Rigidity and bradykinesia most strongly correlate with the strength of beta synchrony (Little and Brown, 2014; Neumann and Kühn, 2017).

Recent studies suggest that the temporal patterning of beta activity in the form of bursts may be the critical feature in PD rather than the overall strength or power of beta activity. Thus, the proportion of longer beta bursts of STN LFPs during OFF medication condition correlates positively with motor impairment (Tinkhauser et al., 2017b). Additionally, motor symptoms can be improved by shortening beta bursts of longer duration with STN adaptive DBS (Tinkhauser

et al., 2017a). STN bursts in PD patients appear to impact motor performance even at the single trial level (Torrecillos et al., 2018; Tinkhauser et al., 2020). Moreover, the percentage of time spent in beta bursts has been shown to be a better feature to predict bradykinesia than average beta power (Lofredi et al., 2019), and in another study the temporal synchrony patterning was suggested to be more predictive of clinical change than the average synchrony (Ahn et al., 2018). Beta burst duration in STN has also been suggested as an indicator for freezing of gait in PD (Anidi et al., 2018).

Whether the relationship between phasic beta synchronization and motor impairment is causal or secondary is unclear. One possible mechanism is that the performance of a neuronal circuit may decrease due to high synchronization through a restriction in information coding capacity (Brittain and Brown, 2014). However, this remains theoretical and hitherto there has been no direct demonstration that periods of elevated oscillatory synchrony can impair the local representation of task-related information in the STN.

1.3 Neuromodulation using deep brain stimulation

DBS is an effective treatment for PD (Rodriguez-Oroz et al., 2005; Deuschl et al., 2006; Benabid et al., 2009), and it is also used for the treatment of other disorders such as dystonia (Kiss 2007; Volkmann et al., 2014) and epilepsy (Salanova et al., 2015; Li and Cook 2018). Various levels of success have been reported when DBS procedures have been tried on other neurological and psychiatric disorders such as Tourette syndrome, depression, Alzheimer’s disease, and anorexia nervosa (Cagnan et al., 2019b; Lozano et al., 2019).

DBS is performed for PD by positioning the electrode first within the STN or the GPi. The electrode has normally either four or eight recording and stimulating contacts. After the electrode implantation surgery, either one contact, or a combination of contacts, is activated to stimulate the STN or the GPi with a default pulse width and high frequency of 60 μs and 130 Hz, respectively (Moro et al., 2002; Dayal et al., 2017; Schor et al., 2019). The stimulation voltage or current is tuned on a case by case with the spread of the stimulation field depending on these and two parameters as well as on the nature of the surrounding tissue (Yousif and Liu, 2008, 2009).

The mechanisms of action of DBS are still not completely clear (Chiken and Nambu, 2016; McIntyre and Anderson 2016; Cagnan et al., 2019b; Lozano et al., 2019). STN DBS results in both excitatory and inhibitory post-synaptic potentials, which overall tend to inhibit local cell bodies. However, at the same time DBS directly activates axons with this activation time-locked to the DBS stimuli or subharmonics therein (Chiken and Nambu, 2016; Lozano et al., 2019). As the resulting activity is disengaged from intrinsic inputs and locked to the rhythm of the DBS it is thought that it might occlude any abnormal intrinsic patterning at lower frequencies, such as occurs in beta bursts. This may account for the beneficial effects of DBS in PD but the same actions can cause side effects such as dysarthria or speech impairment (Skodda, 2012; Dromey and Bjarnason, 2011; Mücke et al., 2018), dystonia or psychiatric side effects which includes disinhibition, depression or hypomania (Michael Schüpbach, 2012; Cyron, 2016; Kardous et al., 2021).

1.4 Closed-loop DBS

Closed-loop DBS aims to improve DBS by stimulating with a pattern which targets the pathology more selectively, relying on feedback signals to adjust the stimulation's various parameters. Typically, a biomarker which has high correlation with symptom severity is used to adapt STN stimulation. The closed-loop DBS feedback signals are recorded using the non-stimulating contacts of the DBS electrode, or via wearable sensors. Closed-loop DBS using cortical feedback was pioneered in non-human primates where it was clearly shown to be more effective than regular high frequency DBS (Rosin et al., 2011). In patients attention has largely focussed on the use of the STN electrodes to record LFP signals which index coordinated local neural activity (i.e. activity that can undergo spatio-temporal summation). Several studies have shown that analysing LFP signals to extract pathological features (i.e. low beta activity elevation), so that the DBS only stimulates STN when pathological activity exceeds a pre-defined threshold, may result in equivalent or even better motor improvement than conventional constant high frequency stimulation (Little et al., 2016a, 2013). As overall stimulation time is reduced this may also reduce dyskinesia or speech side effects (Little et al., 2016b; Rosa et al., 2017; de Almeida Marcelino et al., 2020), and ultimately help in prolonging stimulator battery life. Moreover, regular STN DBS interferes with perceptual decision making tasks (Herz et al., 2018) and value-based choice tasks (Frank et al., 2007; Pham et al., 2015), so this also motivates stimulation paradigms that interfere less with physiological processing in the STN (Cagnan et al., 2019b). More recently, there has been a resurgence of interest in feedback signals for closed loop DBS that can be picked up from the cortex.

Chief among these signals is a finely tuned gamma activity that is closely associated with dyskinesias and which can be used in closed-loop DBS (Swann et al., 2018).

However, LFP activities that might be used to control DBS delivery and patterning need not be limited to beta or gamma activity, and it might even be that multiple LFP components could combined to give the most reliable index of clinical state (or of the hidden internal states that lead to clinical state). Previous work in the literature has shown conflict-related increases in STN's theta activity (Cavanagh et al., 2011; Fumagalli et al., 2011; Zavala et al., 2013, 2014) and that this theta change significantly correlates with reaction time (Zavala et al., 2013), and the delay in movement during conflict (Zavala et al., 2017). Such theta activity is further associated with impulse control disorders (Rodriguez-Oroz et al., 2011; Rosa et al., 2013). Alongside theta activity, alpha STN power is also consistently elevated during cued button presses and paced grips tasks (Klostermann et al., 2007; Anzak et al., 2012; Alegre et al., 2013) and less consistently during self-paced tasks (Singh et al., 2011; Oswal et al., 2013). Additionally, STN alpha power decreases as a response to emotionally arousing unpleasant visual stimuli (Huebl et al., 2011). Higher levels of theta and alpha STN power are correlated with improved motor performance (Anzak et al., 2012; Tan et al., 2013). The reduction in alpha power with emotional stimuli is reported to be associated with depressive symptoms in PD patients (Huebl et al., 2011). STN gamma activity increases during voluntary movements (Brown et al., 2001; Alonso-Frech et al., 2006; Androulidakis et al., 2007) and correlates with movement velocity (Lofredi et al., 2018). Dopaminergic medication increases movement-related gamma activity (Litvak et al., 2012), and this may be functionally

relevant for restoring the PD patients' ability to move. Perhaps related to this, excessive gamma synchrony increases during uncontrolled levodopa-induced dyskinesia movements (Swann et al., 2016). However, a gamma increase has also been linked to movement stopping (Fischer et al., 2017).

The use of diverse LFP features becomes critical if brain signals are to be used to predict tremor in PD as this feature is only poorly related to beta activity (Shah et al., 2018; Yao et al., 2020). Machine learning is the obvious tool with which to predict current motor state from a comprehensive set of features in the LFP, but thus far its use has focussed on the prediction of tremor (with the exception of Gilron et al., 2021).

1.5 Thesis objectives

Above I have identified two specific knowledge gaps that are important to address. First, although it has been hypothesised that the performance of a neuronal circuit may decrease due to strong synchronization through a restriction in information coding capacity (Brittain and Brown, 2014), this has never been directly demonstrated. In this thesis, therefore, I will set out to show that periods of elevated oscillatory synchrony can impair the local representation of task-related information in the STN. To this end I will use directional electrodes which allow high resolution read-outs of changing features in the STN LFP (Zhang et al., 2018), and Machine Learning (ML) to identify the aspects of STN LFP activity that predict whether a voluntary upper or lower limb movement will subsequently be performed. I thereby aim in Chapter 3 to provide a mechanistic explanation for the correlative findings linking bursts of beta activity to parkinsonian motor impairment.

Second, the extent to which multiple LFP features might be used to optimally identify the current state of motor impairment in PD patients has not been established. In particular, the role of bursts of synchrony at frequencies outside of the canonical beta range has not been explored in detail, and there remains uncertainty as to whether the lower and upper ranges of the beta band differentially contribute to the prediction of motor impairment. Here I use hidden Markov modelling to provide an objective index of LFP bursts or states across the frequency spectrum (Quinn et al., 2019; Vidaurre et al., 2018), and combine this with ridge regression to demonstrate the power of LFP states and their features to predict not only akinesia and rigidity, but also tremor (Chapter 4). The inference is that combined features of bursting at different frequencies might provide more faithful feedback of current motor state in closed-loop DBS than just beta bursts alone.

Focussing on the impact of oscillations on prediction of movement and motor impairment in this thesis, I set out to answer the following questions:

- How can ML be used to predict limb movement from deep brain recording signals? Can the forthcoming movement be predicted relying on features extracted from the pre-movement preparation period?
- What is the effect of bursting presence on the information encoded in STN? Which type of burst impairs the local representation of task-related information?
- How can unsupervised time-series models help extract measures which characterise the oscillatory changes caused by medications in PD patients? Which type of bursts correlate with motor impairment and in what way?

- What is the impact of using different measures of bursting at different frequencies on the predication of motor impairment? What is the contribution of each measure in the prediction and how do their contributions to prediction vary when predicting medication-induced changes or impairment during the OFF medication condition?

Chapter 2

General materials and methods

2.1 Ethics

All participants gave their informed written consent in accordance with the Helsinki Declaration. The experimental protocols were approved by the local ethics committees: the National Research Ethics Committee A, Oxford (UK), the Medical Sciences Interdivisional Research Ethics Committee, Oxford (UK), the National Hospital for Neurology & Neurosurgery and Institute of Neurology Joint Research Ethics Committee, London (UK), the Department of Neurosurgery of University Medicine Berlin Research Ethics Committee, Berlin (Germany), and the Department of Neurology of Bern University Hospital Research Ethics Committee, Bern (Switzerland).

2.2 Physiological recordings

Data used in the thesis were recorded by our collaborators for previous studies (Recordings used in chapter 3 have been previously reported in Tinkhauser et al., 2019, and recordings used in chapter 4 have been previously reported in Kuhn et al., 2006; Litvak et al., 2011; and Tinkhauser et al., 2017).

2.2.1 Electromyography and accelerometery recordings

Surface electromyography (EMG) electrodes were placed on the upper limb (forearm flexor muscles) and lower limb (tibialis anterior). Accelerometers were additionally placed on the hand and foot to improve detectability of the

onset of task-related movements for the limb movement experiment (Chapter 3) and to track any movement periods for the levodopa medication experiment during rest (Chapter 4).

In the limb movement experiment (Chapter 3), after a brief recording at rest, patients were asked to perform a block each of contralateral upper and lower limb movements followed by ipsilateral upper and lower limb movements. They were informed of the desired response at the beginning of each block, and instructed that only this movement should be made in response to auditory go cues. Note that whether the assessment began with upper or lower limb blocks was randomised to avoid any order effect. Each single movement was prompted by a verbal ‘go’ command recorded with a microphone. This ensured that beta activity, which rebounds after movement completion (Pfurtscheller and Lopes da Silva, 1999), did not compromise the baseline period of the next movement. 20 trials were aimed to be recorded in each of the 4 blocks. On the other hand, a subset of the patients were asked to perform randomised upper and lower limb movements (both contralateral and ipsilateral). They were informed of the desired response by verbal ‘upper’ and ‘lower’ commands directing movement of the hand or ankle and recorded with the microphone. The upper limb movement consisted of closing and opening of the hand, while the lower limb movement involved foot dorsi-extension and then plantar flexion. Note that whether the assessment began with upper or lower limb blocks was again randomised to avoid any order effect.

In the levodopa medication experiment during rest (Chapter 4), recordings were repeated before and after administration of levodopa, 3–7 days after lead

implantation. The signals were imported onto a computer using Spike2 software (CED, Cambridge, UK), where electromyography and accelerometery data was pre-processed to identify and remove segments where movement occurred.

2.2.2 Local field potential recordings

Both bilateral and directional STN LFP were recorded from Parkinson's disease patients who had undergone DBS surgery. Patients were selected for the surgical procedure if motor symptoms were inadequately controlled by medication and after ensuring that no significant psychiatric conditions were present. Electrode implantation and targeting was performed based on preoperative magnetic resonance or combined computed tomography/ magnetic resonance (CT/MR) imaging. Electrode extension cables were externalized through the scalp to enable post-operative recordings by connecting the cables to an amplifier (TMSi Porti amplifier, TMS International, Netherlands). In a second surgical procedure, up to 7 days later, the cables were connected to a subcutaneously implanted pacemaker that provided chronic high-frequency deep brain stimulation. The electrode models implanted contained either four (Medtronic 3389) or eight (Boston Scientific, Vercise, DB-2201 and Vercise directional, DB2202) platinum-iridium contacts. After optimal electrode placement, the lower most contact (contact 0) should be below or in the lower border of the STN while the upper most contact should be above or at the upper most border of the STN.

The ground electrode was placed on the inside of the wrist. The LFPs were recorded with a common average reference and were re-referenced offline to bipolar montages in the medication conditions study (Chapter 4) resulting in

spatially focal voltage deflections. LFP bipolars were computed by subtracting neighbouring channels of the same recording electrode. If single channels were saturated or inactive, only the remaining neighbouring contacts were subtracted.

Synaptic currents are relatively slow and thus more likely to overlap in time and sum in the population average (Buzsáki et al., 2012). The LFP is therefore thought to predominantly capture postsynaptic membrane potential fluctuations resulting from firing of presynaptic excitatory and inhibitory populations (Haider et al., 2016). It reflects the spatially averaged activity of many cells that are concurrently active, as random activity would cancel itself out. It is important to note that LFP oscillations capture a multitude of extracellular processes in the vicinity of the recording electrode. These processes include any type of transmembrane currents that may also result from synchronous local spiking activity, from afterhyperpolarizations and from hyperpolarization-induced opening of ion channels. Voltage-dependent membrane responses can result in intrinsic resonance properties in response to inputs at preferred frequencies that can give way to self-sustained oscillations (Buzsáki et al., 2012). Importantly, the LFP tracks integrative synaptic processes that could not be inferred from firing activity alone. Although subcortical nuclei lack the structure of cortical columns, there is still some internal organisation so that LFP recordings from the STN capture synchronous sub- and suprathreshold population activity (Magill et al., 2004), albeit with much lower amplitudes than in cerebral cortex.

2.3 Data processing

Spike2 (CED, Cambridge, UK) and OSL (OHBA Software Library; Oxford Centre for Human Brain Activity (OHBA), University of Oxford, Oxford, UK; https://ohba-analysis.github.io/osl-docs/) were used to manually label the onset of the audio cue, and the onset and end of movements based on the microphone, EMG and accelerometer signals (Chapter 3), and to the visual signal inspection and artefact detection and rejection (Chapter 4). MATLAB (2019b, Mathworks, Natick, MA, USA) was used for segmenting trials, preprocessing and further analyses including training and testing for movement classification. After removal of the DC component (2 sec time constant), data were further processed with custom routines in MATLAB. These were performed independently in each subject (Chapter 3). Standard off-line filtering was performed using FieldTrip toolbox (2018, Donders Institute for Brain, Cognition and Behavior, Nijmegen, Netherlands) functions such as *ft_preproc_lowpassfilter* and *ft_preproc_highpassfilter* (Oostenveld et al., 2011). Data were subsequently down-sampled to 1000 Hz in the movement prediction study (Chapter 3).

The bipolar contact pair with the highest beta power in the average of the OFF and ON drug conditions was selected for further analysis based on the presumption that this contact pair was most likely to pick up from the dorsolateral ‘motor’ STN (Chen et al., 2006; Zaidel et al., 2010; Horn et al., 2017). The signals recorded in each medication condition from each hemisphere were bandpass filtered at 2-48 Hz, resampled at 100 Hz and z-normalized on a per session basis to facilitate comparison across different recording systems and to minimise the effects of targeting variance. All

processed LFPs were then concatenated into one vector representing the selected contact pair from all medication conditions and hemispheres. The concatenated signal was then fed to time delay embedded-hidden Markov model (TDE-HMM) which was compared against a percentile thresholding model (Chapter 4).

The down sampled signals were then high-pass filtered at 2 Hz. Frequency decomposition was performed at 1 Hz resolution using the Wavelet method Cohen, 2014). For each hemisphere the directional contact with the highest normalised (relative to its sum) resting beta amplitude was selected to determine the average resting amplitude-frequency spectrum. EMG signals of upper and lower limbs were extracted, z-scored, rectified, and high-pass filtered at 15 Hz for the principal analyses in Chapter 4. The raw signal from each of the six directional electrode contacts was high-pass filtered at 2 Hz, then detrended and z-scored to normalize each channel's data before any trial segmentation or task separation. Frequency decomposition was performed with 1 Hz resolution using the Complex Morlet Wavelet method (Cohen, 2014). A baseline normalization was performed on each segmented trial, where each 1 Hz frequency component in each trial in the time-frequency domain was normalized by a baseline of 500 ms of the same component taken from the beginning of each trial (2 s before auditory cue). Thus, LFPs were expressed as relative change with respect to baseline. This helped normalize changes across hemispheres and subjects, where absolute amplitudes might vary due to targeting variance, differing stun effects and patient's Parkinson's disease symptomatology. In two hemispheres (1 and 13), one directional contact had to be excluded from the analysis because of saturation during the recording (Chapter 3).

2.4 Machine learning

2.4.1 Feature extraction

In the movement prediction study (Chapter 3), a set of 100-ms long non-overlapping windows were used to extract frequency-domain features from the six directional LFP contacts. Normalized LFP powers in nine different frequency bands ranging from 8 to 500 Hz were identified as potential frequency domain features (Shah et al., 2017). These distinct frequency bands were: 8–12 Hz, 13–20 Hz, 21–30 Hz, 31–45 Hz, 56–95 Hz, 106–200 Hz, 201–300 Hz, 301–349 Hz, and 350–500 Hz. After extracting the features, they were standardized to have a zero-mean (by subtracting the mean), and a unit-variance (by dividing by the standard deviation). Low frequency activity (below 7 Hz) was excluded as the 100-ms window used for extracting features was insufficient for reliable estimation. I did, however, explore the additional use of various higher order statistical measures as potential features (entropy, kurtosis, activity, mobility, complexity, skewness, maximum, minimum, mean, and standard deviation; as per Shah et al., 2017) in the classification of the training subsets, but these were seldom prioritized by the feature selection algorithm, and had very low weights compared to the spectral features. As a result, they were excluded from the main analyses.

K-fold cross validation (k: number of groups into which dataset was randomly split) was used to ensure that all trials in the original training dataset were used for both training and validation, and the same subset of data used for training was not used for validation; each trial being used for validation only once. Specifically, I used 4-fold cross-validation, where at each rotation, three folds were used for training, and the remaining one was used for testing. The

ReliefF feature selection algorithm was used to determine important features and eliminate non-important ones (Robnik-Šikonja and Kononenko, 2003). ReliefF first sets all feature weights to 0, then iteratively selects a random trial and finds the nearest trials to it from each class. Finally, it calculates the weights of features through penalizing weights that give different values to neighbours of the same class, and rewarding those that give different values to neighbours of different classes. This was applied on the training subset containing the three folds, and the top six ranked features used for testing the fourth fold. The weight of each feature was estimated by counting how many times it was selected across the four folds as among the top six features, this was then divided by the number of folds (k = 4) to get the final measure of feature importance. These weights were then used as a measure of the contribution of a given feature to the classification.

In the medication conditions study (Chapter 4), states were estimated using the TDE-HMM model (Vidaurre et al., 2018) for 56 different combinations of state number K (5 to 18 states) and time lags L (3 to 15 lags). Details of the TDE-HMM model are explained in section 2.4.3. The time lag L determines the window duration, so that a lag of 10 means that the window includes 10 data points either side of that representing the time under analysis. Longer windows allow better frequency resolution at the expense of temporal resolution (analogous to the time-frequency trade-off when choosing a basis set in wavelets). The state number K denotes the number of states to be detected. For every combination, TDE-HMM states were categorized by their predominant frequency content by cross-correlating the states' time courses with the Hilbert envelopes of the theta, alpha, low beta and high beta frequency bands. Figure 4.2 illustrates the process of ascribing HMM states

to different frequency bands. If the most positive 2 correlations were either within low frequencies (theta and alpha) or high frequencies (low and high beta), then the corresponding state was assigned to the band with highest correlation. Otherwise states were assigned to “background” activity. More than one HMM state could be attributed to a given frequency band. The analysis of multiple different models allows consistent features to emerge, whilst transformation from HMM states to frequency bands was used to facilitate comparisons across different HMM models and their interpretation, especially with respect to existing literature.

This assessment was repeated for the OFF and ON medication conditions. Various extracted measures of interest were extracted from the TDE-HMM models, and changes in them between the two medication conditions, were correlated with the contralateral Unified Parkinson's Disease Rating Scale (UPDRS) hemibody scores to investigate any link to Parkinsonian motor impairment. The extracted features were: probability of transitioning between different states and within states (where a frequency band comprised several HMM states), fractional occupancy (referring to how much time the HMM spends in each state on average), life time (defined as the average duration per visit of each state), interval time (defined as the average time between each state visit), and switching rate between states. Occurrence rate (how often a state gets visited over time) and relative number of visits were deduced from the life time measure as further features describing bursting dynamics. The occurrence rate and relative number of visits are related to the burst rate and relative burst rate reported with the thresholding technique. Inherently, some of these different summary measures of the bursting dynamics are inter-related, e.g. a state with an increase in occurrence or burst rate will see a

corresponding decrease in interval time if the probability of transitioning out of that state remains the same. As such, some of these measures if associated with motor impairment might overall tend to correlate with motor state with opposite polarity, such as the occurrence or burst rate in a given frequency band and the interval time.

HMM method results were contrasted with those from the standard thresholding method of defining beta bursts, to allow comparison with relevant previous work (Tinkhauser et al., 2017a; Tinkhauser et al., 2017b; Torrecillos et al., 2018; Tinkhauser et al., 2020). The one exception was that I did not apply an arbitrary minimum duration for bursts, so that results would parallel as closely as possible to those of the HMM models. Different percentile amplitude thresholds (55-99th in steps of 2 percentiles) were used. For each percentile, the same amplitude threshold was applied on both medication conditions, where that was calculated by taking the mean of amplitude thresholds for both ON and OFF conditions (Tinkhauser et al., 2017b). Measures equivalent to those extracted from the TDE-HMM were extracted, where possible, from the results of the different standard thresholding models and the results combined. These features included bursting rate, relative number of bursts of different durations (<0.1 s, 0.1-0.2 s, ... , 0.8-0.9 s, >0.9 s) and the average burst duration or life time of states in the theta, alpha, low beta and high beta frequency bands.

2.4.2 Naïve Bayes classifier

The Gaussian Naïve Bayes classifier MATLAB (2018b, Mathworks, Natick, MA, USA) implementation was used to differentiate between the upper and lower limb movements in Chapter 3 (Friedman et al., 1997; Rish, 2001; Hand

and Yu, 2011). In this algorithm, features are conditionally independent random variables, given the class. The estimated posterior probability is equal to the prior probability multiplied by the likelihood. Naïve Bayes estimates the densities of the features within each class, and then it models posterior probabilities according to Bayes rule. That is, for all $k = 1, \dots, K$,

$$\hat{P}(Y = k|X_1, .., X_P) = \frac{\pi(Y = k) \cdot \prod_{j=1}^{P} P(X_j|Y = k)}{\sum_{k=1}^{K} \pi(Y = k) \prod_{j=1}^{P} P(X_j|Y = k)}$$

Where Y is the random variable corresponding to the class index of a trial (e.g. which limb is being moved), $X_1, .., X_P$ are the random features of a trial (e.g. the top six ranked features from The ReliefF feature selection algorithm), $\pi(Y = k)$ is the prior probability that a class index is k , which was computed based on the relative frequency distribution of each class. Finally, it classifies a trial by estimating the posterior probability for each class, and then assigns the observation to the class yielding the maximum posterior probability.

2.4.3 Hidden Markov modelling

HMM assumes that a time series can be described using a hidden sequence of a finite number of states, where at each time point only one state is active (Quinn et al. 2019, Vidaurre et al. 2018). However, as HMM is a probabilistic model, the inference process assigns a probability of being active to each state at each time point. Afterwards, the model assumes that the data observed in each state are drawn from a probabilistic observation model. The observation distribution is of the same family for all states, whereas the observation model parameters are different for each state. The different varieties of the HMM are thus given by which family of probabilistic observation distribution is chosen to model the states. Here, if vector

x_t represents the data and s_t represents the hidden state at time point t, the observation model assumes that:

$$x_t|s_t = k \sim \ Multivariate\ Gaussian\ (\mu_k, \Sigma_k),$$

where μ_k is a vector with (number of channels) elements and Σ_k is the (number of channels by number of channels) covariance matrix codifying the variances and covariances between channels when state k is active. This is referred to as the observation model, which, in this case, characterizes the distribution of each state k by parameters (μ_k, Σ_k). Although the chosen model used a multivariate Gaussian, other choices for the observation model are possible; for example, one could use a multivariate autoregressive (MAR) observation model, where the states are defined and identified by their distinct spectral signature (Bosman et al., 2012), or the TDE-HMM model as in Chapter 4 which models the main principal components (eigenvectors) of a Gaussian distribution defined not only over space but also over a window of time around the point of interest.

Additionally, the state sequence is regularized by modelling the probability of transitioning between all pairs of brain states; that is, before observing the data, the probability, $\Pr$, of a certain state. Thus, this probability of a given state being active at time point t is modelled to be dependent on which state was active at time point $t-1$.

$$\Pr(s_t = k) = \ \Sigma_l \ \theta_{l,k} \ \Pr(s_{t-1} = l),$$

where $\theta_{l,k}$ refers to the transition probabilities. Within matrix θ, I can further distinguish between the on-diagonal elements, θ_{kk}, which control the persistence of each state, and the off-diagonal elements, θ_{kl} (with $k \neq l$),

which refer to the actual transitions. Finally, a parameter η encodes the initial state probabilities for each scanning session. Therefore, according to this formulation, the observed data at each time point are effectively modelled as a mixture of Gaussian distributions, with weights given by $w_{tk} = \Pr(s_t = k)$.

The TDE-HMM approach used in the medication conditions study, and inspired by and related to the theory of Gaussian processes, can capture both spatial and spectral properties without overfitting, which is a problem with the alternative HMM method for identifying spatio-spectral states (i.e. the HMM-MAR). The limitation is that the use of dimensionality reduction over (space x time) by (space x time) matrices that represent the states makes the approach relatively insensitive to high frequencies.

A characteristic of the TDE-HMM method is that it is able to identify the frequency of signal segments that are shorter than a full cycle of the signal frequency (see Supplementary note 1 and the simulations in Supplementary Figure 9 in Vidaurre et al., 2018). Unlike the sliding window approach the HMM provides a large number of separated sub-cycle wave segments, from which the spectral estimation of slow frequencies is possible. This is because frequency is defined instantaneously and depends on the gradient of the signal which is theoretically defined at each time point.

In addition, as state visits or episodes of under 200ms duration are indistinguishable in their content from state episodes with longer duration I have opted to retain the former rather than introduce an arbitrary minimum duration, which would detract from the objectiveness of the HMM methodology. The downside of this approach is that I include some episodes

that may be less than one cycle in duration, but to counter this I have differentiated between state visits according to their duration.

Z-normalised concatenated LFPs of the selected contacts were fed to the TDE-HMM analysis to estimate transient spectral bursts. This models the data as a sequence of state visits, where each state can be interpreted as a transient spectral event of a certain type (e.g. beta, alpha etc.) (Quinn et al. 2019). The dynamics of these transient spectral events were then summarized using metrics that characterised states in a particular frequency band; state rate (state onsets per second), fractional occupancy, life time (seconds) and interval time between states (seconds). This assessment was repeated for the OFF and ON medication conditions. Changes in extracted measures between the two conditions were correlated with the contralateral UPDRS hemibody scores to investigate any link to Parkinsonian motor impairment.

2.4.4 Multivariate regression

The intention was to use the multiple HMM features as regressors in linear multivariate regression models to predict clinical and behavioural measures. However, due to the high number of, and multicollinearity existing between, the various HMM features, regular linear multivariate regression models do not afford accurate predictions. Therefore, there was a need to use a non-traditional regression model using L2 regularization, which adds a penalty of the square of the magnitude of coefficients. This method reduces the sum of squares of coefficients to decrease the impact of highly-correlated features.

To be more specific, ridge regression was used to create parsimonious regression models given that the number of extracted features (i.e. regressors) could exceed the number of STN recordings (Hoerl and Kennard,

1970a; Hoerl and Kennard, 1970b; Marquardt, 1970; Marquardt and Snee, 1975). Regression was performed on every single HMM model separately using the full set of features extracted before collapsing states into five bands (theta, alpha, low beta, high beta, and background). Ridge regression uses the equation below to estimate ridge coefficients, $\hat{\beta}$:

$$\hat{\beta} = (X^T X + kI)^{-1} X^T y$$

Where X is the features matrix, y is the predicted score, k is the ridge parameter and I is the identity matrix. Small, positive values of k improve the conditioning of the problem and reduce the variance of the estimates. While biased, the reduced variance of ridge estimates often results in a smaller mean squared error when compared to least-squares estimates. The k parameter was set by varying the k value in the model between -30 and 30, and the final k value chosen when model prediction power converged and stopped changing. To avoid overfitting, k was estimate using leave-one-out cross-validation.

2.5. Statistical analyses

In the movement prediction study (Chapter 3), statistical analyses were performed using MATLAB (2018b, Mathworks, Natick, MA, USA) and SPSS (2017, IBM Corp., Armonk, NY, USA). The area under the receiver operator characteristic curve (AUC) values, features weight values, and average power of EMG signals were tested with MATLAB Lilliefors test to check whether they were normally distributed or not. Prior to inclusion in analysis of variance (ANOVA) and subsequent post-hoc tests, Box-Cox transformation was applied to transform non-Normally distributed data. Greenhouse-Geisser

correction was applied where Mauchly's Test of Sphericity was significant. Post-hoc tests were paired t-tests. All data are presented as means ± standard error of the mean (SEM), and all significance p-values in Chapter 3 are corrected for multiple comparisons using the false discovery rate (FDR) method.

In the medication conditions study (Chapter 4), statistical analyses were performed using MATLAB (2019b, Mathworks, Natick, MA, USA) and SPSS (2019, IBM Corp., Armonk, NY, USA). The HMM and thresholding extracted features were tested with MATLAB Lilliefors test to check whether they were normally distributed. State feature and other distributions were tested against the null hypothesis using permutation testing (Vidaurre et al., 2019). Where several permutation tests were applied to the same data sets these were then corrected for multiple comparisons using the FDR method. Data are presented in the form of modified box-and-whisker plots with a box from the first quartile to the third quartile, a vertical line drawn through the box at the median, and whiskers drawn up to the upper and lower extreme values (excluding outliers). Otherwise, data are presented as means ± standard deviation (SD).

Chapter 3

Bursting activity dynamics and movement prediction

3.1 Introduction

Beta activity is a prominent feature recorded in the basal ganglia of patients with Parkinson's disease and in animal models of the condition (Brown et al., 2001; Mallet et al., 2008; Deffains et al., 2016). It reflects excessive synchronization within basal ganglia circuits (Levy et al., 2002a, b; Kühn et al., 2005; Weinberger et al., 2006; Cagnan et al., 2019) and its central role in parkinsonism is recognized in many computational models of the disease (van Albada et al., 2009; Moran et al., 2011; Marreiros et al., 2013; Pavlides et al., 2015; Müller and Robinson, 2018). Beta activity is attenuated by the dopamine prodrug, levodopa, and by DBS of the STN, a key surgical target in the basal ganglia (Brown et al., 2001; Priori et al., 2004; Kühn et al., 2008b). The degree of beta activity correlates with motoric impairment, and the degree of suppression of beta activity by drugs or DBS correlates with the level of improvement in motoric impairment (Kühn et al., 2006, 2008a; Ray et al., 2008; Neumann et al., 2016; Oswal et al., 2016; Steiner et al., 2017). Recently, it has become evident that beta activity in Parkinson's disease comes in bursts of over 100 ms in duration (Tinkhauser et al., 2017a; Tinkhauser et al., 2017b; Deffains et al., 2018) and that the aforesaid clinical correlations may be even stronger when considering the propensity for such bursts (Torrecillos et al., 2018; Lofredi et al., 2019). That beta bursts may be causally important is suggested by the therapeutic efficacy of using high frequency stimulation to selectively target such bursts (Little et al., 2013; Tinkhauser et al., 2017a).

However, the link between synchronization in the beta band and motoric impairment is somewhat paradoxical given current and well-established theories that ascribe improved communication and more efficient neural processing to oscillatory synchrony (Engel et al., 2001; Salinas and Sejnowski, 2001; Varela et al., 2001; Buzsáki and Draguhn, 2004; Fries, 2005, 2015). One solution to this paradox may be that the performance of a neuronal circuit may deteriorate with too much synchronization, as the restriction in information coding capacity outstrips the improvements in signal-to-noise ratio engendered by synchronization (Brittain and Brown, 2014). Support for this hypothesis comes from studies showing an increase in mutual information between different channels in the STN in animal models of parkinsonism compared to the healthy state (Mallet et al., 2008). However, mutual information is an information theoretic measure that only helps dictate the upper bound of the possible information that can be held by a system; the greater the mutual information across its components the less the information coding capacity of the system. However, mutual information does not necessarily capture those aspects of circuit activity that reflect genuine neural processing as suggested by their association with forthcoming actions.

Here I test the hypothesis that periods of elevated oscillatory synchrony, as marked by bursts in the LFP activity of the STN, impair the local representation of task-related information in the STN. To this end I use directional electrodes allowing a high resolution read-out of changing features in the STN LFP (Zhang et al., 2018), and ML to identify the aspects of wide-band STN LFP activity that predict whether a voluntary upper or lower limb movement will subsequently be performed, either because the identified features are directly important in neural processing or because they are informative surrogates of

such processing. The findings help provide a mechanistic explanation for the correlative findings linking bursts of low frequency activity to parkinsonian motor impairment, while also focusing attention on the STN as a potential alternative or complementary signal source for restorative brain-machine interfaces.

3.2 Material and methods

3.2.1 Patients and surgery

I studied the task-related modulation of STN LFPs before and during voluntary upper and lower limb movements in 18 consecutive Parkinson's disease patients undergoing STN DBS surgery to improve motor symptoms (clinical details are provided in Table 3.1). Recordings were made intraoperatively from both hemispheres, except in seven subjects (Cases 5, 6, 9, 11, 15, 16 and 18) in whom LFPs were recorded in one hemisphere only, due to fatigue and operative constraints. Thus, a total of 29 hemispheres were studied. Patients were recorded OFF dopaminergic medication. All patients were operated at the University Hospital Bern and the local ethics committee approved the use of the data for scientific purposes (2017-00551). Patients were implanted with Boston Vercise Cartesia directional electrodes (Boston Scientific). The contacts of these electrodes are distributed along four vertical levels as shown in Figure 3.1B. The middle two levels each contain three segmented (non-circular) contacts, allowing stimulation and recording focussed in three different directions (each at 120° angles). The top and bottom levels consist of a single ring/omnidirectional contact each. Localization of the STN was performed using the T2-sequence of the

preoperative 3 T MRI and preoperative stereotactic CT scan (with Leksell G frame) assisted by Brainlab iPlan 3.0 Stereotaxy software (Brainlab AG, Germany). Intraoperative targeting was optimized by microelectrode recordings and selective test stimulation.

Table 3.1 Clinical details. Num = number; Hem = hemisphere; R = right; L = left; y = years; m = male; f= female; MDS-UPDRS = Movement Disorder Society - Unified Parkinson's disease rating scale Part III; SEM = standard error of the mean. All but six subjects have been previously reported (cases 1-12 in Tinkhauser et al., 2019).

Subject	Sex	Age DBS (years)	Disease Duration (years)	Dominant Symptom	MDS-UPDRS OFF	MDS-UPDRS ON	Num Hem	STN site	Limb assessment
1	m	49	8	akinetic rigid, left	36	14	1	L	ContraLat, IpsiLat
							2	R	ContraLat, IpsiLat
2	m	55	3	akinetic-rigid right	40	25	3	L	ContraLat, IpsiLat
							4	R	ContraLat, IpsiLat
3	f	73	11	akinetic-rigid right	24	14	5	L	ContraLat, IpsiLat
							6	R	ContraLat, IpsiLat
4	m	64	16	akinetic-rigid, left	56	23	7	L	ContraLat
							8	R	ContraLat, IpsiLat
5	m	53	6	akinetic-rigid, left	30	13	9	L	ContraLat
6	m	34	7	akinetic-rigid, right	29	10	10	L	ContraLat, IpsiLat
7	m	54	11	akinetic-rigid, left	61	27	11	L	ContraLat, IpsiLat
							12	R	ContraLat, IpsiLat
8	m	61	9	akinetic-rigid, right	30	6	13	L	ContraLat
							14	R	ContraLat
9	m	72	9	tremor dominant, right	50	14	15	L	ContraLat
							16	R	ContraLat
10	f	53	5	akinetic rigid, right	27	21	17	R	ContraLat, IpsiLat
11	m	64	13	akinetic rigid, left	40	7	18	L	ContraLat, IpsiLat
							19	R	ContraLat
12	f	70	9	tremor dominant, right	30	6	20	R	ContraLat, IpsiLat
13	f	60	8	akinetic-rigid, right	41	16	21	L	ContraLat
							22	R	ContraLat

14	f	69	16	akinetic-rigid, right	25	3	23	L	ContraLat
							24	R	ContraLat
15	m	65	10	akinetic-rigid, left	38	24	25	R	ContraLat, IpsiLat
16	m	61	8	akinetic-rigid, left	34	15	26	L	ContraLat, IpsiLat
17	m	67	21	akinetic-rigid, left	30	10	27	L	ContraLat
							28	R	ContraLat
18	m	43	11	akinetic-rigid, right	31	11	29	L	ContraLat
Mean ± SEM	**m(13), f(5)**	**59.3 ± 10.4**	**10.1 ± 4.3**		**36.2 ± 10.4**	**14.4 ± 7.1**			

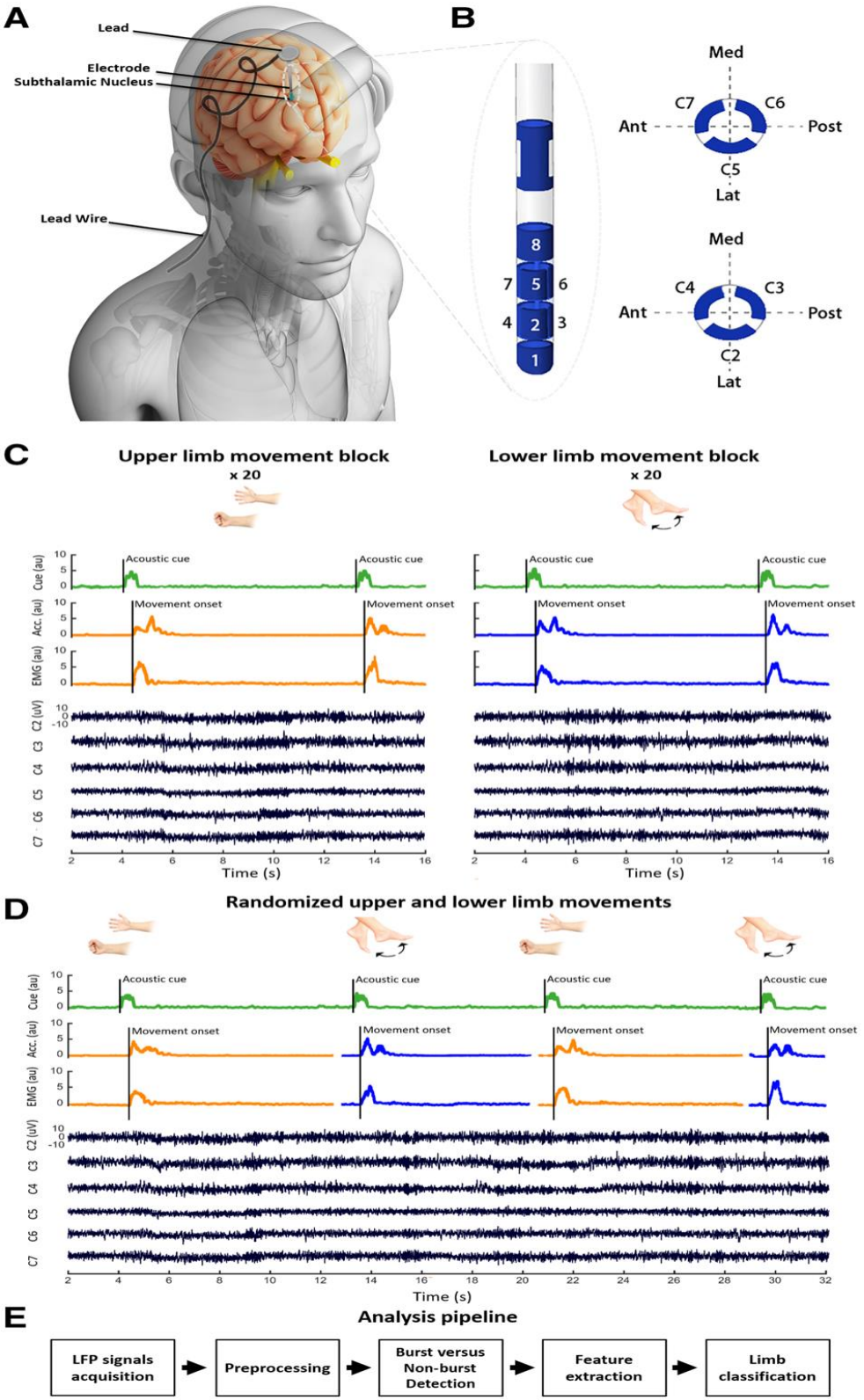

A
Lead
Electrode
Subthalamic Nucleus
Lead Wire
B
8
7
5
6
4
2
3
1
Med
C7
C6
Ant
Post
C5
Lat
Med
C4
C3
Ant
Post
C2
Lat
C
Upper limb movement block
x 20
Lower limb movement block
x 20
Acoustic cue
Movement onset
Cue (au)
Acc. (au)
EMG (au)
C2 (uV)
C3
C4
C5
C6
C7
Time (s)
D
Randomized upper and lower limb movements
Time (s)
E
Analysis pipeline
LFP signals acquisition
Preprocessing
Burst versus Non-burst Detection
Feature extraction
Limb classification

Figure 3.1 Experimental setup and analysis pipeline. (A) Deep brain electrode schematic. (B) The directional DBS lead (Boston Scientific). Contacts are distributed along four levels. On levels two and three, there are three segmented contacts (level two: contacts 2/3/4; level three: contacts 5/6/7). (C) The fixed-limb voluntary movement task; upper and lower limb movements performed in separate blocks, with each block preceded with an instruction describing the limb to be moved after hearing the imperative auditory cue. (D) Random-limb voluntary movement task; upper and lower limb movements randomly instructed within the same experimental block. Here the auditory cue prior to each trial also describes the limb to be moved. (E) Flow chart summarizing analysis pipeline. LFP signals are used to predict the limb moved using the naïve Bayes technique. Acc. = acceleration; Ant = anterior; au = arbitrary units; Lat = lateral; Med = medial; Post = posterior.

3.2.2 Postoperative localization of directional contacts

To visualize the distribution of the directional contacts in the STN I used the Lead-DBS MATLAB toolbox (version 2.1.6) (Horn et al., 2019). Preoperative MRI and postoperative CT scans were co-registered using Advanced Normalization Tools (Avants et al., 2008) and SPM12 (Statistical Parametric Mapping 12; Wellcome Trust Centre for Neuroimaging, UCL, London, UK) and normalized into the MNI 152 2009b space (Montreal Neurological Institute) (Avants et al., 2008). Using the Precise and Convenient Electrode Reconstruction for DBS (PaCER) toolbox, the DBS lead was pre-localized and eventually manually adjusted (Husch et al., 2018). Finally, the x, y, z coordinates of all directional contacts, from the left and right STN, were projected on to the right STN of the DISTAL Atlas (Ewert et al., 2018) using a non-linear flip function (Lead-DBS MATLAB toolbox) as shown in Figure 3.2.

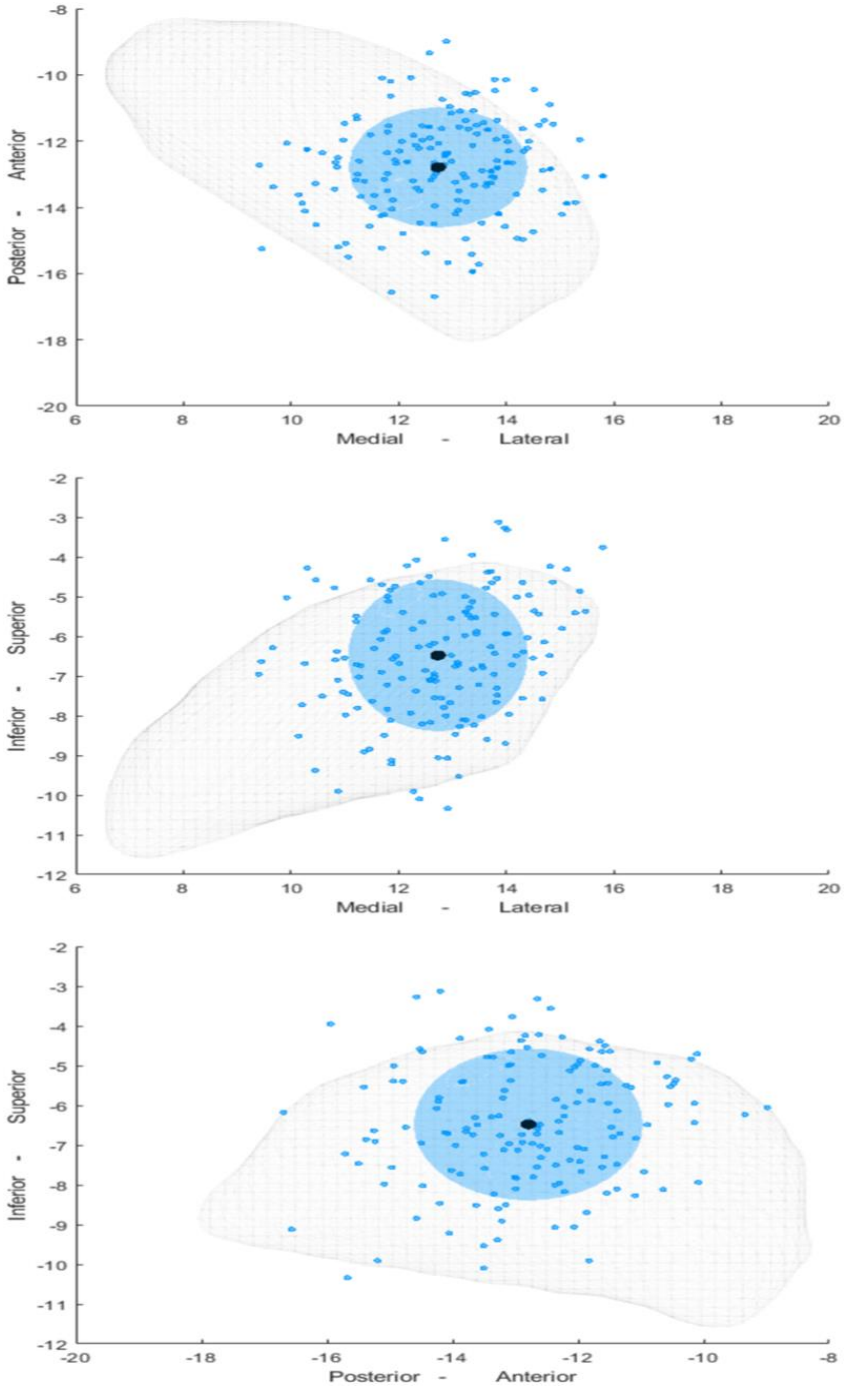


Figure 3.2 Localization of all the directional contacts in all 18 subjects included in the study. Distribution of the contacts (blue dots) and the mean coordinate of these contacts (black dots) are shown relative to the STN (grey mesh) in three different planes. In addition, a blue-shaded sphere is shown where the diameter is separately defined for the x, y, and z coordinates and corresponds to a range of 2.5 standard deviations.

3.2.3 Local field potential recordings and limb assessments

The general experimental set-up has been previously published (Tinkhauser et al., 2019) and is summarized below and in Figure 3.1A-D. After the first electrode was implanted, LFPs were recorded simultaneously from the six directional contacts (contacts 2 to 7, Figure 3.1B) at rest and during movement of the contralateral or ipsilateral limbs. Where time allowed, this procedure was then repeated when the second electrode was implanted. A TMSi-Porti amplifier (Twente Medical Systems International) was used for recordings and these were made with a common average reference, low-pass filter of 550 Hz and a sampling frequency of 2048 Hz. Surface EMG electrodes were taped over the forearm flexor muscles of the upper limb and tibialis anterior of the lower limb. Accelerometers were additionally placed on the dorsum of the hand and foot to further enhance detection of movement onset in each task. Finally, the auditory (verbal) cues were captured by a microphone synchronized with the recording system.

After a brief recording at rest (mean duration: 100.8 ± 36.5 s), patients performed one of two tasks. In the first one (fixed-limb blocks, n = 12 subjects), patients were instructed to perform separate blocks of upper and lower limb movements. Patients were informed of the desired response at the beginning of each block and instructed that only this movement should be made in response to imperative auditory cues during that block (Figure 3.1C). Upper and lower limb blocks were performed in counterbalanced order. In the second task, patients (random-limb blocks, n = 6 subjects) were instructed to perform upper and lower limb movements that were randomly intermixed. Here, patients were informed of the desired response at every auditory cue (Figure

3.1D), which then acted as a combined instruction and imperative cue. Prior to recording in the two tasks, patients were asked to respond ‘promptly and accurately’.

The upper limb movement consisted of closing and opening of the hand, while the lower limb movement involved ankle dorsi-extension and then plantar flexion (Figure 3.1C and Figure 3.1D). For the first experiment, each single movement was prompted by a verbal ‘go’ command recorded with the microphone and the intertrial time was 7.7 ± 1.6 s (range: 6.0–11.9 s). This intertrial duration was selected to avoid compromising the baseline period of the next movement with the beta rebound following the last movement (Pfurtscheller and Da Silva, 1999). For the second experiment, each movement was prompted by verbal ‘upper’ and ‘lower’ commands directing movement of the hand or ankle and recorded with the microphone, and the intertrial time was 7 ± 2.1 s (range: 5.5–14.7 s). The goal was to record 20 trials per STN contralateral to each moved limb per experiment in each subject. However, the exact number of blocks and trials varied due to the intraoperative setting and associated constraints [fixed-limb blocks, 16.54 ± 3.28 trials (range: 10–25 trials); random-limb blocks, 21 ± 11.37 trials (range: 9–40 trials)]. In addition, we were able to record STN activity ipsilateral to upper and lower limb movements in fixed-limb and randomized-limb blocks in 13 and two hemispheres, respectively.

3.2.4 Signal processing

Spike2 software (CED, Cambridge, UK) was used to manually label the onset of the audio cue, and the onset and end of movements based on the microphone, EMG and accelerometer signals. MATLAB (2018b, Mathworks,

Natick, MA, USA) was used for segmenting trials, preprocessing and further analyses including training and testing for movement classification. These were performed independently in each subject. OSL [OHBA Software Library; Oxford Centre for Human Brain Activity (OHBA), University of Oxford, Oxford, UK] was used for artefact detection and rejection. EMG signals of upper and lower limbs were extracted, z-scored, rectified, and high-pass filtered at 15 Hz. A general overview of the LFP processing and analysis pipeline is shown in Figure 3.1E. The raw signal from each of the six directional electrode contacts was high-pass filtered at 2 Hz, then detrended and z-scored to normalize each channel's data before any trial segmentation or task separation. Frequency decomposition was performed with 1 Hz resolution using the Complex Morlet Wavelet method (Cohen, 2014). A baseline normalization was performed on each segmented trial, where each 1 Hz frequency component in each trial in the time-frequency domain was normalized by a baseline of 500 ms of the same component taken from the beginning of each trial (2 s before auditory cue). Thus, LFPs were expressed as relative change with respect to baseline. This helps normalize changes across hemispheres and subjects, where absolute amplitudes might vary due to targeting variance, differing stun effects and patient's Parkinson's disease symptomatology. In two hemispheres (1 and 13), one directional contact had to be excluded from the analysis because of saturation during the recording.

3.2.5 Feature extraction and selection

A set of 100-ms long non-overlapping windows were used to extract frequency-domain features from the six directional LFP contacts. Normalized LFP powers in nine different frequency bands ranging from 8 to 500 Hz were

identified as potential frequency domain features (Shah et al., 2017). These distinct frequency bands were: 8–12 Hz, 13–20 Hz, 21–30 Hz, 31–45 Hz, 56–95 Hz, 106–200 Hz, 201–300 Hz, 301–349 Hz, and 350–500 Hz. After extracting the features, they were standardized to have a zero-mean (by subtracting the mean), and a unit-variance (by dividing by the standard deviation). Low frequency activity (below 7 Hz) was excluded as the 100-ms window used for extracting features was insufficient for reliable estimation. I did, however, explore the additional use of various higher order statistical measures as potential features (entropy, kurtosis, activity, mobility, complexity, skewness, maximum, minimum, mean, and standard deviation; as per Shah et al., 2017) in the classification of the training subsets, but these were seldom prioritized by the feature selection algorithm, and had very low weights compared to the spectral features. As a result, they were excluded from the main analyses.

K-fold cross validation (k: number of groups into which dataset was randomly split) was used to ensure that all trials in the original training dataset were used for both training and validation, and the same subset of data used for training was not used for validation; each trial being used for validation only once. Specifically, I used 4-fold cross-validation, where at each rotation, three folds were used for training, and the remaining one was used for testing. The ReliefF feature selection algorithm was used to determine important features and eliminate non-important ones (Robnik-Šikonja and Kononenko, 2003). ReliefF first sets all feature weights to 0, then iteratively selects a random trial and finds the nearest trials to it from each class, and finally it calculates the weights of features through penalizing weights that give different values to neighbours of the same class, and rewarding those that give different values

to neighbours of different classes. This was applied on the training subset containing the three folds, and the top six ranked features used for testing the fourth fold. The weight of each feature was estimated by counting how many times it was selected across the four folds as among the top six features, this was then divided by the number of folds (k = 4) to get the final measure of feature importance. These weights were then used as a measure of the contribution of a given feature to the classification.

3.2.6 Burst detection

Power spectral densities in the alpha (8–12 Hz), beta (13–30 Hz) and low gamma (35–45 Hz) bands were calculated. The 75th percentile thresholding method was used to find bursts which lasted longer than 100 ms (Tinkhauser et al., 2017b). Because of their higher frequency, gamma bursts are too short-lived to be captured in sufficient quantity by these criteria and were therefore not considered further for analyses. The OFF medication state may have also served to diminish and shorten gamma bursts, as LFP activity in this frequency band and related bursting depends on dopaminergic input (Brown et al., 2001; Androulidakis et al., 2007; Lofredi et al., 2018). The temporal relationship between alpha and beta bursts was screened and overlapping bursts were removed (Figure 3.3). Non-burst periods were defined as periods without alpha, beta, or low gamma bursts. To perform further analysis, a 100 ms duration time window was placed around the centre of every detected burst and non-burst period; feature extraction, selection, and limb movement classification was then performed on these 100-ms periods.

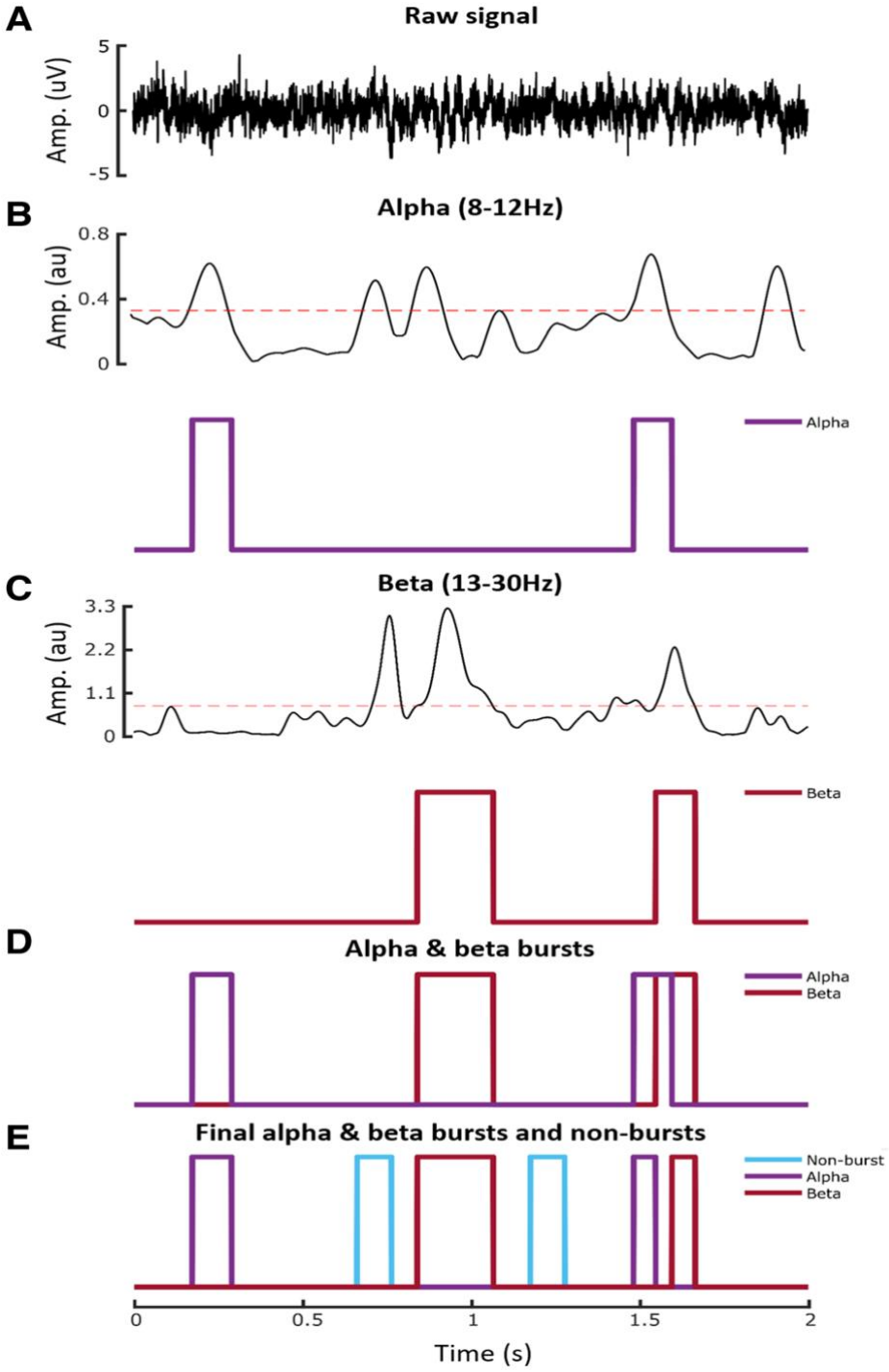


Figure 3.3 Burst detection process. (A) Raw LFP in a 2-s epoch from one of the directional contacts. (B) LFP power in alpha band and detected alpha bursts. Threshold shown by interrupted red line is the 75th percentile power. Note that threshold crossings had to exceed 100 ms in duration to be classified as bursts. (C) LFP power in beta band and detected beta bursts. (D) Detected alpha and beta bursts. (E) Final non-overlapping alpha and beta bursts, and burst-free periods (non-burst). au = arbitrary units.

3.2.7 Decoding algorithm

The Gaussian Naïve Bayes classifier MATLAB implementation was used to differentiate between the upper and lower limb movements (Friedman et al., 1997; Rish, 2001; Hand and Yu, 2011). In this algorithm, features are conditionally independent random variables, given the class. The estimated posterior probability is equal to the prior probability multiplied by the likelihood. Naïve Bayes estimates the densities of the features within each class, and then it models posterior probabilities according to Bayes rule. That is, for all $k = 1, \dots, K$,

$$\hat{P}(Y = k|X_1, .., X_P) = \frac{\pi(Y = k) \cdot \prod_{j=1}^{P} P(X_j|Y = k)}{\sum_{k=1}^{K} \pi(Y = k) \prod_{j=1}^{P} P(X_j|Y = k)}$$

Where Y is the random variable corresponding to the class index of a trial (e.g. which limb is being moved), $X_1, .., X_P$ are the random features of a trial (e.g. the top six ranked features from The ReliefF feature selection algorithm), $\pi(Y = k)$ is the prior probability that a class index is k , which was computed based on the relative frequency distribution of each class. Finally, it classifies a trial by estimating the posterior probability for each class, and then assigns the observation to the class yielding the maximum posterior probability.

3.2.8 Statistical analyses

The main measure of interest was the AUC of the classifier based on the different spectral features of the LFP signal. This was taken as an indicator of task-related information. Statistical analyses were performed using MATLAB (2018b, Mathworks, Natick, MA, USA) and SPSS (2017, IBM Corp., Armonk, NY, USA). The AUC values, features weight values, and average power of

EMG signals were tested with MATLAB Lilliefors test to check whether they were Normally distributed or not. Prior to inclusion in ANOVAs and subsequent post-hoc tests, Box-Cox transformation was applied to transform non-Normally distributed data. Greenhouse-Geisser correction was applied where Mauchly's Test of Sphericity was significant. Post-hoc tests were paired t-tests. All data are presented as means ± SEM, and all significance p-values in this article are corrected for multiple comparisons using the FDR method.

3.3 Results

3.3.1 Subthalamic activity contains information predictive of forthcoming movement

Patients were asked to make voluntary movements of one side following an imperative cue. Prior to the onset of each block patients were informed whether extension of the wrist or dorsiflexion of the ankle would be instructed by the go cue. Patients therefore knew the voluntary movement to be made even before the onset of the first imperative cue in the block. The order of the upper and lower limb blocks was counterbalanced. The cue was the appearance of a target on a PC screen and was the same irrespective of block type. Recordings were made simultaneously from the six segmented contacts of the directional electrode in the STN and these were analysed in non-overlapping 100ms duration windows taken from different periods in the task. Spectral features were extracted for each window and the Naïve Bayes classifier was used to classify serial 100ms duration windows according to whether the wrist or ankle would eventually be moved.

The STN contralateral to the movement was considered first. For each time point (100ms window) AUC was averaged across the six directional electrode contacts. This is illustrated for an exemplar patient in Figure 3.4A and for group data across 23 electrodes in Figure 3.4C. The mean AUC was 0.506 ± 0.013 at rest (prediction at chance levels). However, this increased to 0.798 ± 0.0396, 0.792 ± 0.0521 and 0.804 ± 0.0421 during the pre-cue, pre-movement onset and post-movement onset task periods, respectively (AUC averaged over windows and then across electrodes). An ANOVA of transformed AUC with main effect of period (rest, pre-cue, pre-movement onset and post-movement onset) was significant ($F(1,22)= 206.544$, $p<0.001$). Post-hoc paired significance tests confirmed an increase in AUC in the pre-cue, pre-movement onset and post-movement onset periods compared to rest ($p<0.001$, $p<0.001$, $p<0.001$, respectively). Therefore, the activity of neural ensembles picked up by the subthalamic electrode contained information about the nature of the forthcoming response to be actioned. Remarkably, prediction of the effector to be chosen began in the pre-cue period between instruction and imperative cue even though the transformed EMG average power during pre-cue (0.0058au ± 0.0135au) was not different than that during rest (0.0035au ± 0.0074au, $p=0.4006$).

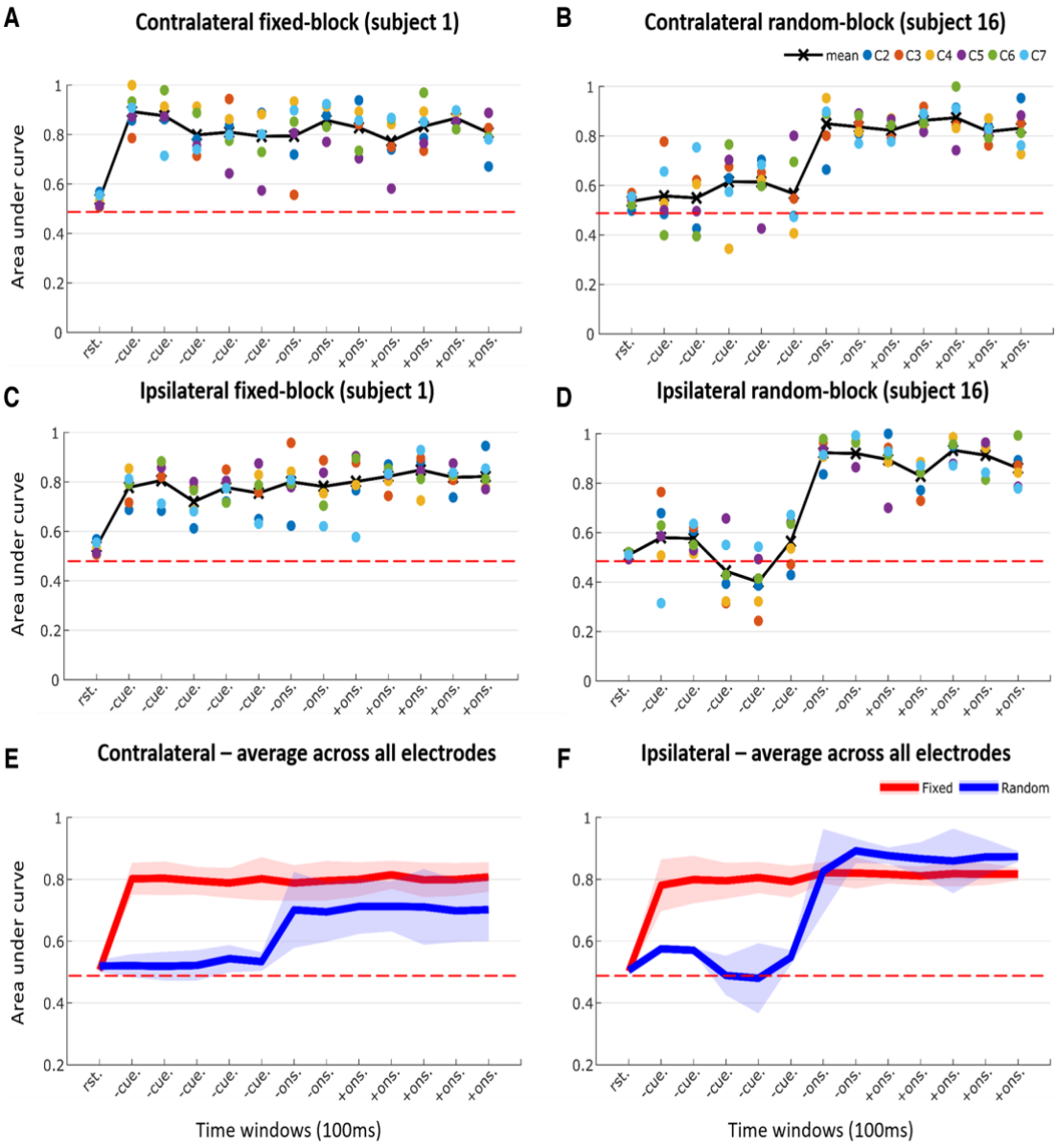


Figure 3.4 Classification AUC across various task periods. Task periods included: rest (rst.), pre-cue (-cue.), pre-movement onset (-ons.), and post-movement onset (+ons.). (A) Example of performance of one contralateral hemisphere during fixed-limb blocks. (B) Example of performance of one contralateral hemisphere during random-limb block. (C) Example of performance of one ipsilateral hemisphere during fixed-limb block. (D) Example of performance of one ipsilateral hemisphere during random-limb block. (E) Average across contralateral hemispheres during fixed-limb block (n = 23) and random-limb block (n = 6) across six directional contacts (c2–c7). (F) Average across ipsilateral hemispheres during fixed-limb (n = 13) and random-limb blocks (n = 2) across six directional contacts (c2–c7). A and C are for the left hemisphere of Subject 1 and B and D are for the left hemisphere of Subject 16. Horizontal dashed red line shows the AUC if classification were at chance level.

To confirm that the information available in the pre-cue period directly related to which limb was to be moved, I performed a control block in a group of 4 subjects (6 electrodes) in whom there was no fore-warning of the limb to be moved at the start of each block of trials. Here, the imperative cue instructed the limb to be moved, and this was randomised across trials in the same block. Under these circumstances the AUC during the pre-cue period was 0.5277 ± 0.0285, which was not different to the AUC during the preceding rest period (0.5198 ± 0.0194, $p = 0.5143$). Exemplar data from one subject are shown in Figure 3.4B and data averaged across 6 electrodes are shown in Figure 3.4C.

Next, I analysed ipsilateral voluntary movements. These were acquired in 8 out of the 18 subjects (13 electrodes), as recording was cut short in five patients due to fatigue. In subjects with paired contralateral and ipsilateral data the AUC was not significantly different between the two sides across any of the task periods. An ANOVA of transformed AUC with main effects task period (rest, pre-cue, pre-movement onset and post-movement onset) and side (contralateral and ipsilateral) confirmed a significant effect of period ($F(1,12) = 178.7$, $p<0.001$), and a significant interaction between period and side ($F(1.884, 22.618)= 112.73$, $p<0.001$). The effect of side was not significant ($F(1,12)= 3.521$, $p=0.085$). As before, the effect of task period was due to an increase in AUC on both ipsilateral and contralateral sides in the pre-cue, pre-movement onset and post-movement onset periods compared to rest ($p<0.001$, $p<0.001$, $p<0.001$, respectively). The interaction between period and side was not further investigated.

I also repeated the control random-limb blocks in two of the 18 subjects whilst they made ipsilateral movements. As before, there was no fore-warning of the

limb to be moved at the start of each block of trials. The imperative cue dictated the responding limb, and this was randomised across trials. Under these circumstances the AUC during the pre-cue period was 0.5325 ± 0.0278, which was not different to that during the preceding rest period (0.5054 ± 0.0058).

To summarise, STN activity over a wide band of frequencies carries significant information about intended contralateral and ipsilateral limb movements even when these are yet to be made, provided that prior instructions enable action selection.

3.3.2 Bursts of 8-30Hz subthalamic activity compromise the prediction of forthcoming movement

My ultimate goal was to determine whether the information about future movement held by local circuits was compromised by bursts of locally synchronised activity, as expressed in the LFP (Figure 3.5A). The incidence of bursts fell off steeply after the imperative cue (Figure 3.5B), but bursts were still frequent during the pre-cue period during which the AUC for predictions of contralateral limb movement was already elevated in the standard forewarned paradigm (alpha burst rate: 1.0125burst/s ± 0.1208burst/s; alpha burst duration: 0.1672s ± 0.0259s, beta burst rate: 0.7342burst/s ± 0.159burst/s, and beta burst duration: 0.2015s ± 0.0225s; Figure 3.5C and Figure 3.5D).

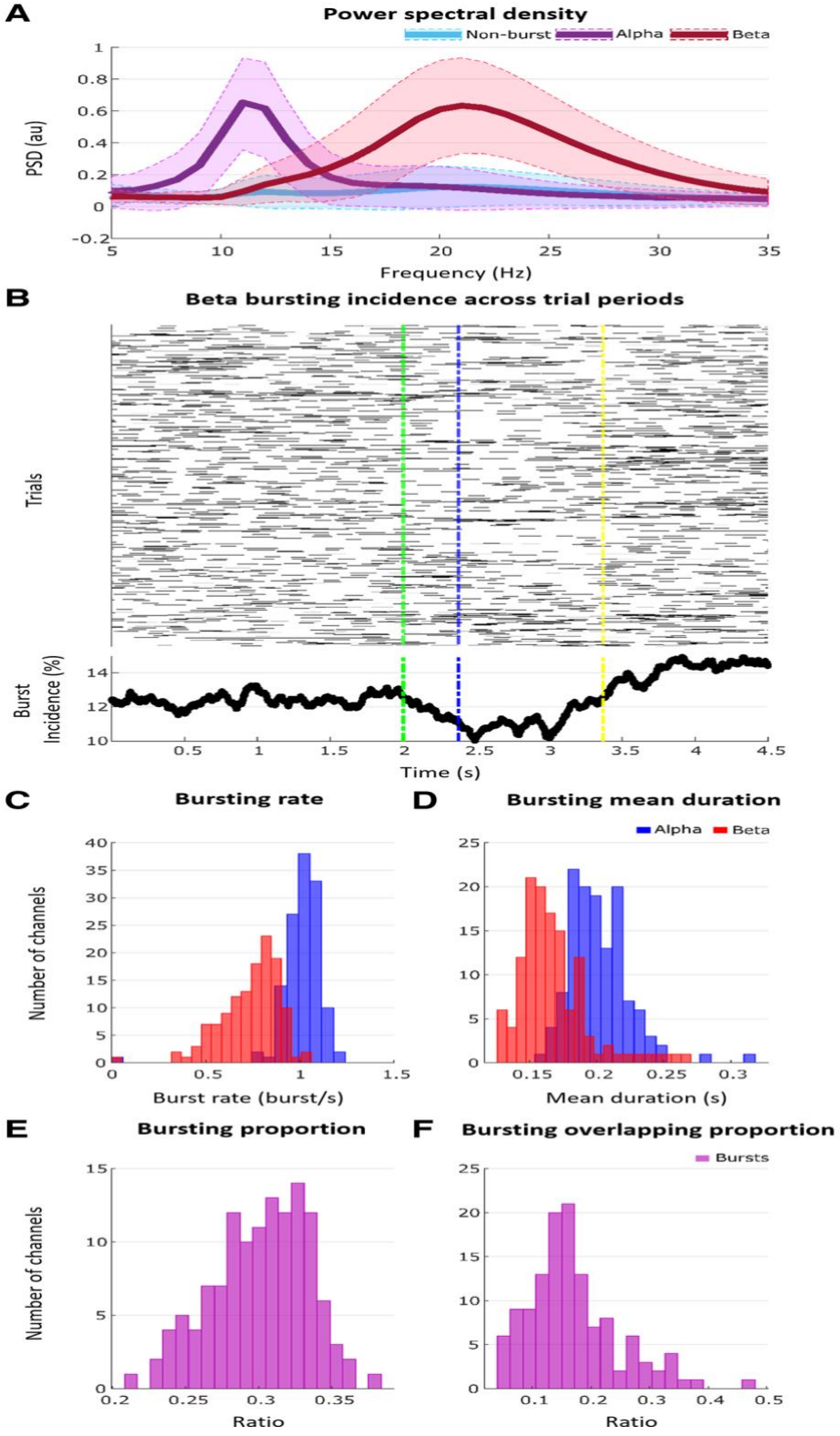

A
Power spectral density
Non-burst
Alpha
Beta
PSD (au)
Frequency (Hz)
B
Beta bursting incidence across trial periods
Trials
Burst Incidence (%)
Time (s)
C
Bursting rate
Number of channels
Burst rate (burst/s)
D
Bursting mean duration
Alpha
Beta
Mean duration (s)
E
Bursting proportion
Number of channels
Ratio
F
Bursting overlapping proportion
Bursts
Ratio

Figure 3.5 Burst characteristics during the pre-cue period in the fixed-limb experiment. (A) Example shows power spectral density for the three bursting states (non-burst, alpha, and beta) from the left hemisphere of Subject 1 (channel 4). (B) Raster plot of bursts (top) and mean of beta burst incidence (% of total trials; bottom) at each time point for all trials of fixed-limb blocks (23 hemispheres, 9801 trials in total) aligned to cue (green vertical line). Mean of trial movement onsets is blue vertical line and mean of trial movement offsets is yellow vertical line. (C) Histogram of burst rate for alpha (blue) and beta (red) bursts across all contralateral hemispheres (n = 23). The overlap between the two burst distributions is dark red. (D) Histogram of mean burst duration for alpha and beta bursts across all contralateral hemispheres (n = 23). (E) Histogram of the proportion of the whole pre-cue period taken up by the combined alpha and beta bursts across all contralateral hemispheres (n = 23). Ratio of 0.2 means, for example, that alpha and beta bursts comprise 20% of the pre-cue period. (F) Histogram of proportion of bursts that overlap between alpha and beta across all contralateral hemispheres (n = 23).

Accordingly, four seconds of pre-cue period were re-classified with respect to whether they contained alpha (8-12Hz) or beta (13-30Hz) bursts or not. Bursts were defined and then a 100ms window centred on the mid-point of each extracted burst. Periods representative of bursts in the beta frequency were selected that did not overlap with bursts in the alpha band, and vice versa (Figure 3.3E). A histogram of proportion of the pre-cue period occupied by alpha and beta bursts (0.3007 ± 0.0328) and a histogram of the proportion of alpha and beta bursts that overlap (0.1699± 0.0772) for all the 23 contralateral hemispheres are shown in Figure 3.5E and Figure 3.5F, respectively. Naïve Bayes classifier was again used to classify alpha, beta and non-burst classified pre-cue sections according to whether the wrist or ankle would eventually be moved. AUCs were averaged across the three directional contacts on each electrode that afforded the best prediction. Averaging was performed separately for two contact configurations. In the first contact configuration, the AUC was averaged across the three burst states (non-burst, alpha burst and beta burst) for each of the six directional contacts and then

the 3 contacts affording the best predictions as measured by the AUC defined (same three contacts, hereafter termed the 3 best contacts). In the second, the 3 best contacts were independently selected for each burst state (different three contacts). This was performed in case there was a shift in the spatial distribution in activities according to burst state, and indeed the mean AUC for the same three best contacts (0.6833 ± 0.0272) was less than that for the different three best contacts (0.7027 ± 0.0258, $p<0.001$) in the non-burst state. Three, rather than six, directional contacts were considered, as when testing the effect of bursting I also wanted to explore the impact of bursting on feature weights, and it was pointless to include directional contacts where features contributed relatively little to classification.

The above revealed that the AUC for contralateral STNs was decreased for pre-cue 100ms windows containing alpha and beta bursts compared with those that only contained non-burst periods, as illustrated for the group data in Figure 3.6A and Figure 3.6B, independently of whether the same or different three contacts were considered. An ANOVA of AUC for the same best three contacts during the pre-cue period with main effect of state confirmed the significance of this factor ($F(2,42)= 65.1$, $p<0.001$). Post-hoc tests demonstrated that the AUC during non-burst windows exceeded that during alpha ($p<0.001$) and beta bursts ($p<0.001$), and the AUC in alpha bursts exceeded that in beta bursts ($p<0.001$) in the pre-cue period of the standard forewarned task. A similar ANOVA for the different best three contacts configuration confirmed the significance of burst state ($F(2,42)= 110.497$, $p<0.001$). Post-hoc tests demonstrated that the AUC during non-burst windows exceeded that during alpha ($p<0.001$) and beta bursts ($p<0.001$), and the AUC in alpha bursts exceeded that in beta bursts ($p<0.001$). Note that

as the difference in AUC between the STN LFP with and without alpha or beta bursts was assessed in the pre-cue period it was likely independent of any change in reaction time, which would arise after the period of evaluation.

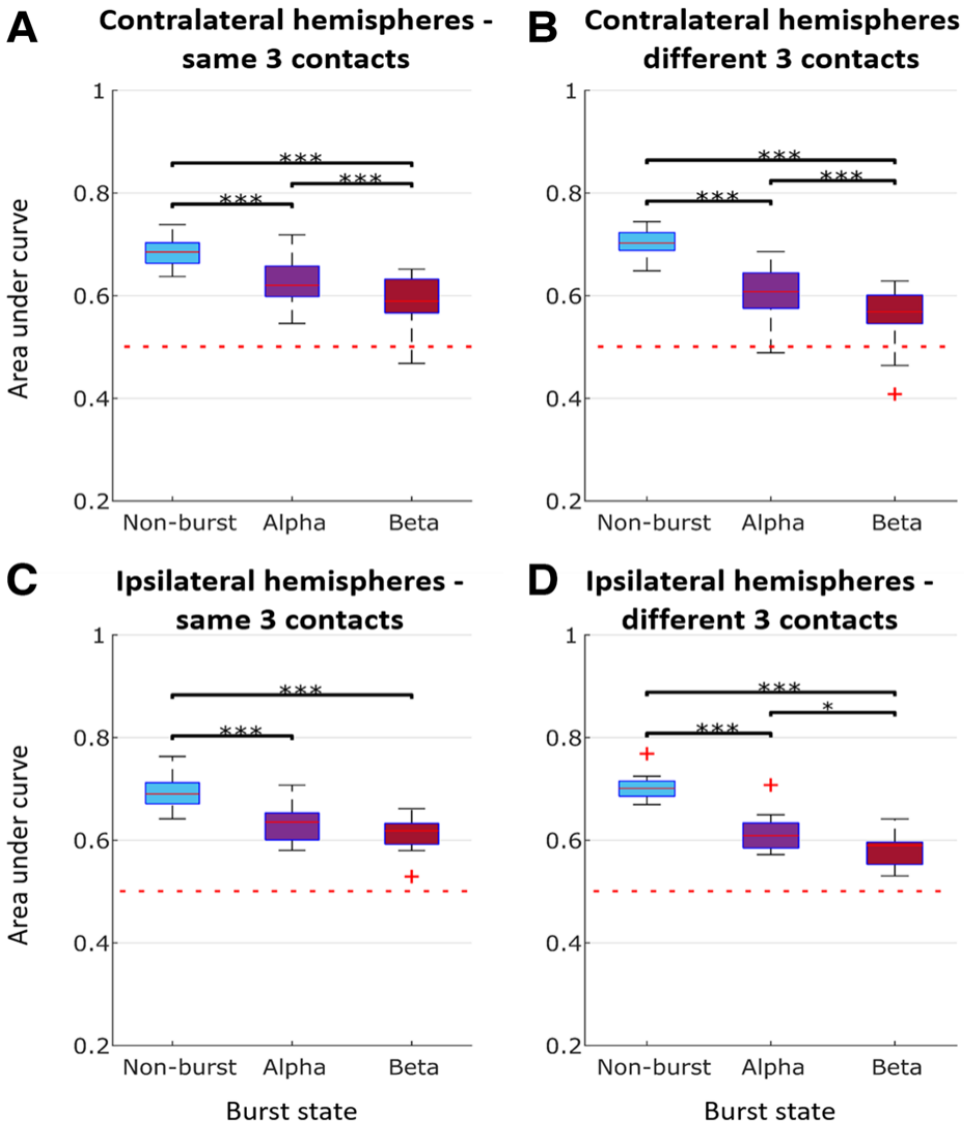


Figure 3.6 Classification AUC during the pre-cue period for different burst conditions [alpha (8–12 Hz), beta (13–30 Hz), and non-burst]. (A) Average across all contralateral hemispheres (n = 23) for same best three contacts (i.e. the three contacts affording the best predictions as measured by the AUC). (B) Average across all contralateral hemispheres (n = 23) for different best three contacts. (C) Average across all ipsilateral hemispheres (n = 13) for same best three contacts. (D) Average across all ipsilateral hemispheres (n = 13) for different best three contacts. ***P < 0.001. Box and whisker plots with median (red horizontal line), 25th and 75th percentiles (bottom and top edges of the box, respectively), and outliers (red+) noted. Horizontal dashed red line shows the AUC if classification were at chance level.

I also repeated the above in the subgroup of 13 subjects in whom I tested both contralateral and ipsilateral voluntary movements. In these subjects with paired data the drop in AUC during alpha and beta bursts did not differ between the two sides (Figure 3.6C and Figure 3.6D). An ANOVA of AUC in the pre-cue period with main effects burst state (non-burst, alpha burst or beta burst) and side (contralateral and ipsilateral) for the same best three contacts confirmed a significant effect of state ($F(2,24)= 59.978$, $p<0.001$), but showed no effect of side ($F(1,12)= 0.054$, $p=0.820$), nor interaction between state and side ($F(2,24)= 0.106$, $p=0.899$). The AUC during non-burst periods exceeded that during alpha ($p<0.001$) and beta bursts ($p<0.001$). However, although the AUC in alpha bursts exceeded that in beta bursts this was no longer significant ($p=0.1277$). An ANOVA of AUC with main effects state (non-burst, alpha burst or beta burst) and side (contralateral and ipsilateral) for the different best three contacts confirmed a significant effect of state ($F(2,24)= 166.471$, $p<0.001$), and showed no effect of side ($F(1,12)= 0.238$, $p= 0.634$), nor interaction between state and side ($F(2,24)= 0.546$, $p=0.586$). As previously, the AUC during non-burst windows exceeded that during alpha ($p<0.001$) and beta bursts ($p<0.001$), and the AUC in alpha bursts exceeded that in beta bursts ($p= 0.0212$).

In summary, regardless of whether the STN contralateral or ipsilateral to movement, or the same or different best three contacts were considered, alpha and beta burst compromised the AUC, with the effect of beta bursts being significantly greater.

3.3.3 Spectral features over a wide frequency range contribute to limb prediction

Spectral features drawn across a wide frequency band (8-500Hz) contributed to prediction of the limb to be moved. This was true for predictions made with the LFP signal during the pre-cue, pre-movement onset and post-movement onset periods of the fixed-limb paradigm before classification into burst states, as indexed by feature weights (Figure 3.7). Moreover, feature weights were significantly and strongly correlated across task periods (see Figure 3.7 legend).

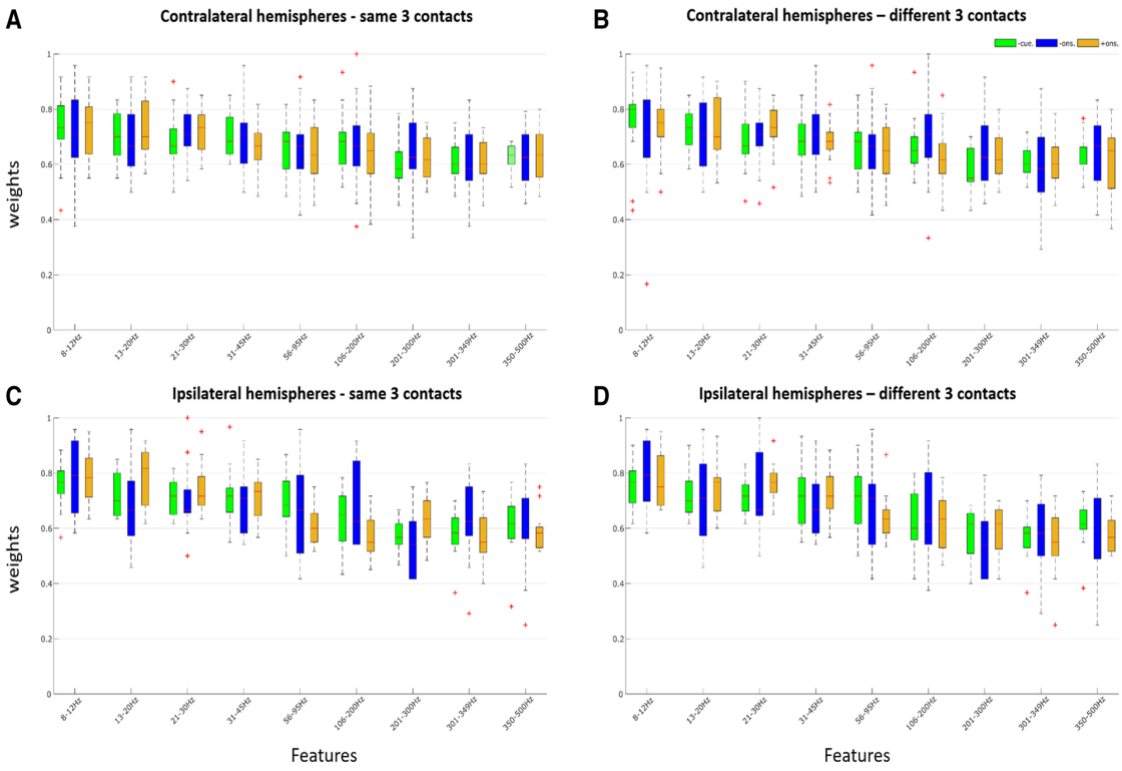


Figure 3.7 Feature importance for prediction during different task periods in fixed-limb blocks for raw LFP before classification into burst conditions. (A) Average across all contralateral hemispheres (n = 23) for the same best three contacts in different task periods. Feature importance was correlated across task periods e.g. between pre-cue and pre-movement onset, Spearman's rho = 0.833, P = 0.008, between pre-cue and post-movement onset, Spearman's rho = 0.933, P < 0.001, and between pre- and post-movement onset, Spearman's rho = 0.85, P = 0.006. (B) Average across all contralateral hemispheres (n = 23) for the different best three contacts. Feature importance was correlated across task periods e.g. between pre-cue and pre-movement onset, Spearman's rho = 0.87, P = 0.003, between pre-cue and post-movement onset, Spearman's rho = 0.862, P = 0.004, and between pre- and post-movement onset, Spearman's rho = 0.917, P = 0.0013. (C) Average across all ipsilateral hemispheres (n = 13) for the same best three contacts. Feature importance was correlated across task periods e.g. between pre-cue and pre-movement onset, Spearman's rho = 0.783, P = 0.0172, between pre-cue and post-movement onset, Spearman's rho = 0.767, P = 0.021, and between pre- and post-movement onset, Spearman's rho = 0.467, P = 0.2125. (D) Average across all ipsilateral hemispheres (n = 13) for the different best three contacts. Feature importance was correlated across task periods e.g. between pre-cue and pre-movement onset, Spearman's rho = 0.967, P < 0.001, between pre-cue and post-movement onset, Spearman's rho = 0.967, P < 0.001, and between pre- and post-movement onset, Spearman's rho= 0.95, P < 0.001. Task periods were pre-cue (-cue.), pre-movement onset (-ons.), and post-movement onset (+ons.).

The same was also true of predictions made with the LFP signal during the pre-cue period of the fixed-limb paradigm after separation into burst states (non-burst, alpha, and beta bursts) (Figure 3.8). Overall, the importance of features was similar between task periods (Figure 3.7), but less between burst states (Figure 3.8).

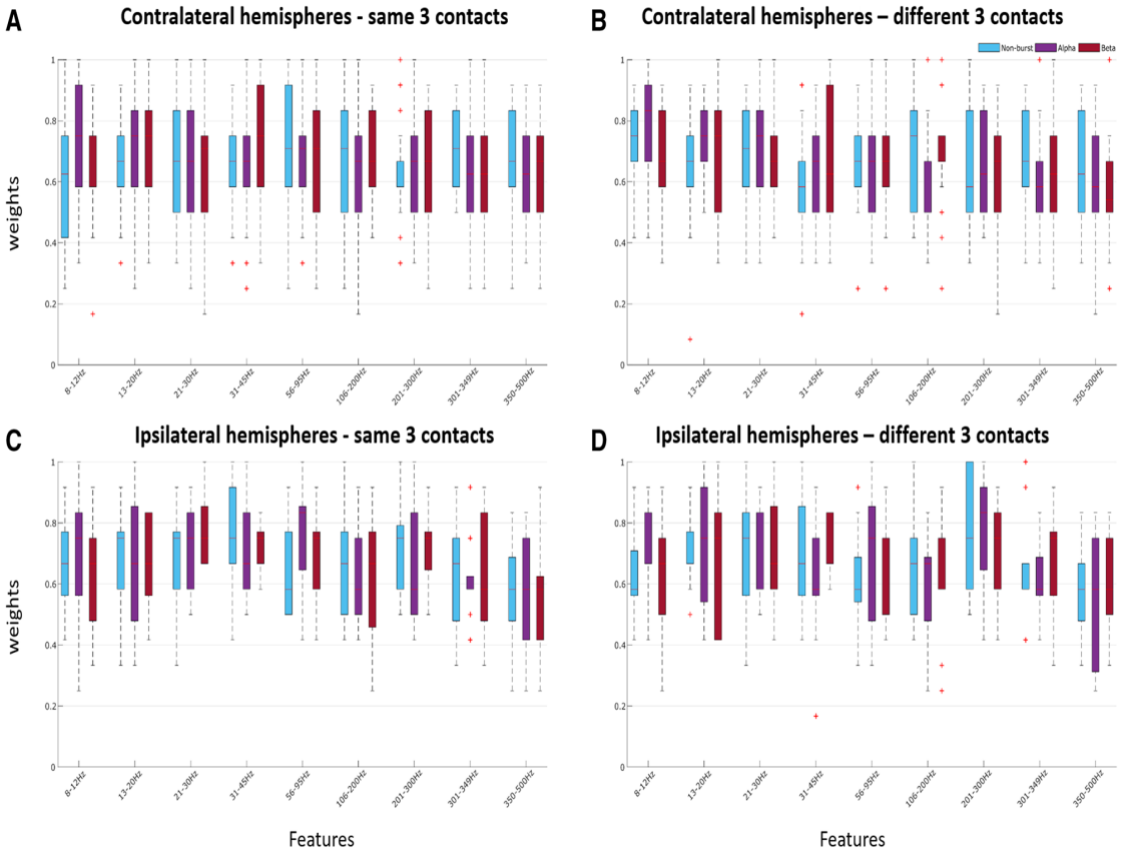


Figure 3.8 Feature importance during the pre-cue period for the burst conditions: non-bursts, alpha bursts, and beta bursts. (A) Average across all contralateral hemispheres (n = 23) for the same best three contacts. (B) Average across all contralateral hemispheres (n = 23) for the different best three contacts. (C) Average across all ipsilateral hemispheres (n = 13) for the same best three contacts. (D) Average across all ipsilateral hemispheres (n = 13) for the different best three contacts.

Finally, in an exploratory analysis I investigated whether bursts weakened feature weights. I focussed on those features that were consistent with high frequency oscillations suspected of being related to local multi-unit activity (features >300Hz; Meidahl et al, 2019). An ANOVA of transformed high frequency (>300Hz) feature weights for the same best three contralateral contacts configuration during the pre-cue period with main effect of burst state showed a significant effect of burst state ($F(2,42)= 17.87$, $p<0.001$). Post-hoc tests demonstrated that the high frequency weights during non-burst windows

exceeded those in alpha bursts ($p<0.001$) and beta bursts ($p<0.001$). Another ANOVA of transformed high frequency feature weights for the different best three contralateral contacts configuration also demonstrated that burst state was a significant main effect ($F(2,42)= 5.482$, $p=0.008$). Post-hoc tests demonstrated that the high frequency weights during non-burst windows exceeded those during alpha ($p= 0.0193$) and beta bursts ($p= 0.0159$).

3.4 Discussion

The findings demonstrate that low frequency (8-30Hz) bursts of activity in the STN LFPs impair the LFP-based prediction of future limb selection during voluntary movements. This is consistent with the hypothesis that the increased synchronisation denoted by bursting compromises information coding capacity in basal ganglia networks (Brittain and Brown, 2014). This effect was maximal in the beta frequency (13-30Hz) band. Bursts in this band are attenuated and shortened in duration by treatment with levodopa in patients with PD (Tinkhauser et al., 2017b), and specifically shutting down long duration bursts using beta-triggered adaptive DBS also leads to improvement in motor impairment (Tinkhauser et al., 2017a). Moreover, the incidence of such bursts correlates with clinical scores of bradykinesia-rigidity (Tinkhauser et al., 2017a; Tinkhauser et al., 2017b) and with the velocity of specific movements (Lofredi et al., 2019; Torrecillos et al., 2018). Together, these observations suggest that bursts of beta activity may be a key abnormality in the Parkinsonian state (Deffains and Bergman, 2019), and the current findings provide a candidate mechanism for their effect and indicate that beta bursts restrict information coding capacity in basal ganglia networks.

The STN bursts are themselves likely to reflect synchronised oscillatory input, given that LFP activities of lower frequency are thought to reflect afferent activity (Buzsáki et al, 2012). In the case of the STN, although LFP beta activity is locally generated (Kühn et al, 2005; Weinberger et al, 2006; Trottenberg et al, 2007; Marmor et al., 2017), it is coherent with, and led by, cortical beta oscillations consistent with cortical driving (Cagnan et al., 2019; Fogelson et al, 2006; Hirschmann et al, 2011; Litvak et al, 2011). However, bursts compromised the feature weights of activities above 300Hz which are believed to be generated within the STN and which have recently been linked to multi-unit activity and phase–amplitude coupling (Foffani et al, 2003; Lopez-Azcarate et al. 2010; van Wijk et al, 2016; van Wijk et al, 2017; Meidahl et al, 2019). Indeed, as the latter is an interaction with the phase of local beta activity (Lopez-Azcarate et al. 2010), and is focussed in beta bursts (Meidahl et al, 2019), it may be that phase-amplitude coupling is a manifestation of the limitation in information coding capacity exerted by relatively sustained periods of increased, afferent driven, beta synchronisation. Microelectrode studies might help confirm whether incoming low frequency bursts serve to limit information coding within the STN that then impacts on STN output in the form of multi-unit activity.

3.4.1 Experimental considerations

Although bursting denotes increased synchronisation (Levy et al. 2002; Kühn et al., 2005; Weinberger et al, 2006; Mallet et al., 2008; Deffains et al., 2018) and excessive synchronisation may potentially limit information coding capacity in basal ganglia networks (Mallet et al., 2008; Brittain and Brown, 2014), it should be acknowledged that low frequency bursting might have its

effects through some alternative unforeseen mechanism. Regardless, however, the effects shown here and the presence of physiological beta bursts in cortical-basal ganglia circuits in the healthy state raise the possibility that the information regarding future voluntary movement in motor circuits is dynamic and punctuated by low frequency bursts that serve to temporarily degrade information favouring one or other course of action. This process, which might under normal circumstances allow for flexibility in response, continues until the imperative cue, when bursting is relatively suppressed and the motor system fully commits to a given action. Of note, time-limited relative increases in beta activity in the STN have previously been linked with the need to delay while more evidence is accumulated when making difficult decisions about action choices (Herz et al, 2018).

It is also worth considering what process might underlie the change in neural activity allowing prediction of forthcoming movement in the first place. In the fixed-limb blocks reliable predictions could be derived from the STN LFP even before presentation of the imperative cue, provided that the subject was forewarned about the limb to be moved. This predictive activity could reflect anticipatory action selection, anticipatory invigoration of the motor response or subtle postural changes made to facilitate the behavioural response when it would eventually be needed. However, the absence of a significant difference in background EMG activity between the rest and pre-cue periods would be against the STN changes denoting an instruction-driven shift in posture or subliminal movement. The observation that LFPs from both the contralateral and ipsilateral STN were equally predictive of the limb to be moved is interesting and may relate to the fact that patients were recorded OFF medication. Lateralised movement-related reactivity effects in the LFP

are dependent on dopaminergic therapy (Androulidakis et al., 2006). However, the finding of predictive LFP activity in both STN does not necessarily mean that the activities within the two STN are identical.

The effect of beta bursts upon information coding capacity was demonstrated for the pre-cue period. However, the incidence of beta bursts dropped after presentation of the go cue and during the movement, so how might a burst related limitation of information coding explain motor impairment? This has been previously shown, although beta bursts appear less frequently after cues instructing movement, they do still do occur in some responses and it is these responses that have slower peak velocities in PD patients (Torrecillos et al., 2018; Tinkhauser et al., 2019). Similarly, beta bursts can re-occur during self-paced repetitive upper limb movements and during gait, and do so in association with bradykinesia and gait freezing, respectively (Lofredi et al., 2019; Anidi et al, 2018). Studies of beta-triggered adaptive DBS also provide evidence that beta bursts occur during movement. Two such studies have assessed repeated reach and return movements (Johnson et al, 2016; Iturrate et al., 2019). They indicate that 30-70% of trials involve the delivery of adaptive DBS at any given point in the movement trajectory. As stimulation is triggered by beta bursts this serves as a surrogate measure for the percentage of trials with beta bursts at any given part point in the movement trajectory. Studies of beta-triggered adaptive DBS also provide some support for a causal link between beta bursts and motor impairment, in so far as stimulation cuts short beta bursts whilst improving kinematic measures of repeated tapping and wrist movements (Tinkhauser et al., 2017; Piña-Fuentes et al., 2019; Velisar et al., 2019).

Alpha band bursts also significantly impaired prediction, albeit not as strongly as beta band bursts. This is interesting as it suggests that increased synchronisation need not necessarily be limited to the beta band to have a deleterious effect. It also has its corollary in clinical studies which often consider the correlations between motor impairment and STN LFP activities in a combined alpha-beta band (Kühn et al, 2006; Kühn et al, 2009; Chen et al, 2010; Neumann et al, 2016). A further study has demonstrated a positive correlation between STN sub-beta frequency oscillations and axial symptoms (Sharott et al., 2014). Alternatively, the alpha band effects seen in the present study might just represent spectral leakage from a dominant effect in the beta band, particularly as some evidence points to the lower frequencies in the beta band as being most linked to motor impairment. For example, it is these that are exaggerated in amplitude in PD relative to obsessive compulsive disorder patients also recorded in the dorsolateral STN, and which are suppressed by levodopa in the same patients. In contrast, LFP activities at higher frequencies in the beta band are more similar in amplitude in this region between the two conditions (Rappel et al., 2018).

3.4.2 Potential applications and limitations

The current findings are also of interest in that they suggest that local STN activity may potentially be decoded to enable effector selection, in addition to force control (Golshan et al., 2018; Mamun et al., 2015; Tan et al., 2016) in brain-machine interface applications. Information about the effector to be selected was present well in advance of the voluntary movement, affording hope that a similar control signal might be present in the STN in the absence of physical movement in paralysed patients or those with amputation. As

already noted, LFPs from both the contralateral and ipsilateral STN were equally predictive of the limb to be moved, although predictions of force are better achieved from the contralateral STN (Tan et al, 2016). Here, it is probably relevant that the LFP activity which was recorded with directional electrodes, it allows a higher resolution sampling of local activity than conventional quadrapolar DBS electrodes (Zhang et al., 2018). Under these circumstances I was able to predict the selected limb with an AUC of about 0.8 from single time windows of 100ms duration when averaging across three electrode contacts. It is likely that predictions could be strengthened still further if information were derived from several windows and the spatial patterning of activity across the six different directional contacts considered.

I should acknowledge several limitations of the experiments in this chapter. These were performed intra-operatively and hence the number of movement trials and blocks were limited. Features were therefore necessarily selected on empirical grounds and could not be independently identified through advanced ML algorithms. Predictions might have been improved with such algorithms, and also had recordings been achieved in chronically implanted patients, in whom any acute stun effects (Chen et al., 2006) compromising STN processing would have abated.

In conclusion, using a STN LFP-based ML approach I have been able to distinguish forthcoming upper limb from lower limb movements and have shown that the predictive information within the LFP is compromised during bursts of alpha and beta activity, with the major effect occurring in the latter frequency band. These results support the hypothesis that bursts of low frequency activity in the subthalamic nucleus restrict the overall capacity of

the system to encode physiologically relevant information about intended actions. Given that such bursts are exaggerated in PD, the findings provide mechanistic insight into the pathological relevance of beta dynamics, whilst also encouraging consideration of the STN as an alternative or complementary signal source in restorative brain-computer interfaces.

3.5 Summarized findings

The main findings of this chapter are:

- ML applied to STN LFPs can be used to predict which contralateral or ipsilateral limb is going to move, not only during movement execution, but also during planning and intention.
- Mean AUC is ~0.8, and this is likely a lower bound estimate of the predictive capabilities of the new 8-contact directional electrode.
- Activity of neural ensembles manifest in beta bursts and picked up by the subthalamic electrode contain information about the nature of the forthcoming response to be actioned.
- Information about the nature of the forthcoming response to be actioned is degraded by bursts of alpha and beta activity.
- The combination of STN LFPs and ML is promising for future neuro-prosthetic applications, particularly as it leverages relatively safe and routine surgery.

Chapter 4

Balance between competing states and motor impairment

4.1 Introduction

PD symptomatology is partially reversed by the dopamine prodrug, levodopa, but more advanced disease may necessitate deep brain stimulation (DBS). This therapy involves the chronic electrical stimulation of key targets in the basal ganglia, like the STN, that have been functionally compromised by the effects of dopaminergic denervation (Deuschl et al., 2006). The effectiveness of DBS has increased interest in the nature of activity in the neural circuits modulated by stimulation. Pathological synchronisation in the beta (~ 20Hz) frequency band has emerged as a key abnormality in PD linked to motor impairment (Hammond et al., 2007). In particular, the reduction in mean beta power in the LFP recorded in the STN after administration of levodopa or during DBS is positively correlated with the attendant improvement of motor impairment (Kuhn et al., 2006, 2008, 2009; Chen et al., 2010; López-Azcárate et al., 2010; Eusebio et al., 2011; Ozkurt et al., 2011; Oswal et al., 2016; Trager et al., 2016).

More recently, it has been stressed that beta activity consists of transient bursts in PD and that burst characteristics like rate and duration may correlate more strongly with motor impairment than mean beta power (Tinkhauser et al., 2017a; Tinkhauser et al., 2017b; Deffains et al., 2018; Anderson et al., 2020). The link between STN beta power, and particularly beta bursts, and motor impairment has prompted consideration of this signal as a feedback marker suitable for the closed-loop control of DBS. Closed-loop control may

potentially be at least as effective as conventional, continuous DBS, and in acute studies incurs fewer stimulation-induced side effects, such as speech impairment and dyskinesias (Little et al., 2013a, 2016a, b; Rosa et al., 2015, 2017; Pina-Fuentes et al., 2020).

However, in the correlative studies cited above, beta power, or even beta bursting, is only moderately indicative of the severity of motor impairment. So what of other oscillatory activities in the STN LFP? Broadly the STN LFP can be divided into lower frequency activities in the theta, alpha, low beta and high beta bands and higher frequency activities such as finely tuned gamma (Alonso-Frech et al., 2006; Androulidakis et al., 2007; Swann et al., 2016) and high frequency oscillations (Foffani et al., 2003; López-Azcárate et al., 2010; Özkurt et al., 2011). Higher frequency activities have lower amplitude in the STN, and are therefore challenging to track with the ultra-low power electronics needed for chronic DBS systems (see, for example, Figure 2 in López-Azcárate et al., 2010). Moreover, two key higher frequency activities, the finely tuned gamma band feature and high frequency oscillations, are also frequently absent (López-Azcárate et al., 2010; Wiest et al., 2020; Wiest et all., 2021). Lower frequency activities, on the other hand, are more consistent, of greater amplitude, and more easily tracked by chronically implanted bidirectional DBS systems. However, although registerable, with the exception of low beta activity, their relationship to motor impairment has hitherto been obscure.

Here, I use HMM to objectively detect different types of LFP states (or bursts) in the theta, alpha, low beta and high beta frequency (Quinn et al., 2019; Vidaurre et al., 2018). When a given state visits lasts more than one oscillation

cycle this may be considered a burst. I define how LFP states are modulated by dopaminergic therapy and how changes in state characteristics predict changes in parkinsonian motor impairment. In so doing I demonstrate that motor impairment is predicted not only by the predilection for episodes of low beta synchronisation, but also by the rate of occurrence and the nature of state visits in the theta, alpha, and high beta frequency bands. Together these different states compete to determine motor impairment with high fidelity in patients with PD.

4.2 Material and methods

4.2.1 Patients and surgery

I investigated spectral states in the STN LFP before and after administration of levodopa in 32 patients (64 hemispheres) with advanced PD undergoing DBS surgery targeting the STN. Patients had an average age of 58.5 years (range 34 to 79 years) and an average disease duration of 11.7 years (range 5 to 18 years). Twelve were female (Table 4.1). All patients were diagnosed with PD according to the Queen Square Brain Bank criteria (Gibb and Lees, 1988). The mean of the part III of the UPDRS score OFF medication was 37.9 (range 15-72) whilst the mean score on medication was 14.4 (range 3 to 30). The DBS electrodes were model 3389 (Medtronic) with four platinum–iridium cylindrical surfaces of 1.27 mm diameter, 1.5 mm length, and 2 mm center-to-center separation. The contacts were numbered 0 (lowermost) to 3 (uppermost). Correct placement of the DBS electrodes was confirmed by intraoperative microelectrode recordings in 18 patients and by postoperative imaging in all patients. All experimental procedures had received prior

approval from the local research ethics committee in accordance with the standards set by the Declaration of Helsinki, and patients gave their written informed consent.

Table 4.1 Clinical details. Where UPDRS motor scores were derived with half points these have been rounded up. SD =standard deviation. All but five subjects have been previously reported (cases 12-19 in Kuhn et al., 2006; cases 1, 2, 5, 7-9, 11, and 13- 17 in Litvak et al., 2011; cases 1-8 in Tinkhauser et al., 2017).

Subject	Sex	Age (years)	Disease duration (years)	Total UPDRS III OFF Drugs OFF DBS	Total UPDRS III ON Drugs OFF DBS
1	M	63	10	21	7
2	F	67	18	46	27
3	F	64	6	47	25
4	M	49	7	20	11
5	F	64	11	30	8
6	F	53	12	27	18
7	F	73	16	48	10
8	M	79	7	27	13
9	M	34	8	22	3
10	F	59	13	21	6
11	F	62	12	37	17
12	M	69	18	53	30
13	F	48	8	22	4
14	M	69	11	24	18
15	M	57	17	30	18
16	M	65	14	38	29
17	F	63	5	15	11
18	M	67	16	47	26
19	M	58	13	43	25
20	M	57	17	54	14
21	M	60	15	56	10
22	M	61	9	28	5
23	M	48	11	72	16
24	M	52	12	35	10
25	M	51	9	49	21
26	F	58	14	71	18
27	F	61	7	34	4
28	M	54	15	53	19
29	F	58	10	55	16
30	M	55	15	19	5
31	M	40	10	30	9
32	M	54	8	38	9
Mean ± SEM	**m(20), f(12)**	**58.5 ± 9.2**	**11.7 ± 3.7**	**37.9 ± 15.1**	**14.4 ± 7.9**

4.2.2 Experiment and recordings

DBS electrodes were temporarily externalized, prior to connection to the implantable pulse generator. LFP recordings were performed with the patient

quietly seated with their eyes open following overnight withdrawal of antiparkinsonian medication and were repeated before and after administration of levodopa (see below) 3–7 days after lead implantation. In 18 patients LFPs were recorded on-line from adjacent bipolar contact pairs (01, 12, 23) to limit volume conduction (Marmor et al., 2017). These LFP signals were amplified and filtered at 1–250 Hz using a custom-made, high-impedance amplifier (which had at its front end input stage the INA 128 instrumentation amplifier, Texas Instruments) and recorded through a 1401 analogue/digital converter (Cambridge Electronic Design) onto a computer using Spike2 software (CED, Cambridge, UK). Signals were sampled at either 625 Hz, 1 kHz, or 2.4 kHz. Fourteen patients were recorded using the EEG system integrated in a CTF 275-channel magnetoencephalography (MEG) scanner (CTF/VSM MedTech, Vancouver, Canada). Their signals were filtered 1-600 Hz and sampled at 2.4 kHz. Four LFP channels were recorded on each side, referenced to a cephalic reference. When LFP recordings were not recorded directly bipolarly, they were converted off-line to a bipolar montage between adjacent contacts (three bipolar channels per side) to limit the effects of volume conduction.

4.2.3 Clinical assessment

Patients were evaluated using the UPDRS part III after omitting all dopaminergic medication overnight and after administration of at least 200 mg of levodopa, with the exception of case 11 who received 100mg of levodopa. Clinical evaluation was performed at the same time as LFP recordings, except for 14 patients in whom it was performed up to 3 months pre-operatively. Changes in motor impairment with levodopa was calculated using hemibody

scores for bradykinesia-rigidity (sum of UPDRS motor score sub-items 22–26 including finger taps, open and close hand movements, rapid alternating pronation and supination hand movements, and leg movements) and tremor (sum of UPDRS motor score sub-items 20-21 for arm and leg), either in combination or separately, contralateral to the recording site. The clinical improvement was defined as the percentage of the reduced UPDRS hemibody score in ON condition compared with OFF condition.

4.2.4 Signal processing and determination of bursts

Figure 4.1 and Figure 4.2 illustrate the processing steps involved in extracting various LFP states and ascribing them to the theta, alpha, low beta and high beta bands, or to a background state if no dominant peak existed. After visual signal inspection and artefact detection and rejection using Spike2 Software (CED, Cambridge, UK) and OSL (OHBA Software Library; Oxford Centre for Human Brain Activity (OHBA), University of Oxford, Oxford, UK; https://ohba-analysis.github.io/osl-docs/), data were imported into MATLAB (2019b; Mathworks, Natick, MA, USA), where all further signal processing steps took place. Signal durations ranged from 127.9 s to 639.9 s with a mean signal duration of 392.4 ± (standard deviation) 111.9 s for both the OFF and the ON conditions (data duration OFF and ON medication was matched in each subject).

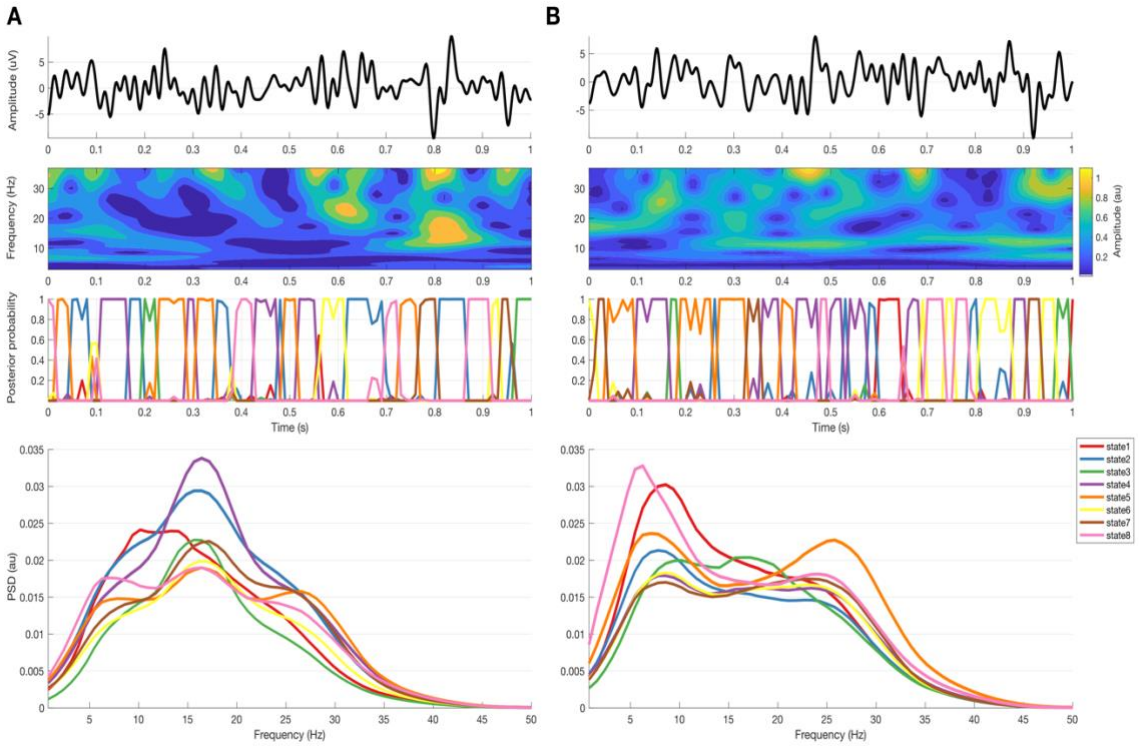


Figure 4.1 Data recorded during OFF (A) and ON (B) medications. First row is raw LFP of 1-second data sample, second row is the corresponding amplitude of the wavelet transform, third row is the corresponding HMM states posterior probability (with 8 states and 11 lags). Fourth row are the spectra corresponding to the HMM states derived from the complete recording in all subjects.

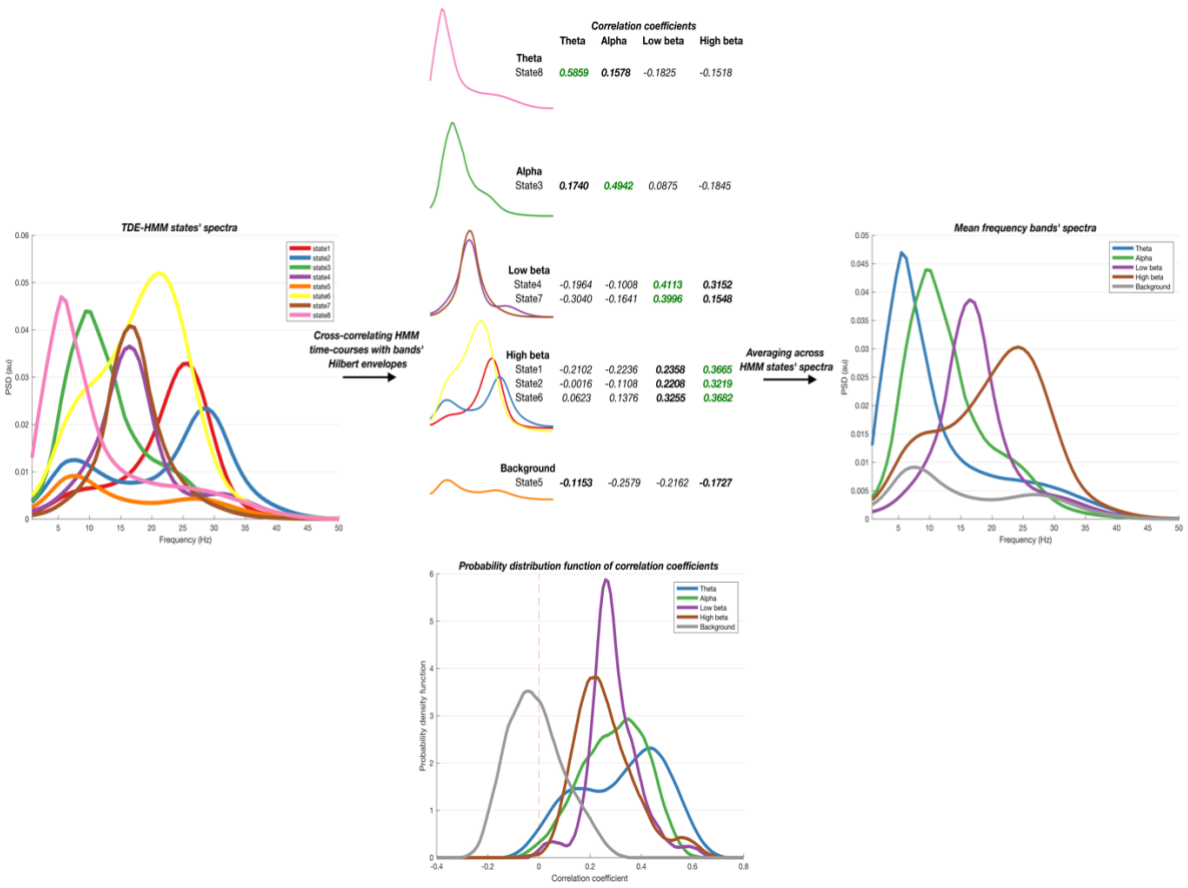


Figure 4.2 Example of HMM model with 8 states and 7 lags showing the process of assigning states to frequency bands. First, HMM state time courses in the STN LFP of a given subject are correlated with the Hilbert envelopes of the four different frequency bands (theta, alpha, low beta, and high beta) in that subject. Afterwards, if the two most positive correlations were either within the 2 low frequency bands (theta & alpha) or high frequency bands (low & high beta), then the state is assigned to the band with highest correlation; otherwise, if the strongest 2 correlations were split within the low and high frequency bands, then the state is assigned to a background band (see values of correlation coefficients in the middle panel). This results in 5 state bands. This process allows comparisons across various HMM combinations (e.g. with potentially different numbers of states). Probability distribution function panel (bottom) shows correlation coefficients used to ascribe states defined in each HMM model to the theta, alpha, low beta and high beta frequency bands. Y-axis shows probability distribution functions and x-axis shows the correlation coefficients extracted when classifying HMM states into corresponding frequency bands.

The bipolar contact pair with the highest beta power in the average of the OFF and ON drug conditions was selected for further analysis based on the presumption that this contact pair was most likely to pick up from the

dorsolateral ‘motor’ STN (Chen et al., 2006; Zaidel et al., 2010; Horn et al., 2017). The signals recorded in each medication condition from each hemisphere were bandpass filtered at 2-48 Hz, resampled at 100 Hz and z-normalized on a per session basis to facilitate comparison across different recording systems and to minimise the effects of targeting variance. All processed LFPs were then concatenated into one vector representing the selected contact pair from all medication conditions and hemispheres. The concatenated signal was then fed to TDE-HMM model which was compared against a percentile thresholding model.

4.2.5 Time-Delay Embedded Hidden Markov Model for Burst Detection

A principled way to detect bursts is to use HMMs. This can overcome many limitations of standard threshold-based approaches to burst detection, such as an over-dependence on the choice of arbitrary thresholds (Quinn et al., 2019). The approach used here, i.e. time-delay embedded HMM, is also able to concurrently detect different types of bursts, each with distinct spectral content, without the need to predefine frequency bands of interest.

In general, HMMs assume that a time series can be described using a hidden sequence of a finite number of states (Baker et al., eLife, 2014; Quinn et al., 2019; Vidaurre et al., 2018), This assumes that at each time point only one state is active (‘visited’); although, as probabilistic Bayesian inference is used here, a probability of being active is assigned to each state at each time point. The HMM then assumes that the data observed in each state are drawn from a probabilistic observation model, i.e. a probability distribution, where the distribution parameters are different for each state.

The variant of HMM used here is the TDE-HMM. This uses a multivariate Gaussian distribution as the observation model, but, crucially, the HMM is inferred on a time-delay embedded version of the (z-normalised and concatenated) LFP data; i.e. copies of the LFP data, each shifted by different time lags which define the time window around the point of interest, are fed in concurrently as multiple data channels to the HMM inference. Each HMM state then captures periods of time that have distinct auto-covariance, which translates into distinct spectral content. The net result is that the TDE-HMM models the data as a sequence of state visits, where each state can be interpreted as a transient spectral event of a certain type (Quinn et al., 2019). Note that the TDE HMM approach is also able to identify the frequency of signal segments that are shorter than the period of the signal frequency (Vidaurre et al., 2018).

4.2.6 Data analysis and statistics

States were estimated using the TDE-HMM model for 56 different combinations of state number K (5 to 18 states) and time lags L (3 to 15 lags). The time lag L determines the window duration so that a lag of 10 means that the window includes 10 data points either side of that representing the time under analysis. Longer windows allow better frequency resolution at the expense of temporal resolution (analogous to the time-frequency trade-off when choosing a basis set in wavelets). The state number K denotes the number of states to be detected. For every combination, TDE-HMM states were categorized by their predominant frequency content by cross-correlating the states' time courses with the Hilbert envelopes of the theta, alpha, low beta and high beta frequency bands. Figure 4.2 illustrates the process of

ascribing HMM states to different frequency bands. If the most positive 2 correlations were either within low frequencies (theta and alpha) or high frequencies (low and high beta), then the corresponding state was assigned to the band with highest correlation. Otherwise states were assigned to “background” activity. More than one HMM state could be attributed to a given frequency band. The analysis of multiple different models allows consistent features to emerge, whilst transformation from HMM states to frequency bands was used to facilitate comparisons across different HMM models and their interpretation, especially with respect to existing literature.

This assessment was repeated for the OFF and ON medication conditions. Various extracted measures of interest were extracted from the TDE-HMM models, and changes in them between the two medication conditions, were correlated with the contralateral UPDRS hemibody scores to investigate any link to Parkinsonian motor impairment. The extracted measures were: probability of transitioning between different states and within states (where a frequency band comprised several HMM states), fractional occupancy (referring to how much time the HMM spends in each state on average), life time (defined as the average duration per visit of each state), interval time (defined as the average time between each state visit), and switching rate between states. Occurrence rate (how often a state gets visited over time) and relative number of visits were deduced from the life time measure as further features describing bursting dynamics. The occurrence rate and relative number of visits are related to the burst rate and relative burst rate reported with the thresholding technique and described below. Inherently, some of these different summary measures of the bursting dynamics are inter-related, e.g. a state with an increase in occurrence or burst rate will see a

corresponding decrease in interval time if the probability of transitioning out of that state remains the same. As such, some of these measures if associated with motor impairment might overall tend to correlate with motor state with opposite polarity, such as the occurrence or burst rate in a given frequency band and the interval time.

HMM method results were contrasted with those from the standard thresholding method of defining beta bursts, to allow comparison with relevant previous work (Tinkhauser et al., 2017a; Tinkhauser et al., 2017b; Torrecillos et al., 2018; Tinkhauser et al., 2020). The one exception was that I did not apply an arbitrary minimum duration for bursts, so that results would parallel as closely as possible those of the HMM models. Different percentile amplitude thresholds (55-99th in steps of 2 percentiles) were used. For each percentile, the same amplitude threshold was applied on both medication conditions by calculating the mean of amplitude thresholds for both ON and OFF conditions (Tinkhauser et al., 2017b). Measures equivalent to those extracted from the TDE-HMM were extracted, where possible, from the results of the different standard thresholding models and the results combined (Figure 4.3). These features included bursting rate, relative number of bursts of different durations (<0.1 s, 0.1-0.2 s, ... , 0.8-0.9 s, >0.9 s) and the average burst duration or life time of states in the theta, alpha, low beta and high beta frequency bands.

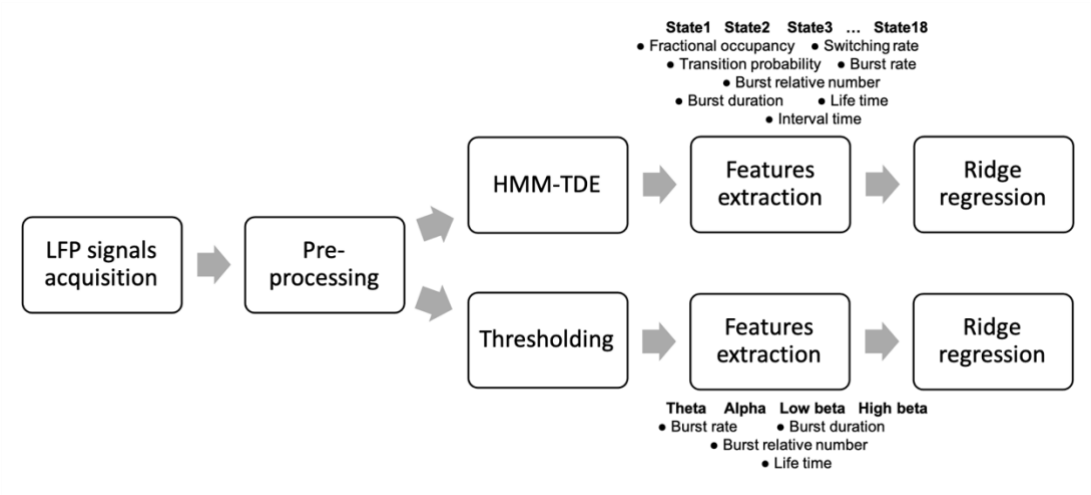


Figure 4.3 Flow chart summarizing analysis pipeline. LFP signals are used to predict motor impairment. Features used in ridge regression methods are extracted from HMM-TDE and thresholding models. Note that burst duration refers to the rate of bursts of different duration (<0.1 s, 0.1-0.2 s, ... , 0.8-0.9 s, >0.9 s) whereas life time refers to the average burst duration of states in the different frequency bands.

Ridge regression was used to create parsimonious regression models given that the number of extracted features (i.e. regressors) could exceed the number of STN recordings (Hoerl and Kennard, 1970a; Hoerl and Kennard, 1970b; Marquardt, 1970; Marquardt and Snee, 1975). Regression was performed on every single HMM model separately using the full set of features extracted before collapsing states into five bands (theta, alpha, low beta, high beta, and background). Ridge regression uses the equation below to estimate ridge coefficients, $\hat{\beta}$:

$$\hat{\beta} = (X^T X + kI)^{-1} X^T y$$

Where X is the features matrix, y is the predicted score, k is the ridge parameter and I is the identity matrix. Small, positive values of k improve the conditioning of the problem and reduce the variance of the estimates. While biased, the reduced variance of ridge estimates often results in a smaller

mean squared error when compared to least-squares estimates. The k parameter was set by varying the k value in the model between -30 and 30, and the final k value chosen when model prediction power converged and stopped changing. To avoid overfitting, I performed leave-one-out cross-validation. Finally, to evaluate the results I used the previously described method to ascribe states defined in each HMM model to the chosen frequency bands so that I could then attribute the corresponding ridge coefficients to these frequency bands.

Note that the TDE-HMM approach is also able to identify the frequency of signal segments that are shorter than the period of the signal frequency (Vidaurre et al., 2018). As the content of such short segments is statistically indistinguishable from that of longer segments I included both short and long state visits, but distinguished between the contributions of state visits of differing duration in the results. This limited the number of additional constraints on the data (no minimum duration), and I have included the results of simple thresholding without a minimum duration constraint for direct comparison.

Statistical analyses were performed using MATLAB (2019b, Mathworks, Natick, MA, USA) and SPSS (2019, IBM Corp., Armonk, NY, USA). The HMM and thresholding extracted features were tested with MATLAB Lilliefors test to check whether they were normally distributed. State feature and other distributions were tested against the null hypothesis using permutation testing (Vidaurre et al., 2019). Where several permutation tests were applied to the same data sets these were then corrected for multiple comparisons using the FDR method. Data are presented in the form of modified box-and-whisker

plots with a box from the first quartile to the third quartile, a vertical line drawn through the box at the median, and whiskers drawn up to the upper and lower extreme values (excluding outliers).

4.3 Results

4.3.1 Medication-induced changes in STN LFP states

TDE-HMM was run on the STN LFP data to identify a temporal sequence of states in each STN LFP channel, where each state can be interpreted as a transient spectral event of a certain type, including, but not limited to, beta bursts (Quinn et al., 2019). Motor impairment in PD is partially reversible after oral treatment with the dopamine prodrug, levodopa. Accordingly, I began by determining which LFP states change following levodopa treatment before seeking correlations between these changes and the improvement in motor impairment. Fifty-six TDE-HMM models of the STN LFP with different numbers of states (5-18) and time embedding lags (3-15) were separately tested ON and OFF medication.

Initially, I focussed on activities with frequencies under 40Hz, as these are more consistently found and more readily registered with the ultra-low power amplifiers that are necessary in chronic recording systems that might, in the future, deliver closed-loop DBS. Identified LFP states with clear spectral peaks were then ascribed to the theta, alpha, low beta and high beta bands, or to a background state if no dominant peak existed (Figure 4.2). Overall, following the dopamine prodrug levodopa, LFP states in the low beta band became less common and relatively briefer, whereas those in the theta band, and to a lesser extent, alpha band became more common, and relatively longer in

duration. Different TDE-HMM models could differ in the extent to which they identified levodopa induced changes in LFP states and in their ability to predict change in motor impairment. Accordingly, in the following I focus on results that have been collapsed across all 56 TDE-HMM models.

The occurrence rate of LFP states (or burst rate, i.e. how often a state gets visited over time) significantly increased when ON compared to OFF levodopa for the state visits of the shortest duration in all frequency bands, except low and high beta (Figure 4.4). In contrast, the occurrence rate of LFP states decreased in the low beta band regardless of state duration ON compared to OFF levodopa. These changes could represent shifts from one spectral band state to another, or shifts to and from the background LFP state. This issue was addressed by considering state transition probabilities (Figure 4.5). Dopaminergic medication significantly drove subthalamic activity away from the low beta state to the theta, alpha, high beta and background states, in so far as these latter states were more likely to follow the low beta state than precede it ON medication. In addition, high beta and background states were significantly driven into the theta and alpha states, and the alpha state further driven into the theta state by levodopa.

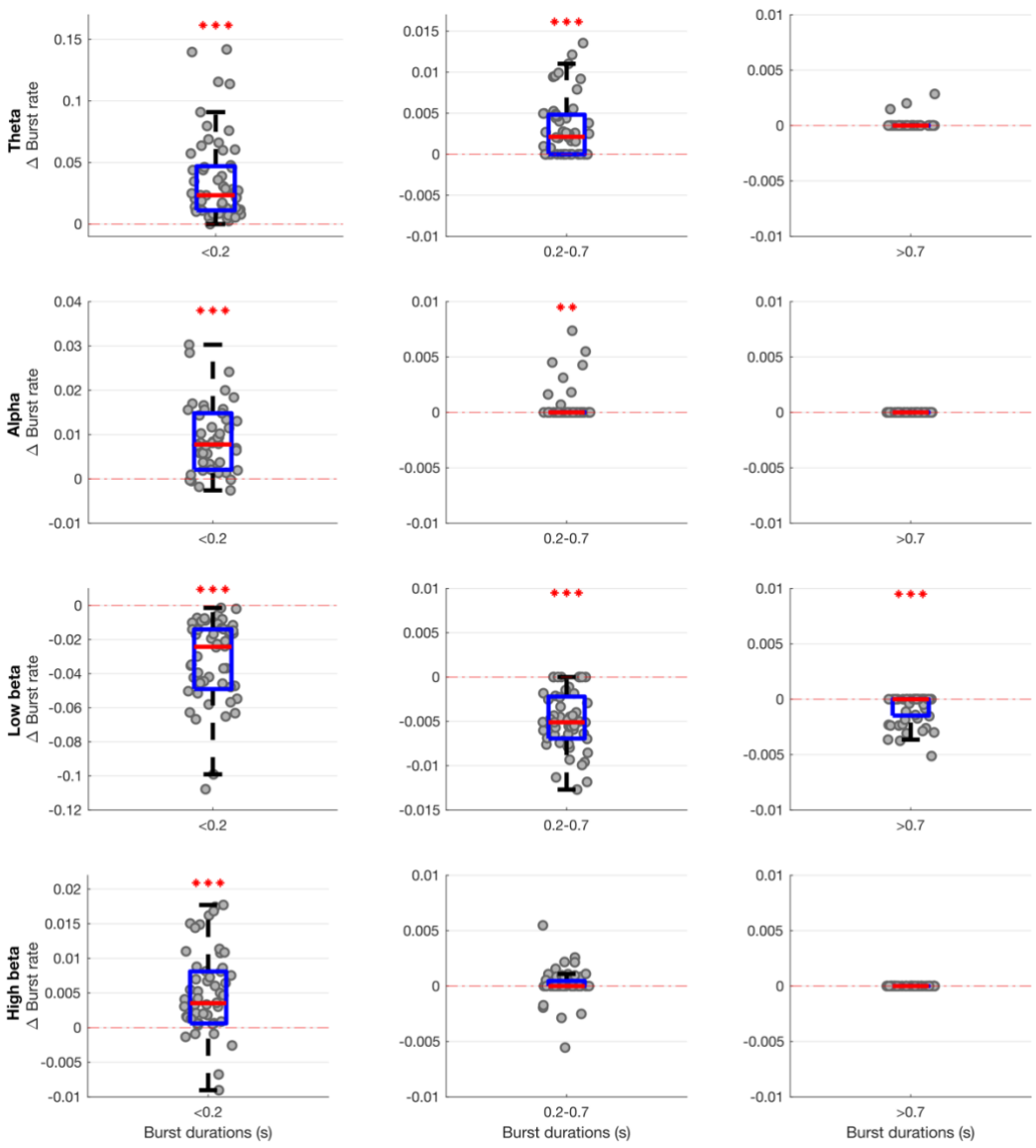


Figure 4.4 Box-and-whisker plots of change (ON-OFF) in the rate of theta (4-7 Hz), alpha (8–12 Hz), low beta (13–21 Hz) and high beta (22-35 Hz) states identified by the combination of different HMM models. There are widespread changes in the burst rate of states between the OFF and ON medication condition, with these most marked for theta and low beta states. Each dot represents the median value across the 64 hemispheres in one HMM model (data from 56 different models are plotted). Statistics were derived after performing permutation testing and thereafter corrected for multiple comparisons using the false discovery rate (FDR) method. Data are presented in the form of modified box-and-whisker plots with a box from the first quartile to the third quartile, a vertical line drawn through the box at the median, and whiskers drawn up to the upper and lower extreme values (excluding outliers). *: $p<0.05$, **:$p<0.01$, ***: $p<0.001$.

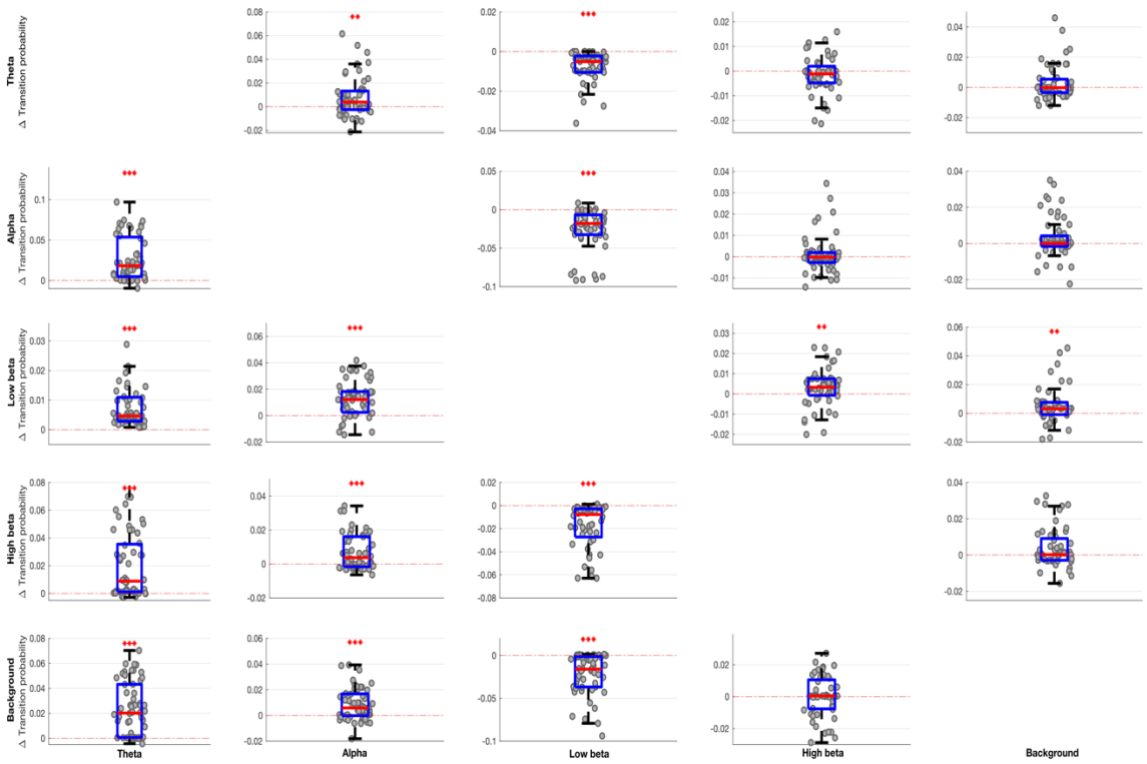


Figure 4.5 Box-and-whisker plots of medication-linked change in transition probability between various state bands (theta, alpha, low beta, high beta, and background) for different HMM models. Medication significantly drives activity away from the low beta state (shown as negative change) and into the theta and alpha states (shown as positive change). Changes in the high beta and background states are less marked, with the exception that transitions of the low beta state to the high beta and background states are increased by medication. Each dot represents the median value across the 64 hemispheres in one HMM model (data from 56 different models are plotted). Statistics were derived after performing permutation testing and thereafter corrected for multiple comparisons using the false discovery rate (FDR) method. Data are presented in the form of modified box-and-whisker plots with a box from the first quartile to the third quartile, a vertical line drawn through the box at the median, and whiskers drawn up to the upper and lower extreme values (excluding outliers).*: p<0.05, **:p<0.01, ***: p<0.001.

To better compare the present findings in the beta band with previously reported results of the standard thresholding technique, I also plotted the change in the relative rate of different durations of states (compared to the rate of all durations of states) within the beta frequency band with levodopa (Figure 4.6). There was a significant increase in the relative rate of short

duration low beta states and a decrease in the relative rate of longer duration low beta states ON levodopa. This is consistent with previous reports using the thresholding technique (Tinkhauser et al., 2017; Anderson et al., 2020).

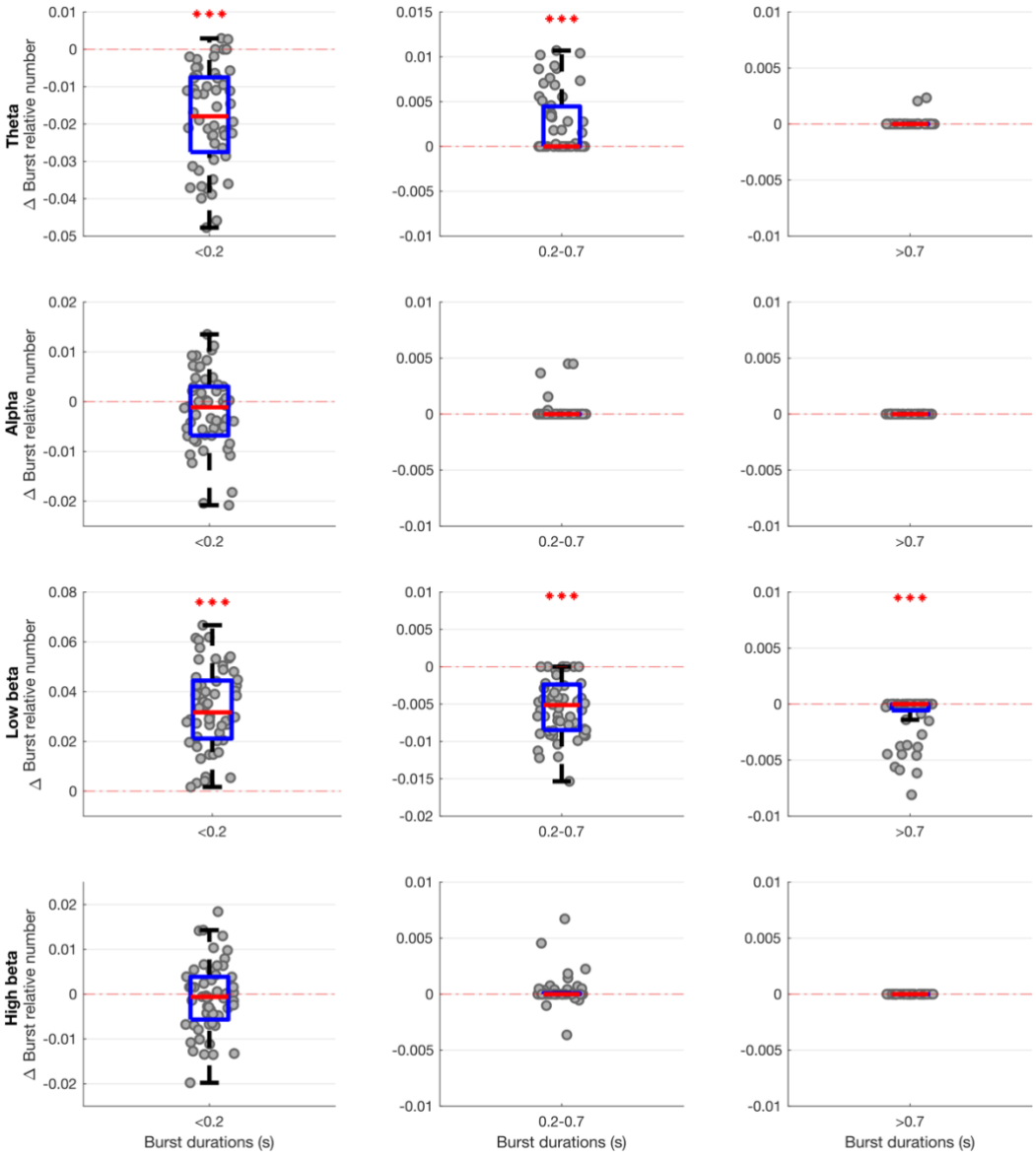


Figure 4.6 Box-and-whisker plots of change (ON-OFF) in number of theta, alpha, low beta and high beta states relative to the total number of states identified by the combination of different HMM models. There are widespread changes in the relative number of states between the OFF and ON medication condition, with these most marked in the theta and low beta bands. Each dot represents the median value across the 64 hemispheres in one HMM model (data from 56 different models is plotted). Statistics were derived after performing permutation testing and thereafter corrected for multiple comparisons using the false discovery rate (FDR) method. Data are presented in the form of modified box-and-whisker plots with a box from the first quartile to the third quartile, a vertical line drawn through the box at the median, and whiskers drawn up to the upper and lower extreme values (excluding outliers).*: $p<0.05$, **:$p<0.01$, ***: $p<0.001$.

In addition, there were significant decreases in fractional occupancy and life time, and corresponding increases in state-interval time in the low beta band ON levodopa, and significant converse changes in the theta, and to a lesser extent, alpha and high beta bands (Figure 4.7). Changes in the background activity were small.

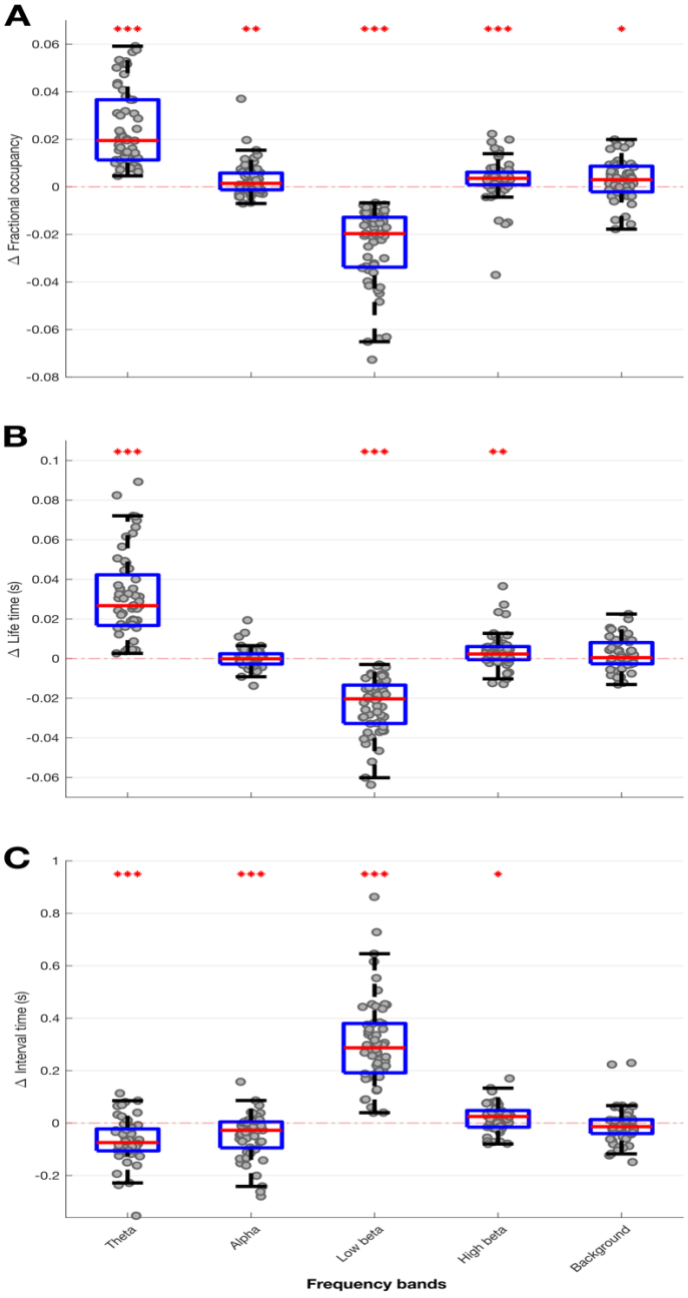


Figure 4.7 Box-and-whisker plots of medication-induced change (ON-OFF medication) in fractional occupancy (A), life time (B) and interval time (C) for different HMM models. Low beta state is reduced ON medication for fractional occupancy and life time, and increased ON medication for interval time. Theta, alpha, and high beta states show the converse pattern. Each dot represents the median value across the 64 hemispheres in one HMM model (data from 56 different models are plotted). Statistics were derived after performing permutation testing and thereafter corrected for multiple comparisons using the false discovery rate (FDR) method. Data are presented in the form of modified box-and-whisker plots with a box from the first quartile to the third quartile, a vertical line drawn through the box at the median, and whiskers drawn up to the upper and lower extreme values (excluding outliers). *: $p<0.05$, **:$p<0.01$, ***: $p<0.001$.

4.3.2 Medication-induced changes in STN LFP states correlate with motor impairment

The levodopa induced changes in low beta and theta-alpha states were also associated with opposing effects on motor impairment (Figure 4.8A). The change in the occurrence rate of the low beta states between ON versus OFF levodopa was significantly consistently positively correlated with the change in motor impairment with levodopa, so that decreases in the occurrence of low beta states were linked to improvements in motor impairment ON drug. Conversely, changes in the occurrence rates of theta and alpha band states were significantly consistently negatively correlated with change in motor impairment ON drug, so that increases in the frequency of theta and alpha states were linked to improvements in motor impairment ON drug. These contrasting effects were similar across states of different absolute durations, although the bivariate correlations themselves were relatively weak.

To better compare the present findings with previously reported results of standard thresholding in the beta band, I also estimated the correlation with the relative number of states in each frequency band (Figure 4.8B). As with the previous results, there was a reversal in correlation sign whereby the change in the relative occurrence rate of short duration low beta states negatively correlated with change in motor impairment and change in the relative occurrence rate of longer duration low beta states positively correlated with change in motor impairment, although the variance between different models was relatively large. Thus a relative increase in the occurrence rate of short duration beta states was linked to diminution in motor impairment ON

medication, whereas a relative decrease in longer beta states was linked to less motor impairment ON drug. This is consistent with previous reports using the thresholding technique (Tinkhauser et al., 2017b). The opposite pattern was seen in the theta state. A relative increase in the occurrence rate of short duration theta states was linked to greater motor impairment ON medication, but a relative increase in longer theta states was linked to less motor impairment ON drug. Smaller, less consistent effects were seen in the relative number of alpha states.

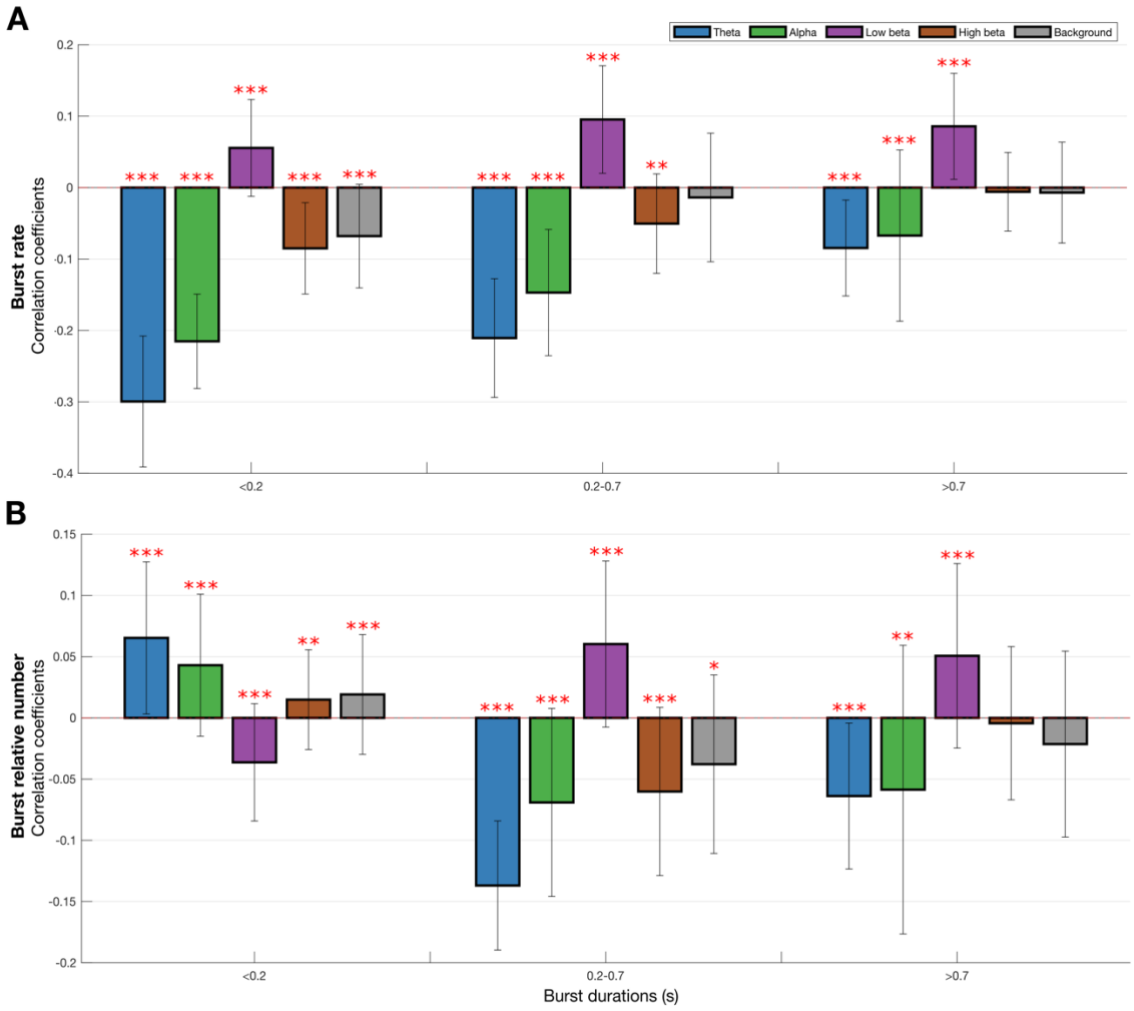


Figure 4.8 Correlation between medication-induced change (ON-OFF medication) in bursting and % change (ON-OFF medication) in contralateral hemibody UPDRS score including tremor items. Correlations for change in rate of states (A) and relative burst number (B) are shown for theta, alpha, low beta, high beta and background states identified by 56 different HMM models. Increase in rate of theta and alpha states is coupled with contralateral hemibody UPDRS Part III score reductions ON medication across all state durations. However, this pattern is reversed for the relative number of the shortest alpha states. Increase in rate of the low beta state positively correlates with contralateral hemibody motor UPDRS Part III score reductions ON medication across all burst durations. However, this is only true of longer durations when it comes to change in relative state numbers in the low beta band. Results were corrected for multiple comparisons using false discovery rate (FDR) method. Median correlations ± SD are shown. *: $p<0.05$, **:$p<0.01$, ***: $p<0.001$ and refer to whether the 56 bivariate correlations for each frequency band and state episode duration were significantly more positive or negative than zero following FDR correction.

4.3.3 Medication-induced changes across STN LFP states predict motor impairment

Changes in the absolute and relative occurrence rate of states in the different frequency bands were linked to frequency specific and often opposing changes in motor impairment. However, the bivariate correlations reported above and illustrated in Figure 4.8 are relatively modest in strength, and the statistics only confirm the consistency of the sign of frequency specific correlations using features from different HMM models. The potential importance of the correlations lies not only in the mechanistic insight afforded, but also in the potential for the different states and their features to provide comprehensive feedback about motor impairment for closed-loop control of DBS. The question therefore arises whether multivariate models that include multiple features derived from multiple TDE-HMM states can lead to stronger predictions of motor impairment. To answer this I performed Ridge regression.

The regression model derived from the TDE-HMM analysis was further contrasted with that derived from standard thresholding (Figure 4.9), using the same feature sets where possible. The median coefficient of determination across the 56 different TDE-HMM models was 0.52 (using leave-out one cross-validation), indicating that the multiple regression models explained just over 50% of the variance in the change in motor impairment following medication. This is a substantial effect and contrasts with the results across multiple thresholding models using the same data, with different threshold percentiles in the theta, alpha, low beta and high beta frequency bands (23 combinations; 55-99th percentiles). Here the median coefficient of determination was only 0.16.

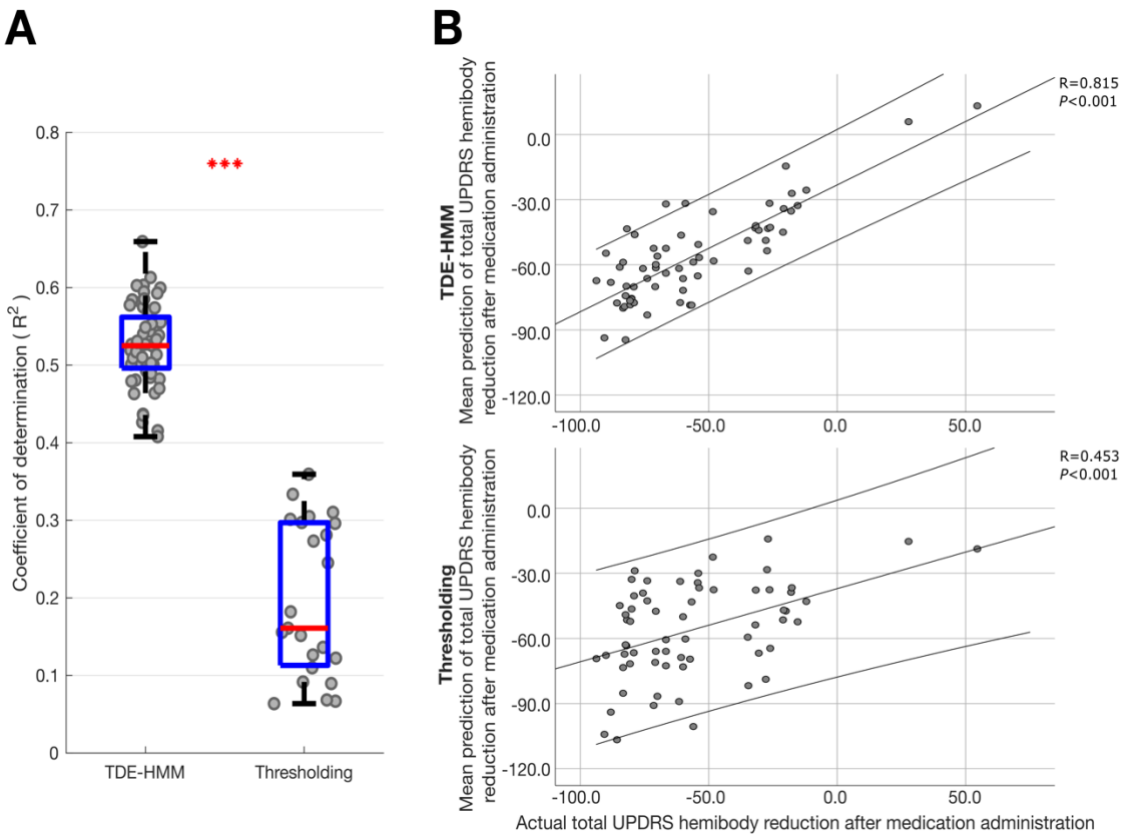


Figure 4.9 LFP HMM state prediction of change in contralateral hemibody UPDRS score including tremor items upon treatment with levodopa. (A) Box-and-whisker plot of coefficient of determination (r^2) between predicted and actual percentage improvement in contralateral hemibody UPDRS score including tremor items. Prediction was performed using ridge regression which utilized features extracted from different HMM models (left) and different percentile thresholding models across different frequency bands (right). Each dot represents data from one HMM model (n=56) on the left and one thresholding model (n=23; different threshold levels 55-99) on the right. ***: $p<0.001$. (B) Illustrative examples showing correlation between the mean predicted (across the 56 HMM and 23 thresholding models) and actual percentage improvement in contralateral hemibody bradykinesia-rigidity items of the UPDRS Part III. Prediction was performed using ridge regression which utilized multiple HMM state features (top) or multiple thresholded frequency-bands features (bottom). Each dot in B represents data from one hemisphere in one subject (n=64). Linear fits and 95% confidence limits are shown. Negative changes represent % reductions in UPDRS score after medication administration.

I also considered the contributions made to the regression model by states in the different frequency bands and their features (Figure 4.10). The normalised regression coefficients for features in the low beta state and for those in the remaining spectral states tended to have opposing signs, in line with the contrasting effect of levodopa on these features and with the results of bivariate correlations between changes in these features and change in motor impairment with medication.

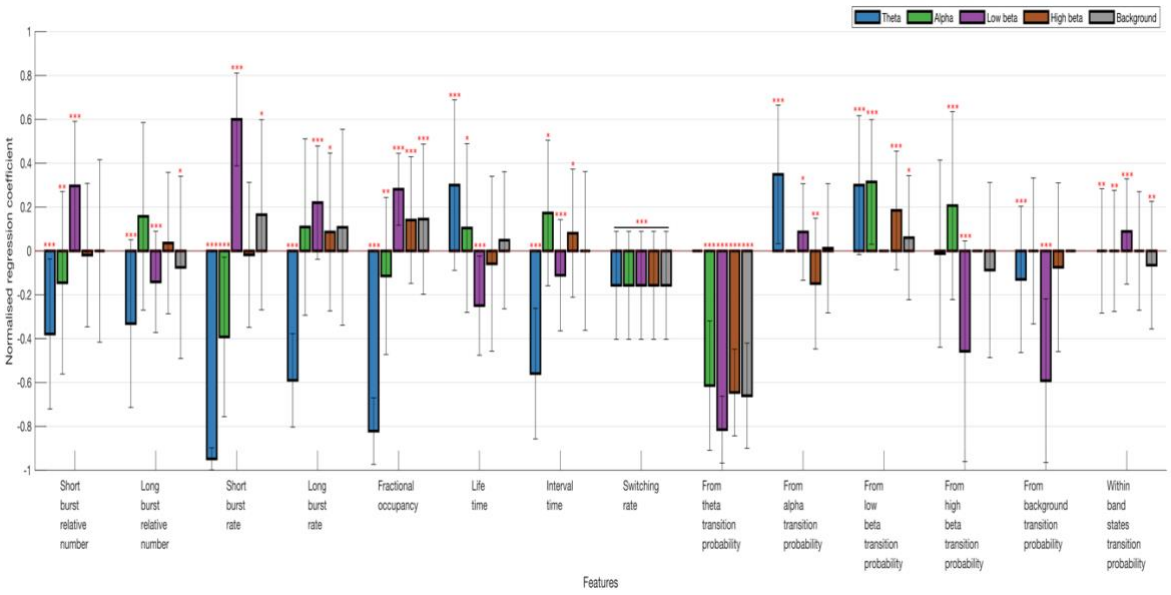


Figure 4.10 Normalised ridge regression coefficients for the features used to predict change in contralateral hemibody UPDRS score ON medication across different HMM models. Change was defined as ON-OFF hemibody UPDRS scores that included tremor items. The most negative contributions (more negative than -0.5) to the regression models came from medication-induced changes in theta; the short and long burst occurrence rate, fractional occupancy, interval time and transition probability from the theta state, although there were many other significant but weaker negative correlations. The most positive contribution (more positive than +0.5) to the regression models come from medication-induced changes in the occurrence rate of short duration low beta states, although again there were many other significant but weaker positive correlations. Median normalised regression coefficients across the 56 different HMM models ± SD are shown. *: p<0.05, **:p<0.01, ***: p<0.001.

The change in contralateral UPDRS Part III hemibody scores predicted above in Figure 4.9 included both the change in bradykinesia-rigidity and tremor items. Results were similar if changes in tremor items were excluded (Figure 4.11). Conversely, prediction of change in contralateral hemibody tremor scores alone was weaker than prediction of change in bradykinesia-rigidity, although the narrower range of changes in tremor score may have contributed to this difference (Figure 4.12). Still, ridge regression based on TDE-HMM

features was able to predict about 30% of the variance in the change in contralateral tremor scores. This was greater than the prediction of variance in the change in contralateral tremor scores with thresholding models (Figure 4.12). It was also greater than the prediction of tremor change using just bradykinesia-rigidity scores, which was 8%, suggesting that some LFP features were of additional benefit in predicting tremor variance. I also considered the contributions made to the regression model for tremor by states in the different frequency bands and their features (Figure 4.13).

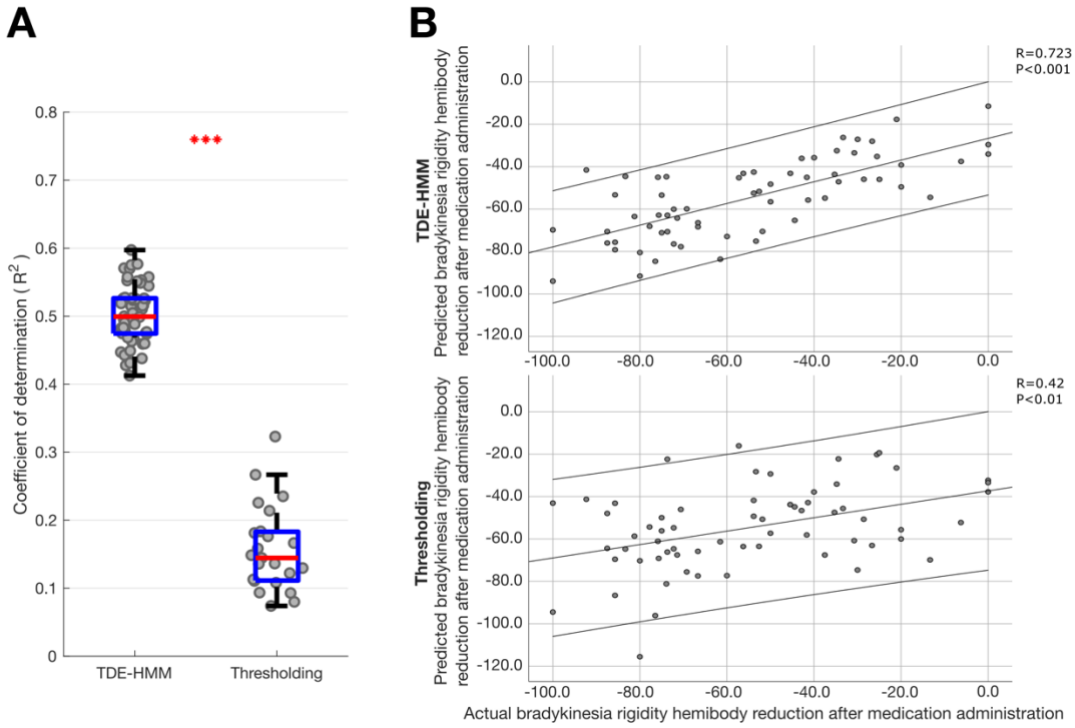


Figure 4.11 LFP HMM state prediction of change in contralateral bradykinesia-rigidity without tremor items upon treatment with levodopa. (A) Box-and-whisker plot of coefficient of determination (r^2) between predicted and actual percentage improvement in contralateral hemibody bradykinesia-rigidity items of the UPDRS Part III. Prediction was performed using ridge regression which utilized features extracted from different HMM models (Left; compare with left hand HMM result in Fig 6) and thresholding method (right). Each dot represents data from one HMM model (n=56) and one thresholding model (n=23; one for each threshold applied across the four frequency bands). ***: p<0.001. (B) Illustrative example of single HMM and thresholding models show correlation between predicted and actual percentage improvement in contralateral hemibody bradykinesia-rigidity items of the UPDRS Part III. Prediction was performed using ridge regression which utilized multiple HMM state features extracted from an example 8-state and 7 lags HMM model (top) or a 75th percentile thresholding model (bottom) for the different frequency bands. Results of leave-out one cross-validation are presented for the ridge regression model. Each dot represents data from one hemisphere in one subject (n=64). Linear fits and 95% confidence limits are shown as straight lines. Negative changes represent % reductions in UPDRS score after medication administration.

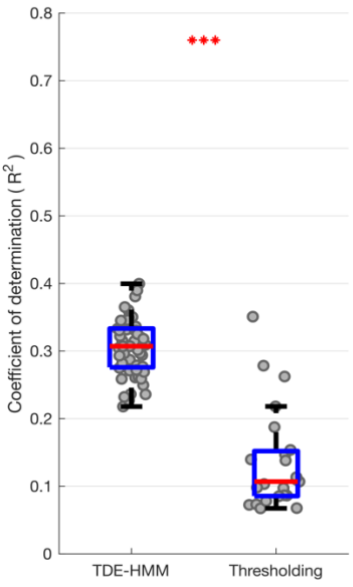


Figure 4.12 Box-and-whisker plot of LFP HMM state prediction of change in contralateral tremor upon treatment with levodopa. Coefficient of determination (r^2) between predicted and actual percentage improvement in contralateral hemibody tremor items of the UPDRS Part III. Prediction was performed using ridge regression which utilized features extracted from different HMM (left) and thresholding models (right); compare with left and right hand HMM result in Figure 4.11A, respectively) . Each dot represents data from one HMM model (n=56) and one thresholding model (n=23; different threshold levels 55-99). ***: p<0.001.

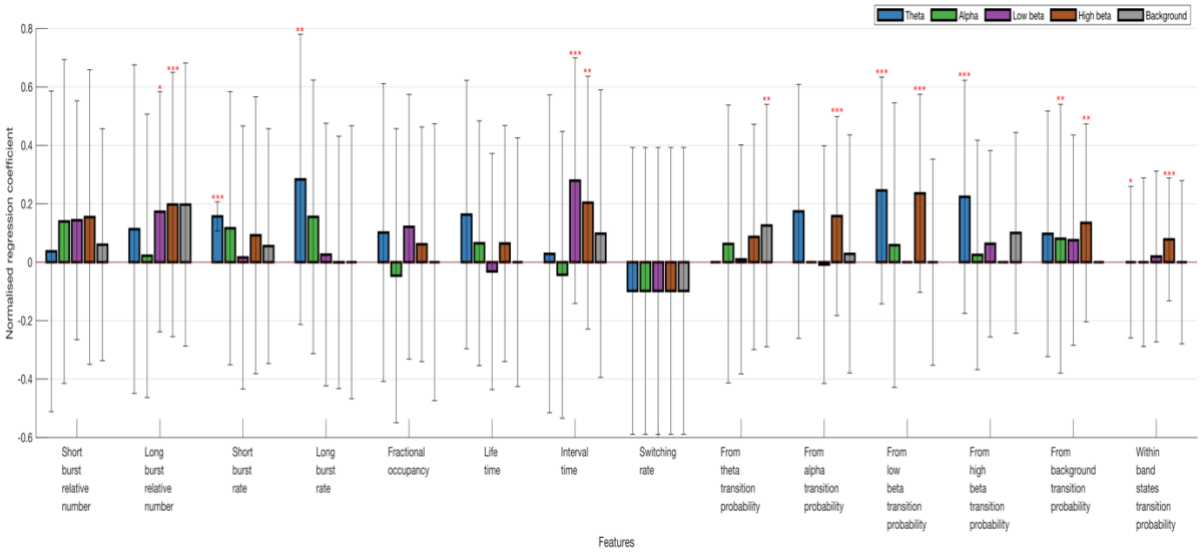


Figure 4.13 Normalised ridge regression coefficients for the features used to predict change in contralateral hemibody tremor score across different HMM models. The most significant (P<0.001) contributions to the regression models for change in tremor come from medication-induced changes in the relative number of longer bursts in the high beta band, occurrence rate of shorter bursts in the theta band, longer interval time in the low beta band and higher transition probabilities from the alpha to the high beta state, from the low beta to the theta and high beta states, from the high beta states to the theta state, and within detected high beta states. All these contributions were positive, i.e. predicted a greater reduction in tremor. Median normalised regression coefficients across the 56 different HMM models ± SD are shown. *: p<0.05, **:p<0.01, ***: p<0.001.

4.3.4 Both low beta and other spectral states contribute to prediction of change in motor impairment with levodopa

The normalised ridge regression coefficients reported in Figure 4.10 suggested that STN LFP states at frequencies other than low beta also contributed to the prediction of change in motor impairment with levodopa, albeit their effect was opposite in sign to that of the corresponding features in the low beta state. Ridge regression creates parsimonious regression models that generalise well when doing prediction, even in the presence of collinearity between multiple regressors (such as the occurrence rate and relative burst rate which themselves were deduced from the life time measure) (Hoerl and Kennard, 1970b). However in doing so the estimates of the normalised regression coefficients of the different inputs may be biased, even though they have a smaller variance than with ordinary least squares estimators. Estimates of the normalised regression coefficients should therefore be interpreted cautiously. With this in mind I sought further evidence that low beta and other frequency states both contributed to the prediction of change in contralateral hemibody UPDRS score upon treatment with levodopa. To this end I separated those features relating to the low beta state and those relating to the theta, alpha, high beta and background states, and performed ridge regression as before on these feature subsets. Figure 4.14 indicates that both were able to predict the change in motor impairment with levodopa, although the respective coefficients of determination (r^2) values were about half of those of the combined model (Figure 4.9A).

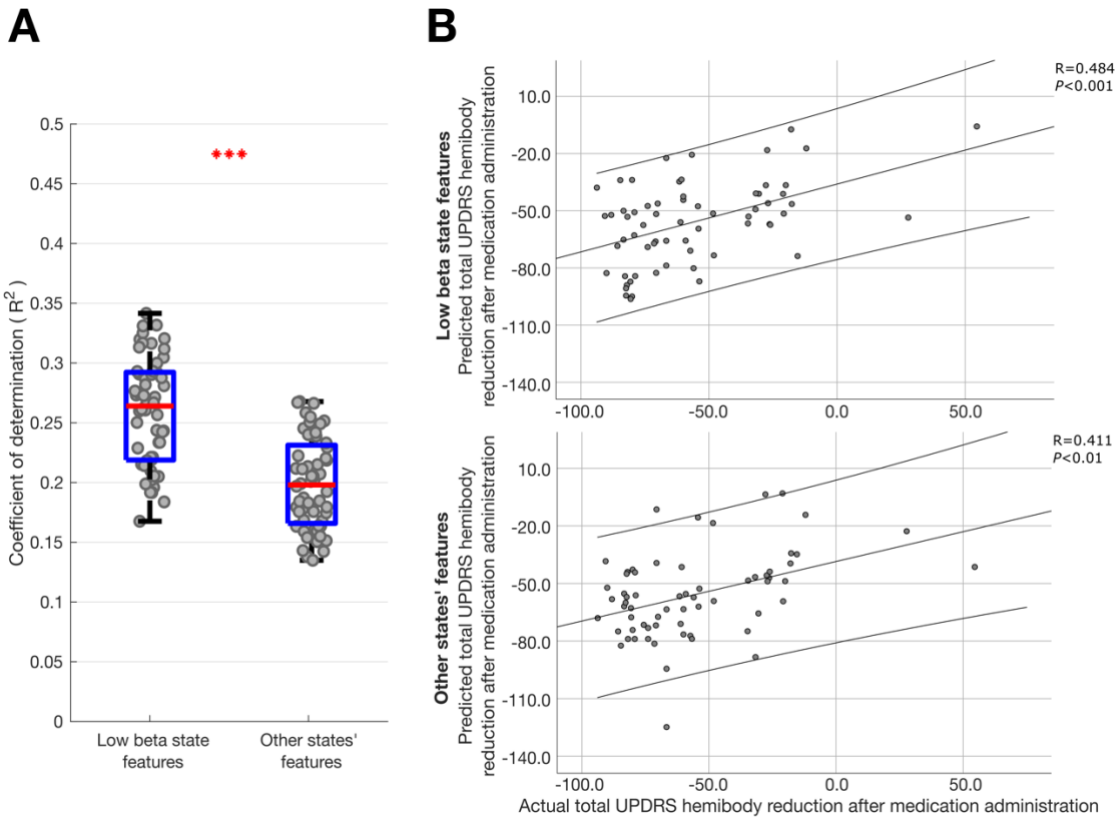


Figure 4.14 LFP HMM state prediction of change in contralateral hemibody UPDRS score upon treatment with levodopa using different feature sets. (A) Box-and-whisker plots of coefficients of determination (r^2) between predicted and actual percentage improvement in contralateral hemibody UPDRS score including tremor items, estimated by ridge regression utilizing only low beta features (Left) and theta, alpha and high beta features (right) extracted from different HMM models. Each dot represents data from one HMM model (n=56). ***: p<0.001. (B) Illustrative example of single HMM model showing correlation between predicted and actual percentage improvement in contralateral hemibody UPDRS score including tremor items. Prediction was performed using ridge regression which utilized only low beta (top) or utilized theta, alpha and high beta features (bottom) from an 8-state HMM model. Results of leave-out one cross-validation are presented for the two ridge regression models. Each dot in B represents data from one hemisphere in one subject (n=64). Linear fits and 95% confidence limits are shown. Negative changes represent % reductions in UPDRS score after medication administration.

My core analysis considered data low-pass filtered at 45 Hz but did not include amplitude information features or gamma activity. Figure 4.15 gives the results of including amplitude features in the ridge regression models illustrated in

Figure 4.9. This addition increased the variance in change in motor impairment with levodopa explained by TDE-HMM models to 0.57 ± 0.06 (Figure 4.15A, Left) and by thresholding models to 0.22 ± 0.12 (Figure 4.15A, Right). In order to explore the possible additional contributions of gamma activity in predicting change in motor impairment with levodopa, I performed an additional TDE-HMM analysis of the same data now pass-band filtered over 55-95 Hz. This time I identified the states with time courses that best cross-correlated with the Hilbert envelope of gamma power, where this was defined as 60-90Hz. The gamma band state features were then added to the ridge regression models illustrated in Figure 4.15A. Adding gamma features increased variance explained by TDE-HMM models to 0.59 ± 0.06 (Figure 4.15B, Left) and by thresholding models to 0.23 ± 0.12 (Figure 4.15B, Right). The signs of the amplitude coefficients in the ridge regression model depended on the frequency band. A reduction in amplitude in the low beta band ON medication was associated with a greater improvement in motor impairment ON medication, whereas the opposite was seen in the remaining frequency bands. The signs of the gamma coefficients in the ridge regression were opposite to those of corresponding low beta coefficients and similar in sign to those of the theta, alpha and high beta frequencies coefficients.

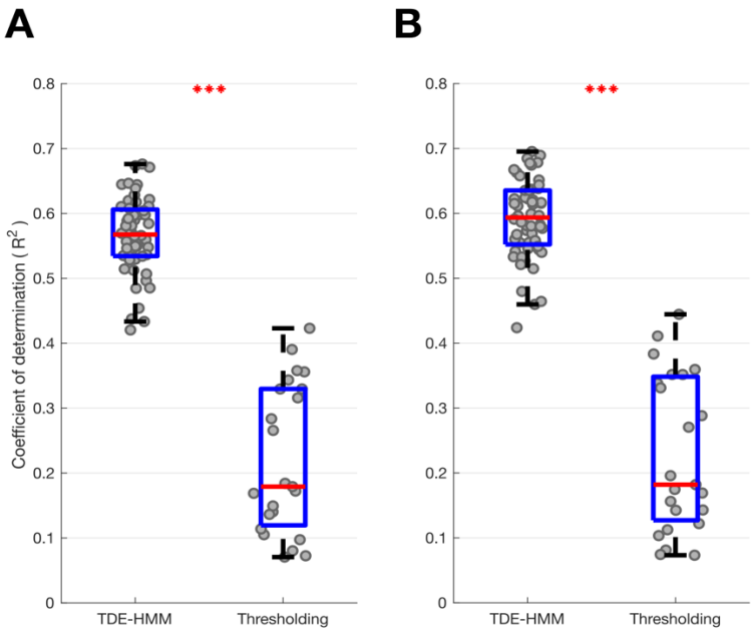


Figure 4.15 Box-and-whisker plots of LFP HMM state prediction of change in contralateral hemibody UPDRS score including tremor items upon treatment with levodopa after including states and bands amplitude information (A) and both amplitude and gamma features (B). Coefficient of determination (r^2) between predicted and actual percentage improvement in contralateral hemibody UPDRS score including tremor items. Prediction was performed using ridge regression which utilized features extracted from different HMM models (left) and different percentile thresholding models across different frequency bands (right). Each dot represents data from one HMM model (n=56) on the left and one thresholding model (n=23; different threshold levels 55-99) on the right. ***: p<0.001.

4.3.5 Multivariate correlations between STN LFP states and motor impairment OFF medication

Next, I considered whether multivariate models that include multiple TDE-HMM states and their features based on LFPs recorded OFF dopaminergic medication were also able to give comprehensive prediction of the motor impairment across patients OFF medication (Figure 4.16). Again ridge regression based on TDE-HMM features performed very well, predicting about 50% of the variance in contralateral combined bradykinesia-rigidity and tremor

scores OFF medication (Figure 4.16), or contralateral bradykinesia-rigidity alone (Figure 4.17A), much better than ridge regression based on thresholding models. The HMM states and features contributing to the regression models predicting contralateral UPDRS Part III hemibody scores OFF medication were very similar to those contributing to regression models predicting the change in contralateral UPDRS Part III hemibody scores with medication (compare Figure 4.18 with Figure 4.10). To highlight this Figure 4.19 presents a scatter plot of all the median normalised regression coefficients from the two sets of models. These tend to lie on a diagonal, which suggests that the LFP features that predict motor impairment OFF medication are those that may be modulated by treatment with levodopa to achieve improvement in motor state.

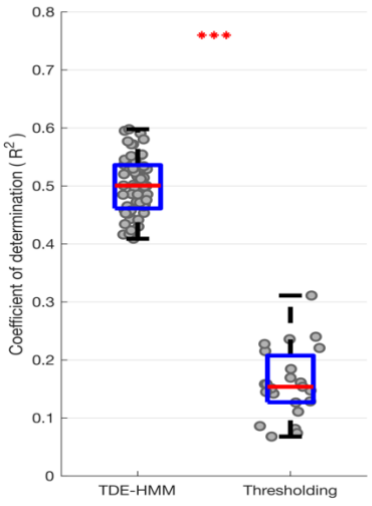


Figure 4.16 Box-and-whisker plot of coefficient of determination (r^2) between predicted and actual contralateral hemibody UPDRS score, including tremor items, OFF medication. Prediction was performed using ridge regression which utilized features extracted from different HMM models (left) and different percentile thresholding models based on LFPs recorded OFF medication (right). Each dot represents data from one HMM model (n=56) on the left and one thresholding model (n=23; one for each threshold applied across the four frequency bands) on the right. ***: p<0.001.

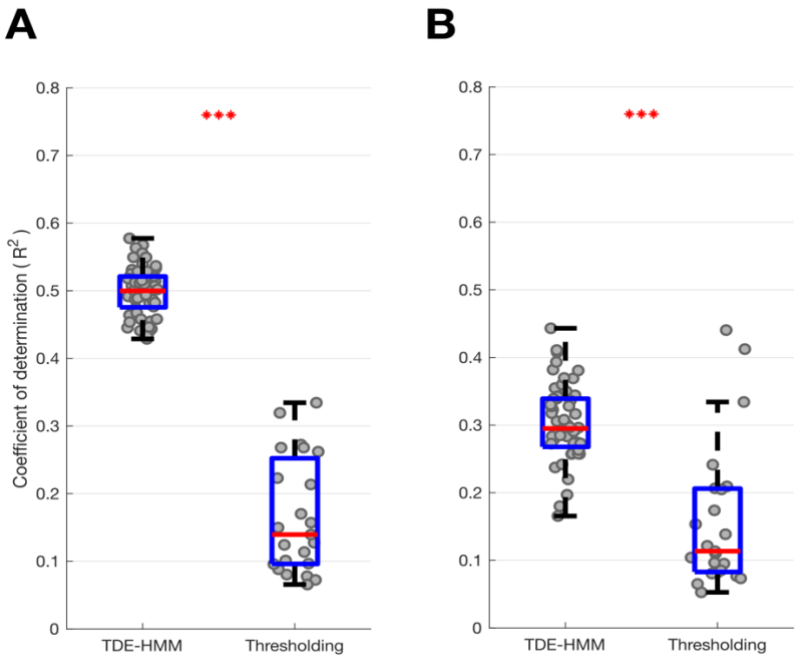


Figure 4.17 Box-and-whisker plots of LFP HMM state prediction of contralateral bradykinesia-rigidity (A) and contralateral tremor (B) OFF levodopa. Coefficient of determination (r^2) between predicted and actual hemibody items of the UPDRS Part III. Prediction was performed using ridge regression which utilized features extracted from different HMM and thresholding models. Each dot represents data from one HMM model (n=56) and one thresholding model (n=23; different threshold levels 55-99). ***: p<0.001.

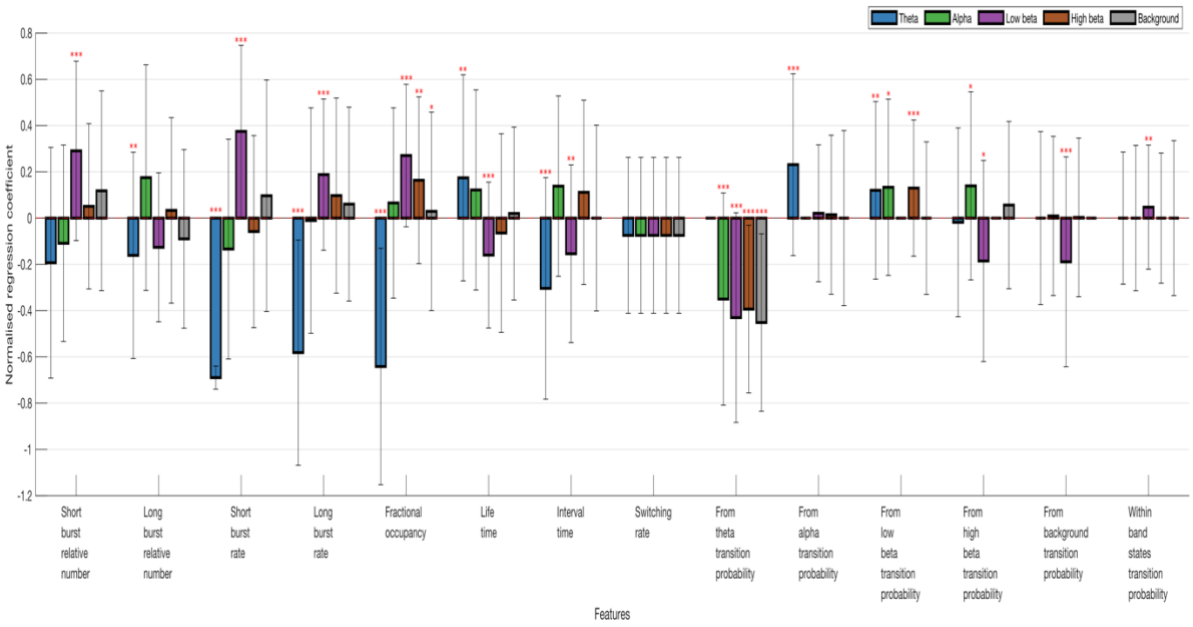


Figure 4.18 Normalised ridge regression coefficients for the features used to predict contralateral hemibody UPDRS scores including tremor items during OFF medication across different HMM models. The states and features contributing to the regression models are very similar to those contributing to regression models predicting the change in motor impairment with levodopa (see Figure 4.10). Median normalised regression coefficients across the 56 different HMM models ± SD are shown.*: p<0.05, **:p<0.01, ***: p<0.001.

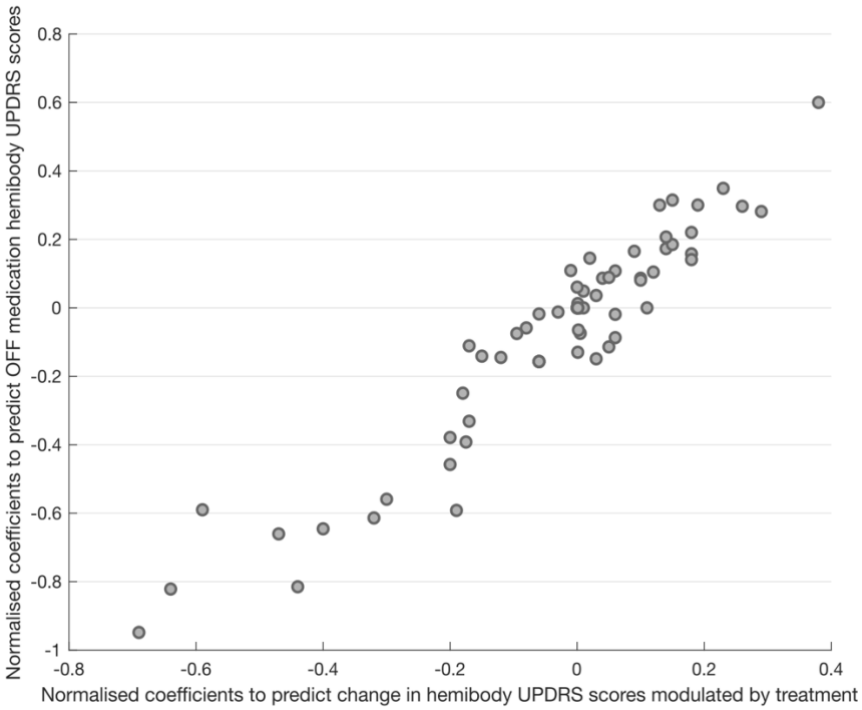


Figure 4.19 Scatterplot of normalised ridge regression coefficients for the features used to predict change in contralateral hemibody UPDRS score including tremor items ON medication and for the features used to predict contralateral hemibody UPDRS scores including tremor items during OFF medication, both across the 56 different HMM models. These tend to lie on a diagonal which means that the LFP features that predict motor impairment OFF medication are those that are modulated by treatment with levodopa to achieve improvement in motor state.

As before, prediction of contralateral hemibody tremor scores alone was weaker than prediction of bradykinesia-rigidity, but ridge regression based on TDE-HMM features was still able to predict about 30% of the variance in the contralateral tremor score OFF medication (Figure 4.17B).

To explore the effect of expanding the feature set for prediction of OFF medication contralateral UPDRS Part III hemibody scores, I included amplitude and gamma features in the ridge regression model. The result for adding amplitude information is illustrated in Figure 4.20 which demonstrates that the variance in contralateral combined bradykinesia-rigidity and tremor

scores OFF medication explained by TDE-HMM models increased to 0.54 ± 0.05 (Figure 4.20A, Left) and that explained by thresholding models increased to 0.18 ± 0.07 (Figure 4.20A, Right). Adding gamma features to the model illustrated in Figure 4.20A increased the variance explained by TDE-HMM models to 0.56 ± 0.06 (Figure 4.20B, Left) and that explained by thresholding models to 0.18 ± 0.07 (Figure 4.20B, Right). The signs of the amplitude coefficients depended on the frequency band as before and the signs of the gamma coefficients in the ridge regression were opposite to those of corresponding low beta coefficients.

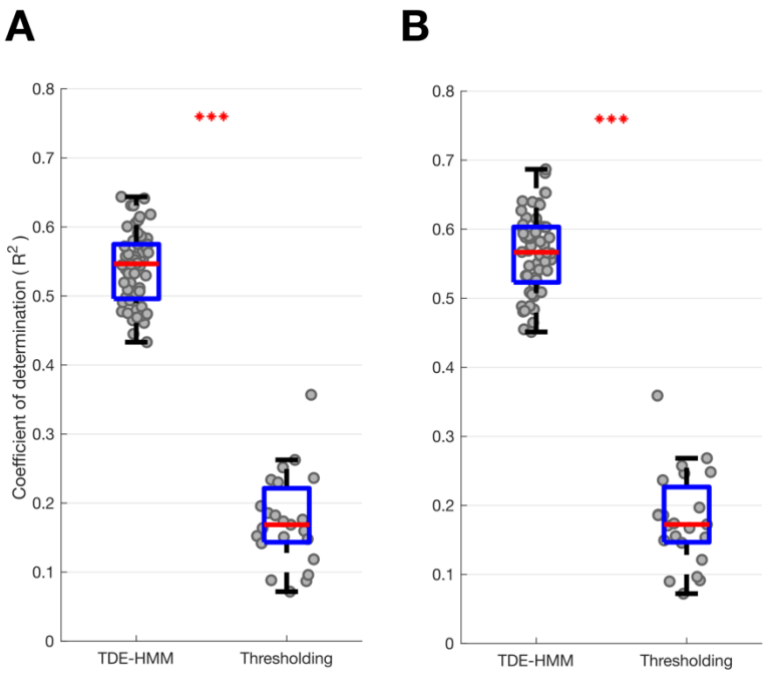


Figure 4.20 Box-and-whisker plots of LFP HMM state prediction of contralateral hemibody UPDRS score including tremor items after including states and bands amplitude information (A) and both amplitude and gamma features (B) OFF levadopa. Coefficient of determination (r^2) between predicted and actual contralateral hemibody UPDRS score, including tremor items. Prediction was performed using ridge regression which utilized features extracted from different HMM models (left) and different percentile thresholding models across different frequency bands (right). Each dot represents data from one HMM model (n=56) on the left and one thresholding model (n=23; different threshold levels 55-99) on the right. ***: p<0.001.

4.4 Discussion

I have demonstrated that multiple spectral states in the STN LFP have a bearing on motor impairment in PD patients, and that levodopa modulates these states and shifts the balance between them in a way that predicts clinical change with high fidelity. Using group-level time-delay embedded Hidden Markov Modelling I showed that the preponderance, rate of occurrence and duration of LFP states in the low beta frequency range positively correlates with motor impairment in patients withdrawn from their antiparkinsonian medication. Levodopa reduced the preponderance (fractional occupancy), rate of occurrence and duration of low beta states, with this reduction correlating with the improvement in motor impairment. These observations are consistent with earlier reports using a standard thresholding approach to state or burst identification in PD patients, although these did not distinguish between the low and high beta band and only determined the relative numbers of states of a given duration, and hence could not unequivocally detect whether short or long duration beta bursts were independently detrimental as measured by motor UPDRS score (Tinkhauser et al., 2017a; Tinkhauser et al., 2017b). The deleterious effects of the LFP states I identified were limited to the low beta band, in line with reports of correlations between averaged LFP power and motor impairment that are similarly limited to the low beta band (Oswal et al., 2016; Neumann et al., 2016), and studies that suggest that low and high frequency beta activities may be functionally distinct (Priori et al., 2004; Marceglia et al., 2009; Zaidel et al., 2010).

In addition, bivariate correlations and the normalised regression coefficients from ridge regression models suggested that STN LFP states at other frequencies (up to 40Hz) had opposing effects to the low beta state. Thus the preponderance, occurrence rate and duration of LFP states in the theta, alpha and high beta frequency ranges negatively correlated with motor impairment in patients withdrawn from their antiparkinsonian medication, and levodopa increased the preponderance, occurrence rate and duration of these states, with the increase correlating with the improvement in motor impairment. Changes in LFP state behaviour were biggest in the theta frequency band. Although averaged power spectra of LFP need not faithfully mirror LFP state behaviour in the STN, there are past reports of theta, and to a lesser extent alpha, activity being increased by levodopa in PD (Priori et al., 2004; Alonso-Frech et al., 2006; Rodriguez-Oroz et al., 2011; Alegre et al., 2012; Giannicola et al., 2013; Quinn et al., 2015). These are consistent with the observation that the occurrence rates, fractional occupancies and life times of theta and alpha states were significantly increased when ON compared to OFF levodopa for the state visits of the shortest duration. Moreover, a recent study also suggested that theta increases might oppose the effects of beta bursts, as theta increased as beta bursts became disorganised and attenuated (Yeh et al., 2020).

The opposing effects of the low beta state and theta, alpha and high beta states were together able to account for just over 50% of the variance in patients' hemibody impairment OFF medication, and in the change in hemibody impairment following ingestion of the dopamine prodrug, levodopa. The features of the different states contributing to the regression model for hemibody UPDRS scores OFF medication were very similar to those

contributing to the regression model predicting the change in contralateral hemibody scores with medication. This suggests that the LFP features that predict motor impairment OFF medication are those that are modulated by treatment with levodopa to achieve improvement in motor state. Hence these features, like the elements of the motor impairment which they predict, are modulated by the current status of dopaminergic activity.

My core analysis sought features of HMM states with a frequency of under 40 Hz that predicted motor impairment. However, I did not include amplitude information, and omitted the effects of gamma band activities. In a secondary analysis I therefore included these features in the ridge regression. Information on signal amplitude and inclusion of HMM states in the gamma band led to modest further increases in the prediction of motor impairment OFF medication and in the change in this with levodopa treatment. Perhaps the most parsimonious explanation for the modest effect of incorporating amplitude information is that the pattern of spectral states under 40Hz determines signal amplitude or *vice versa*. Thus adding features related to absolute amplitude did not greatly improve predictions. Gamma activity may have had modest impact because it is not a consistent feature in LFP recordings across patients, and, because the information contained within may be shared by reciprocal changes at lower frequencies (Wiest et al., 2020; Wiest et al., 2021).

4.4.1 Experimental considerations

The HMM approach serves to define states on objective statistical grounds and does not necessitate the application of arbitrary filtering within a canonical frequency band or of arbitrary thresholds. Indeed, the derived features were

consistently more predictive of motor impairment than features drawn from simple, standard thresholding used for burst detection. However, the HMM will identify as many states as are defined in the model, and if one or more related states react in a particular way then the converse may be reflected in the remaining state features, where these are considered relative to other states. Yet this is unlikely to explain the reciprocal nature of low beta and non-low beta features, both in terms of their response to levodopa and their prediction of motor impairment. This is because multiple (5 to 18) states were prescribed and systematic differences between frequency bands other than low beta were identified. Thus the major reciprocal effects occurred in the theta band and the least were seen in the background activity. Moreover, had changes in the non-low beta band been secondary to those in the low beta band, then I should not have seen additional predictive value from non-low beta band features; the ridge regression model with all features was able to predict much more of the variance in motor UPDRS than the model with just low beta band features. Finally, not all of the state features considered in this study were relative to other states. Life time, interval time and occurrence rate take absolute values, and yet were also reciprocal in nature in the low beta and non-low beta bands.

A clear limitation of the HMM is that only one state is visited at any given time. Although this state will have the most evidence and can be considered dominant at that moment in time, my approach will miss independent subsidiary states that might overlap in time, as might come from other neural generators.

By focussing on frequency bands (as a post-hoc analysis step performed after HMM state identification and feature prediction by ridge regression), I facilitated comparison with the existing literature, but this approach meant that multiple HMM states could get combined together into a given frequency band, and I could therefore be overlooking detail available in the underlying states. For example, it is possible that different HMM states could be differentially affected by medication status (e.g. change in burst rate, interval rate etc.) and this detail get lost when states are combined into a single frequency band. In addition, the number of states to be classified by HMM has to be predefined, as does the number of lags utilised, although by collapsing the results across many realisations of the HMM, as here, I can identify robust features in the data. I should also note that the attribution of different HMM states to canonical frequency bands was certainly not perfect, partly because the frequency ranges of these bands are somewhat arbitrary when applied to the basal ganglia and predominantly defined on the basis of cortical physiology.

It is tempting to assume that theta, alpha and high beta states promote normal movement, but I did not assess the presence of levodopa-induced dyskinesias in the cohort and so it remains to be seen whether any of these LFP sates are linked to dyskinesias ON medication. Indeed, there is some evidence that excessive theta activity in dorsolateral motor STN might be related to dyskinesias (Alonso-Frech et al., 2006; Rodriguez-Oroz et al., 2011; Alegre et al., 2012). Gamma oscillations in the STN LFP have also been associated with dyskinesias on levodopa (Alonso-Frech et al., 2006; Alegre et al., 2012; Fogelson et al., 2006). Ultimately, it must be acknowledged that the link between different LFP states in the STN and motor impairment is correlational

in nature, and further studies are needed to determine whether any of these LFP states are mechanistically involved in determining motor impairment.

With respect to the clinical data it should be noted that I had a mix of motor UPDRS values determined at the time of the recording in some subjects and values determined up to three months pre-operatively in others. This may increase the variance in the clinical measure, as clinical impairment may have been greater in those assessed pre-operatively given that the post-operative stun effect would have been absent. This may have potentially led me to under-estimate the regression coefficients linking burst features to motor impairment. Finally, it should be noted that bursts can be defined by means other than the original thresholding method (Tinkhauser et al., 2017a). It is possible that these newer methods might have led to increased regression coefficients estimates in the low beta band (Anderson et al., 2020; Schmidt et al., 2020). However, the use of the original threshold method allowed me to more easily contrast my findings with those in the literature (Tinkhauser et al., 2017a; Tinkhauser et al., 2017b; Torrecillos et al., 2018; Tinkhauser et al., 2020).

4.4.2 Implications for therapy

The most immediate therapeutic significance of the present findings lies in the potential identification of a more informative feedback signal for closed-loop DBS than beta activity alone (Little and Brown, 2020). When all LFP states and corresponding features were considered in a multivariate Ridge regression model it was possible to predict just over 50% of the variance in patients' hemibody impairment. This is remarkable, and potentially valuable as feedback, regardless of whether the signals have mechanistic relevance.

Moreover, although the strongest prediction was seen for bradykinesia and rigidity, tremor could also be predicted. The latter is not the case when beta power or bursts are considered alone (Kuhn et al., 2006; Kuhn et al., 2009; Neumann et al., 2016; Tinkhauser et al., 2017b).

However, several points need addressing before the tracking of the pattern of multiple LFP states can be used as feedback. First, it should be noted that LFP state correlations with motor impairment were shown across subjects rather than within subjects. However, recent studies relating beta bursts to trial-to-trial variations in motor performance make it possible that my findings will extrapolate to the individual (Torrecillos et al., 2018; Lofredi et al., 2019; Tinkhauser et al., 2020). Second, until there is an online version of Hidden Markov Modelling, this technique will have to be limited to the off-line identification of the most informative states and state characteristics within a given subject, so that these features can then be used to focus supervised machine learning techniques that can be applied on-line.

The findings are also important in suggesting that whilst some LFP states might be usefully downregulated for therapeutic benefit, others could potentially be upregulated to better mimic the effect of dopaminergic therapy and improve parkinsonism. Current conventional DBS serves to suppress low beta activity in the STN, but also potentially beneficial activities in other frequency bands (Wiest et al., 2020). The present findings therefore further motivate closed-loop DBS as this is more selective in its suppression of LFP states when it is only triggered by beta bursts (Tinkhauser et al., 2017a), and encourage the development of phase-locked stimulation techniques that can

both selectively up and down regulate target brain states (Cagnan et al., 2017; Holt et al., 2019; Peles et al., 2020).

4.5 Summarized findings

The main findings of the chapter are:

- Multiple spectral states in STN LFP have bearing on motor impairment in PD patients.
- Levodopa modulates states and shifts the balance between them in a way that predicts clinical change with high fidelity.
- STN LFP states outside of low beta band had opposing effects to the low beta state.
- There is potential for identification of more informative feedback for closed-loop DBS than beta activity alone.
- Some states might usefully be upregulated to improve parkinsonism.

Chapter 5

General discussion

In this thesis I investigated the contribution of machine learning approaches in extracting informative features in order to perform better prediction of motor measures when only using data from STN local field potential recordings. The specific questions I set out to answer at the beginning of this thesis were:

- How can ML be used to predict limb movement from deep brain recording signals? Can the forthcoming movement be predicted by relying on features extracted from the pre-movement preparation period?
- What is the effect of bursting presence on the information encoded in STN? Which types of bursts impair the local representation of task-related information?
- How can unsupervised time-series models help extract measures which characterise the oscillatory changes caused by medications in PD patients? Which types of bursts correlate with motor impairment and in what way?
- What is the impact of using different measures of bursting at different frequencies on the predication of motor impairment? What is the contribution of each measure in the prediction, and how do their contributions to prediction vary when predicting medication-induced changes or impairment during the OFF medication condition?

I studied electrophysiological signals in a limb movement paradigm and during different medication conditions. The results of both experiments indicate the important role of bursts of theta, alpha, low beta, high beta, and gamma oscillations in predicting motor impairment. Moreover, they highlight the potential value of applying newly developed machine learning and time-series analysis methods to electrophysiological signals from the basal ganglia. Thus multivariate dynamical features extracted with an unsupervised machine learning method, hidden Markov modelling, outperformed traditional thresholding models in predicting motor impairment.

5.1 Machine learning for clinical applications

Using ML for motor prediction and thereby as feedback in closed-loop DBS has the potential to transform DBS therapy in PD. Here I found (1) potential applications for ML in end effector selection for neuroprosthetics; (2) insights into pathological effects on information encoded in the brain (see also Heideman et al., 2020); (3) data-driven analysis approaches that exploit more of the information encoded in brain signals (see also Heideman et al., 2020); and (4) motor impairment prediction/correlation as a feedback biomarker for closed-loop DBS.

The application of the ML methods which I used in PD could in the future be expanded to accommodate the non-motor features which present an extra level of burden in PD patients. More specifically, it may be possible to predict aspects of non-motor symptomatology to further inform control policies during DBS, although the time-course of LFP changes related to non-motor phenomena and hence the prediction of corresponding symptoms may be

much longer than with motor state, so that control policies may need to take this in to consideration.

Although ML applications in PD are relatively early in their development, the preliminary evidence favouring their use more broadly in clinical practice is very promising (Kubota at al., 2016; Belić et al., 2019; Mei et al., 2021). Their ability to extract underlying patterns within patients' data offers the potential to improve patient selection (Geraedts et al., 2021), facilitate surgical targeting (Kim et al., 2019), and optimise programming approaches to achieve rapid and robust clinical enhancements (Shamir et al., 2015; Anderson et al., 2018; Boutet et al., 2021). Moreover, ML applications are playing a vital role in shaping next-generation prosthetics due to their ability to provide high precision and low-latency real-time control (Carmena, 2013; Kim and Kim, 2018; Khawaldeh et al., 2020). Those ML models which offer interpretable learning pipelines also allow specialists to understand the ML decision-making criteria, and have the potential of providing more insights into pathophysiology (Corrado and Doya, 2007; Perugini et al., 2018; Bore et al., 2020). With the growing trend of digitising clinical data, ML is expected to flourish as it benefits from larger datasets, which make solutions more robust, generalisable, and accurate (Bohr and Memarzadeh, 2020).

5.2 Involvement of beta activity in motor impairment

Beta activity at both cortical and basal ganglia levels is known to be modulated with movement and by medications affecting movement. Hence it desynchronises prior to and during movement and then increases at the end of movement execution, and is reduced by treatment with levodopa. Chapter

3 suggests one possible mechanism for the impairment of movement when beta activity, and thereby related neuronal synchrony, is high. Under these circumstances there is a degradation in the classification accuracy of limb movements using STN LFPs, which implies disruption of the information encoded in the STN. As a result this causes low limb prediction accuracy from STN LFPs. Chapter 4 provides clear evidence that the link between beta activity and motor impairment in PD is attributable to that activity that is in the lower beta band. Lower frequency beta states/bursts positively predict impairment. In contrast, higher frequency beta states oppose this effect and negatively predict motor impairment.

5.3 Involvement of non-beta activity in motor impairment

The effects of the low beta state were opposed by theta, alpha and high beta states so that together these states explained a high percentage of the variance in patients' hemibody impairment OFF medication, and in the change in hemibody impairment following ingestion of the dopamine prodrug, levodopa. Considering features from both the beta and non-beta bands I found that these could collectively predict about 50% of the variance in hemibody UPDRS scores. When considered separately beta state features predicted 27% of the variance in hemibody UPDRS scores, whereas non-beta state features predicted 20% of the variance in hemibody UPDRS scores. The inclusion of LFP states outside the lower beta frequency range also meant that tremor, as well as bradykinesia-rigidity, could be reasonably well predicted.

The features of the different states contributing to the regression model for hemibody UPDRS scores OFF medication were very similar to those contributing to the regression model predicting the change in contralateral hemibody scores with medication. This finding suggests that the LFP features that predict motor impairment OFF medication are those that are modulated by treatment with levodopa to achieve improvement in motor state. Hence these features, like the elements of the motor impairment which they predict, are modulated by the current status of dopaminergic activity.

The importance of non-beta states in motor function has previously been noted at the cortical level (Varela et al., 2001; Buzsáki and Draguhn, 2004; Schnitzler and Gross, 2005). For example, cortical alpha activity shows a movement-related desynchronization (Pfurtscheller, 1981; Pfurtscheller and Andrew, 1999; Toro et al., 1994; Deiber et al., 2012). Additionally, motor-cortical alpha (and beta) activity modulation is observed during motor sequence learning in healthy younger adults (Pollok et al., 2021, 2014).

5.4 Why should bursts of different frequency have contrasting properties?

One paradox highlighted by the work in this thesis is that bursts of different frequency can have different functional associations. How this comes about is uncertain, but there may be several possible explanations. First, LFP bursts indicate brief periods of elevated local synchronisation of post-synaptic potentials through synchronised afferent input. Weaker synchronisation may have positive effects through temporal summation, as captured in the ‘Communication through Coherence’ hypothesis where a selective

communication within neural networks is obtained by the coherence captured between the sending region firing rate oscillation and the receiving region gain modulation (Fries, 2005), but stronger bouts of synchronisation may reduce the information coding capacity of local circuits (Brittain and Brown, 2014). As a general rule weaker synchronisation and hence lower amplitude LFP bursts are seen at higher frequencies and this might broadly explain why bursts at these frequencies are predictive of less impaired movements in patients with PD. But why then should phasic synchronisation in the low beta band be associated with motor impairment whereas bouts of synchronisation at theta and alpha frequencies, which can be of even higher amplitude, are predictive of less impaired movements? Perhaps the functional effects of phasic low beta synchrony is more related to its ability to induce a short-lived plasticity, as demonstrated in the cerebral cortex (Zanos et al., 2018). This might also explain why the functional associations of beta bursts tend to outlive bursts by a second or so (Torrecillos et al., 2018; Tinkhauser et al., 2020).

It is tempting to consider low beta bursts in the LFP of the STN as deleterious events with negative consequences, and bursts at other frequencies as having positive consequences and promoting normal movement. However, beta bursts can be associated with more effective behaviour under some conditions, such as when responses must be inhibited for behavioural success (Jana et al., 2020; Wessel, 2020). This serves as a reminder that LFP-motor impairment correlations depend on the precise context; beta bursts can be positive phenomena promoting more effective behaviour and non-beta bursts potentially negative phenomena under some circumstances.

5.5 Potential improvement in closed-loop deep brain stimulation

Conventional regular high frequency DBS is already a well-established treatment approach for multiple neurological and psychiatric diseases, however further progress depends on unlocking the potential of closed-loop DBS (Priori et al., 2012). Closed-loop DBS has several advantages compared to open-loop DBS. For example it performs an automatic and continuous tuning to changes in the disease occurring over time, and it decreases the risk of side-effects (Rosin et al., 2011; Santos et al., 2011).

Closed-loop DBS still faces several challenges. Firstly, the stimulation affects significantly the quality of the recorded signal which makes detecting biomarkers more challenging due to the artefacts on recording. To solve this, the recording instruments can be modified to supress these artefacts (Kent and Grill, 2012), signal processing methods can be applied to filter the recorded signals (Rossi et al., 2007), or distant cortical electrodes can be used for feedback recording (Swann et al., 2018).

Another challenge is selecting a feedback signal or combination of signals that will provide the most instructive information to the control algorithm. Studies have so far mostly relied on beta activity as a feedback signal to the closed-loop DBS system (Little et al., 2013, 2016a; Rosa et al., 2015, 2017; Piña-Fuentes et al., 2020). Here I show that it is not only beta which predicts motor impairment, but other types of oscillations as well. Therefore, I argue that the next generation closed-loop DBS systems should not only use beta as a feedback to modulate the timing and nature of stimulation, but also consider

other activities such as theta, alpha, and gamma in combination. Additionally, as discussed in section 5.2, newly developed ML approaches such as HMM, appear to be successful at preserving a high amount of the information available in the LFP, as they capture both stationary and non-stationary features, which potentially can provide the closed-loop DBS algorithm with a stronger combination of features to be used for more precise and targeted stimulation.

5.6 Thesis limitations

I should acknowledge a few limitations in the experiments of this thesis. In chapter 3 experiment, the recordings were performed intraoperatively and hence the number of movement trials and blocks were limited with the time constraints and patient fatigue, also a confounding stun effect cannot be excluded (Koop et al., 2006). The features extracted from the LFP data for the classification of limb movement were selected on empirical grounds and not independently identified through a feature selection algorithm (Robnik-Šikonja and Kononenko, 2003). Predictions might been improved with using such algorithms and, also, if recordings were achieved in chronically implanted patients, in whom any acute stun effects (Koop et al., 2006) compromising STN processing, would have been abated. Additionally, the Naive Bayes classifier used in Chapter 3 implicitly assumes that all features used are mutually independent, which is almost impossible in real life (Rish, 2001; Hand and Yu, 2001).

In chapter 4, I had a mix of motor UPDRS values determined at the time of the recording in some subjects and values determined up to three months pre-

operatively in others. This may have increased the variance in the clinical measure, as clinical impairment may have been greater in those assessed pre-operatively given that the post-operative stun effect would have been absent. This may have potentially led me to under-estimate the regression coefficients linking burst features to motor impairment.

In chapter 4, a limitation of the HMM method is that only one state is visited at any given time point (Vidaurre et al., 2017). This means that the approach will miss independent subsidiary states that might overlap in time, as might come from other neural generators. Moreover, when I performed the post-hoc analysis step after HMM state identification, states were matched to commonly known frequency bands (i.e. theta, alpha, low beta, high beta, and gamma), to facilitate the comparison with the existing literature. However this approach meant that multiple HMM states could get combined together into a given frequency band, where I might have overlooked details available in the underlying states. Below I suggest that this mixture of LFP states within a band might have contributed to the contrasting functional relationships of alpha activities in Chapters 3 and 4. Furthermore, it should be noted that LFP state correlations with motor impairment were shown across subjects rather than within subjects. Within subject studies would have the advantage of greater relevance to personalised optimisation of the feedback signal for closed-loop DBS (Gilron et al., 2021). However, across subject studies are still of value in allowing the initialisation of supervised or hybrid unsupervised clustering algorithms, and in hypothesis testing. Also, until there is an online version of HMM, the technique used in Chapter 4 will have to be limited to the off-line identification of the most informative states and state characteristics, so that

these features can then be used to inform supervised machine learning techniques that can be applied on-line.

In both chapter 3 and 4, it should be noted that bursts could have been defined by means other than the original thresholding method (Tinkhauser et al., 2017a) or the HMM approach taken here. Both chapters evidence that LFP activities across a very broad frequency band contribute to the prediction of motor measures. However, findings in chapter 4 which indicated that beta states in the lower frequency beta range were specifically positively correlated with motor impairment suggest that I should have also explored differences between lower and higher frequency beta bursts in chapter 3. In addition, I could have usefully considered the impact of bursts in frequency ranges other than the alpha and beta bands in this chapter.

In addition to the above, I should highlight an apparent inconsistency. Whereas, alpha states negatively correlated with motor impairment in chapter 4, alpha bursts degraded the information about the nature of the forthcoming response to be actioned demonstrated in chapter 3, albeit less than the degrading effect of beta bursts. Possible explanations for this discrepancy are included in the discussion of experimental limitations in section 4.4.1. Perhaps the most important of these is that multiple HMM states may occur within a given frequency band, and the mix of states may not necessarily be fixed across experimental conditions. For example, the nature of different states within the alpha frequency band could be differentially affected by medication status thereby leading to contrasting functional correlates. In chapter 3, I explored time periods around voluntary movements in the intra-operative OFF medication state whereas in chapter 4 I explored post-operative patients who

were at rest both OFF and ON medication. The impact of differing states within a frequency band may have been heightened by my use of a form of multivariate correlation in chapter 4. In chapter 3, I defined alpha bursts and their respective impact on information coding independently of bursts in other bands. In chapter 4 the impact of alpha bursts was considered in the context of other burst types as well, and it may be that this stressed the positive effects of alpha bursts. For example, suppose alpha bursts were contaminated by spectral leakage from beta bursts. This would manifest as a detrimental effect of alpha bursting in chapter 3, but this association might have been be lost in the analysis applied in chapter 4.

5.7 Conclusion

In this thesis, I used STN local field potential recordings with a ML approach to predict forthcoming limb movements and show that motor information stored in the STN is compromised during alpha and especially beta bursts. These findings suggest that bursts of low frequency activity in the STN restrict the overall capacity to encode movement-related information. The results provide a mechanistic insight into how bursts of synchronised oscillations might contribute to motor dysfunction in PD. In addition, the ability of the STN LFP between bursts of alpha and beta activity in predicting the limb to be moved encourages the consideration of the STN as an alternative or complementary signal source in restorative neuroprosthetic applications. Additionally, I used an unsupervised ML approach on STN LFPs to assess dopaminergic medication effects and predict motor impairment. The study results suggest that whilst some LFP states (i.e. low beta) might be usefully downregulated for therapeutic benefit, others (i.e. theta, alpha, and high beta)

could potentially be upregulated to better mimic the effect of levodopa therapy and improve parkinsonism. In theory, this could be achieved using phase-locked stimulation at phases suppressing and enhancing oscillations respectively (Holt et al., 2019). Current conventional and closed-loop DBS therapy presently only suppress low beta power in STN, and it may be that better improvements can be had by additionally elevating activity in other frequency bands. These results prompt refinements of the feedback signal in closed-loop DBS to give more faithful information on motor state, and motivate the development of phase-locked stimulation techniques which both selectively up and down regulate target brain activities.

References

Alegre M, López-Azcárate J, Alonso-Frech F, Rodríguez-Oroz MC, Valencia M, Guridi J, Artieda J, Obeso JA. Subthalamic activity during diphasic dyskinesias in Parkinson's disease. Movement disorders. 2012 Aug;27(9):1178-81.

Alegre M, Valencia M. Oscillatory activity in the human basal ganglia: more than just beta, more than just Parkinson's disease. Experimental neurology. 2013 Oct 1;248:183-6.

Allman MJ, Meck WH. Pathophysiological distortions in time perception and timed performance. Brain. 2012 Mar 1;135(3):656-77.

Alloway KD, Smith JB, Mowery TM, Watson GD. Sensory processing in the dorsolateral striatum: the contribution of thalamostriatal pathways. Frontiers in systems neuroscience. 2017 Jul 25;11:53.

Almeida QJ, Wishart LR, Lee TD. Bimanual coordination deficits with Parkinson's disease: the influence of movement speed and external cueing. Movement Disorders. 2002 Jan;17(1):30-7.

Alonso-Frech F, Zamarbide I, Alegre M, Rodriguez-Oroz MC, Guridi J, Manrique M, Valencia M, Artieda J, Obeso JA. Slow oscillatory activity and levodopa-induced dyskinesias in Parkinson's disease. Brain. 2006 Jul 1;129(7):1748-57.

Anderson DN, Osting B, Vorwerk J, Dorval AD, Butson CR. Optimized programming algorithm for cylindrical and directional deep brain stimulation electrodes. Journal of neural engineering. 2018 Jan 24;15(2):026005.

Anderson RW, Kehnemouyi YM, Neuville RS, Wilkins KB, Anidi CM, Petrucci MN, Parker JE, Velisar A, Brontë-Stewart HM. A novel method for calculating beta band burst durations in Parkinson's disease using a physiological baseline. Journal of neuroscience methods. 2020 Sep 1;343:108811.

Androulidakis AG, Kühn AA, Chu Chen C, Blomstedt P, Kempf F, Kupsch A, Schneider GH, Doyle L, Dowsey-Limousin P, Hariz MI, Brown P. Dopaminergic therapy promotes lateralized motor activity in the subthalamic area in Parkinson's disease. Brain. 2007 Feb 1;130(2):457-68.

Anidi C, O'Day JJ, Anderson RW, Afzal MF, Syrkin-Nikolau J, Velisar A, Bronte-Stewart HM. Neuromodulation targets pathological not physiological beta bursts during gait in Parkinson's disease. Neurobiology of disease. 2018 Dec 1;120:107-17.

Anzak A, Tan H, Pogosyan A, Foltynie T, Limousin P, Zrinzo L, Hariz M, Ashkan K, Bogdanovic M, Green AL, Aziz T. Subthalamic nucleus activity optimizes maximal effort motor responses in Parkinson's disease. Brain. 2012 Sep 1;135(9):2766-78.

Aquino CC, Fox SH. Clinical spectrum of levodopa-induced complications. Movement Disorders. 2015 Jan;30(1):80-9.

Avants BB, Epstein CL, Grossman M, Gee JC. Symmetric diffeomorphic image registration with cross-correlation: evaluating automated labeling of elderly and neurodegenerative brain. Medical image analysis. 2008 Feb 1;12(1):26-41.

Baker AP, Brookes MJ, Rezek IA, Smith SM, Behrens T, Smith PJ, Woolrich M. Fast transient networks in spontaneous human brain activity. Elife. 2014 Mar 25;3:e01867.

Belić M, Bobić V, Badža M, Šolaja N, Đurić-Jovičić M, Kostić VS. Artificial intelligence for assisting diagnostics and assessment of Parkinson's disease—A review. Clinical neurology and neurosurgery. 2019 Sep 1;184:105442.

Benabid AL, Chabardes S, Mitrofanis J, Pollak P. Deep brain stimulation of the subthalamic nucleus for the treatment of Parkinson's disease. The Lancet Neurology. 2009 Jan 1;8(1):67-81.

Beste C, Saft C, Andrich J, Müller T, Gold R, Falkenstein M. Time processing in Huntington's disease: a group-control study. PLoS One. 2007 Dec 5;2(12):e1263.

Bezard E, Brotchie JM, Gross CE. Pathophysiology of levodopa-induced dyskinesia: potential for new therapies. Nature Reviews Neuroscience. 2001 Aug;2(8):577-88.

Bieńkiewicz M, Craig CM. Parkinson's is time on your side? Evidence for difficulties with sensorimotor synchronization. Frontiers in neurology. 2015 Nov 27;6:249.

Bloem BR, Hausdorff JM, Visser JE, Giladi N. Falls and freezing of gait in Parkinson's disease: a review of two interconnected, episodic phenomena. Movement disorders: official journal of the Movement Disorder Society. 2004 Aug;19(8):871-84.

Bosman CA, Schoffelen JM, Brunet N, Oostenveld R, Bastos AM, Womelsdorf T, Rubehn B, Stieglitz T, De Weerd P, Fries P. Attentional stimulus selection through selective synchronization between monkey visual areas. Neuron. 2012 Sep 6;75(5):875-88.

Bore JC, Campbell BA, Cho H, Gopalakrishnan R, Machado AG, Baker KB. Prediction of mild parkinsonism revealed by neural oscillatory changes and machine learning. Journal of Neurophysiology. 2020 Dec 1;124(6):1698-705.

Bohr A, Memarzadeh K. The rise of artificial intelligence in healthcare applications. InArtificial Intelligence in healthcare 2020 Jan 1 (pp. 25-60). Academic Press.

Bostan AC, Dum RP, Strick PL. The basal ganglia communicate with the cerebellum. Proceedings of the national academy of sciences. 2010 May 4;107(18):8452-6.

Boutet A, Madhavan R, Elias GJ, Joel SE, Gramer R, Ranjan M, Paramanandam V, Xu D, Germann J, Loh A, Kalia SK. Predicting optimal deep brain stimulation parameters for Parkinson’s disease using functional MRI and machine learning. Nature communications. 2021 May 24;12(1):1-3.

Brittain JS, Brown P. Oscillations and the basal ganglia: motor control and beyond. Neuroimage. 2014 Jan 15;85:637-47.

Brown P. Oscillatory nature of human basal ganglia activity: relationship to the pathophysiology of Parkinson's disease. Movement disorders: official journal of the Movement Disorder Society. 2003 Apr;18(4):357-63.

Brown P, Oliviero A, Mazzone P, Insola A, Tonali P, Di Lazzaro V. Dopamine dependency of oscillations between subthalamic nucleus and pallidum in Parkinson's disease. Journal of Neuroscience. 2001 Feb 1;21(3):1033-8.

Brown P, Eusebio A. Paradoxes of functional neurosurgery: clues from basal ganglia recordings. Movement Disorders. 2008 Jan;23(1):12-20.

Buzsáki G, Anastassiou CA, Koch C. The origin of extracellular fields and currents—EEG, ECoG, LFP and spikes. Nature reviews neuroscience. 2012 Jun;13(6):407-20.

Buzsáki G, Draguhn A. Neuronal oscillations in cortical networks. Science304, 1926–1929. DOI: https://doi. org/10. 2004;1126.

Byblow WD, Summers JJ, Lewis GN, Thomas J. Bimanual coordination in Parkinson's disease: deficits in movement frequency, amplitude, and pattern switching. Movement Disorders. 2002 Jan;17(1):20-9.

Cagnan H, Denison T, McIntyre C, Brown P. Emerging technologies for improved deep brain stimulation. Nature biotechnology. 2019 Sep;37(9):1024-33.

Cagnan H, Mallet N, Moll CK, Gulberti A, Holt AB, Westphal M, Gerloff C, Engel AK, Hamel W, Magill PJ, Brown P. Temporal evolution of beta bursts in the parkinsonian cortical and basal ganglia network. Proceedings of the National Academy of Sciences. 2019 Aug 6;116(32):16095-104.

Cagnan H, Pedrosa D, Little S, Pogosyan A, Cheeran B, Aziz T, Green A, Fitzgerald J, Foltynie T, Limousin P, Zrinzo L. Stimulating at the right time: phase-specific deep brain stimulation. Brain. 2017 Jan 1;140(1):132-45.

Carmena JM. Advances in neuroprosthetic learning and control. PLoS biology. 2013 May 21;11(5):e1001561.

Cavanagh JF, Wiecki TV, Cohen MX, Figueroa CM, Samanta J, Sherman SJ, Frank MJ. Subthalamic nucleus stimulation reverses mediofrontal influence over decision threshold. Nature neuroscience. 2011 Nov;14(11):1462-7.

Chen CC, Hsu YT, Chan HL, Chiou SM, Tu PH, Lee ST, Tsai CH, Lu CS, Brown P. Complexity of subthalamic 13–35 Hz oscillatory activity directly correlates with clinical impairment in patients with Parkinson's disease. Experimental neurology. 2010 Jul 1;224(1):234-40.

Chen CC, Pogosyan A, Zrinzo LU, Tisch S, Limousin P, Ashkan K, Yousry T, Hariz MI, Brown P. Intra-operative recordings of local field potentials can help localize the subthalamic nucleus in Parkinson's disease surgery. Experimental neurology. 2006 Mar 1;198(1):214-21.

Chevalier G, Vacher S, Deniau JM, Desban M. Disinhibition as a basic process in the expression of striatal functions. I. The striato-nigral influence on tecto-spinal/tecto-diencephalic neurons. Brain research. 1985 May 20;334(2):215-26.

Chevalier G, Vacher S, Deniau JM. Inhibitory nigral influence on tectospinal neurons, a possible implication of basal ganglia in orienting behavior. Experimental brain research. 1984 Jan;53(2):320-6.

Chiken S, Nambu A. Mechanism of deep brain stimulation: inhibition, excitation, or disruption?. The neuroscientist. 2016 Jun;22(3):313-22.

Cohen MX. Analyzing neural time series data: theory and practice. MIT press; 2014 Jan 17.

Corrado G, Doya K. Understanding neural coding through the model-based analysis of decision making. Journal of Neuroscience. 2007 Aug 1;27(31):8178-80.

Cyron D. Mental side effects of deep brain stimulation (DBS) for movement disorders: The futility of denial. Frontiers in integrative neuroscience. 2016 Apr 20;10:17.

Dayal V, Limousin P, Foltynie T. Subthalamic nucleus deep brain stimulation in Parkinson's disease: the effect of varying stimulation parameters. Journal of Parkinson's disease. 2017 Jan 1;7(2):235-45.

de Almeida Marcelino AL, Mainka T, Krause P, Poewe W, Ganos C, Kühn AA. Deep brain stimulation reduces (nocturnal) dyskinetic exacerbations in patients with ADCY5 mutation: a case series. Journal of Neurology. 2020 Dec;267(12):3624-31.

Deffains M, Bergman H. Parkinsonism-related β oscillations in the primate basal ganglia networks–recent advances and clinical implications. Parkinsonism & related disorders. 2019 Feb 1;59:2-8.

Deffains M, Iskhakova L, Katabi S, Haber SN, Israel Z, Bergman H. Subthalamic, not striatal, activity correlates with basal ganglia downstream activity in normal and parkinsonian monkeys. Elife. 2016 Aug 23;5:e16443.
Deffains M, Iskhakova L, Katabi S, Israel Z, Bergman H. Longer β oscillatory episodes reliably identify pathological subthalamic activity in Parkinsonism. Movement Disorders. 2018 Oct;33(10):1609-18.

Deiber MP, Sallard E, Ludwig C, Ghezzi C, Barral J, Ibañez V. EEG alpha activity reflects motor preparation rather than the mode of action selection. Frontiers in Integrative Neuroscience. 2012 Aug 14;6:59.

Desmurget M, Turner RS. Motor sequences and the basal ganglia: kinematics, not habits. Journal of Neuroscience. 2010 Jun 2;30(22):7685-90.

Deuschl G, Schade-Brittinger C, Krack P, Volkmann J, Schäfer H, Bötzel K, Daniels C, Deutschländer A, Dillmann U, Eisner W, Gruber D. A randomized trial of deep-brain stimulation for Parkinson's disease. New England Journal of Medicine. 2006 Aug 31;355(9):896-908.

Diedrichsen J, Shadmehr R, Ivry RB. The coordination of movement: optimal feedback control and beyond. Trends in cognitive sciences. 2010 Jan 1;14(1):31-9.

Dromey C, Bjarnason S. A preliminary report on disordered speech with deep brain stimulation in individuals with Parkinson's disease. Parkinson’s Disease. 2011 Oct 16;2011.

Dudman JT, Krakauer JW. The basal ganglia: from motor commands to the control of vigor. Current opinion in neurobiology. 2016 Apr 1;37:158-66.

Engel AK, Fries P, Singer W. Dynamic predictions: oscillations and synchrony in top–down processing. Nature Reviews Neuroscience. 2001 Oct;2(10):704-16.

Eusebio A, Thevathasan W, Gaynor LD, Pogosyan A, Bye E, Foltynie T, Zrinzo L, Ashkan K, Aziz T, Brown P. Deep brain stimulation can suppress

pathological synchronisation in parkinsonian patients. Journal of Neurology, Neurosurgery & Psychiatry. 2011 May 1;82(5):569-73.

Ewert S, Plettig P, Li N, Chakravarty MM, Collins DL, Herrington TM, Kühn AA, Horn A. Toward defining deep brain stimulation targets in MNI space: a subcortical atlas based on multimodal MRI, histology and structural connectivity. Neuroimage. 2018 Apr 15;170:271-82.

Feng XJ, Greenwald B, Rabitz H, Shea-Brown E, Kosut R. Toward closed-loop optimization of deep brain stimulation for Parkinson's disease: concepts and lessons from a computational model. Journal of neural engineering. 2007 Feb 23;4(2):L14.

Fischer P, Pogosyan A, Herz DM, Cheeran B, Green AL, Fitzgerald J, Aziz TZ, Hyam J, Little S, Foltynie T, Limousin P. Subthalamic nucleus gamma activity increases not only during movement but also during movement inhibition. elife. 2017 Jul 25;6:e23947.

Foffani G, Priori A, Egidi M, Rampini P, Tamma F, Caputo E, Moxon KA, Cerutti S, Barbieri S. 300-Hz subthalamic oscillations in Parkinson’s disease. Brain. 2003 Oct 1;126(10):2153-63.

Fogelson N, Pogosyan A, Kühn AA, Kupsch A, Van Bruggen G, Speelman H, Tijssen M, Quartarone A, Insola A, Mazzone P, Di Lazzaro V. Reciprocal interactions between oscillatory activities of different frequencies in the subthalamic region of patients with Parkinson's disease. European Journal of Neuroscience. 2005 Jul;22(1):257-66.

Fogelson N, Williams D, Tijssen M, van Bruggen G, Speelman H, Brown P. Different functional loops between cerebral cortex and the subthalmic area in Parkinson's disease. Cerebral cortex. 2006 Jan 1;16(1):64-75.

Frank MJ, Samanta J, Moustafa AA, Sherman SJ. Hold your horses: impulsivity, deep brain stimulation, and medication in parkinsonism. science. 2007 Nov 23;318(5854):1309-12.

Friedman N, Geiger D, Goldszmidt M. Bayesian network classifiers. Machine learning. 1997 Nov;29(2):131-63.

Fries P. A mechanism for cognitive dynamics: neuronal communication through neuronal coherence. Trends in cognitive sciences. 2005 Oct 1;9(10):474-80.

Fries P. Rhythms for cognition: communication through coherence. Neuron. 2015 Oct 7;88(1):220-35.

Fumagalli M, Giannicola G, Rosa M, Marceglia S, Lucchiari C, Mrakic-Sposta S, Servello D, Pacchetti C, Porta M, Sassi M, Zangaglia R. Conflict-dependent dynamic of subthalamic nucleus oscillations during moral decisions. Social neuroscience. 2011 Jun 1;6(3):243-56.

Gauggel S, Rieger M, Feghoff TA. Inhibition of ongoing responses in patients with Parkinson’s disease. Journal of Neurology, Neurosurgery & Psychiatry. 2004 Apr 1;75(4):539-44.

Gelb DJ, Oliver E, Gilman S. Diagnostic criteria for Parkinson disease. Archives of neurology. 1999 Jan 1;56(1):33-9.

Geraedts VJ, Koch M, Kuiper R, Kefalas M, Bäck TH, van Hilten JJ, Wang H, Middelkoop HA, van der Gaag NA, Contarino MF, Tannemaat MR. Preoperative Electroencephalography-Based Machine Learning Predicts Cognitive Deterioration after Subthalamic Deep Brain Stimulation. Movement Disorders. 2021 Jun 3.

Giannicola G, Rosa M, Marceglia S, Scelzo E, Rossi L, Servello D, Menghetti C, Pacchetti C, Zangaglia R, Locatelli M, Caputo E. The effects of levodopa and deep brain stimulation on subthalamic local field low-frequency oscillations in Parkinson's disease. Neurosignals. 2013;21(1-2):89-98.

Gibb WR, Lees A. The relevance of the Lewy body to the pathogenesis of idiopathic Parkinson's disease. Journal of Neurology, Neurosurgery & Psychiatry. 1988 Jun 1;51(6):745-52.

Golshan HM, Hebb AO, Hanrahan SJ, Nedrud J, Mahoor MH. A hierarchical structure for human behavior classification using STN local field potentials. Journal of neuroscience methods. 2018 Jan 1;293:254-63.

Greenland JC, Williams-Gray CH, Barker RA. The clinical heterogeneity of Parkinson's disease and its therapeutic implications. European Journal of Neuroscience. 2019 Feb;49(3):328-38.

Guo Y, Rubin JE, McIntyre CC, Vitek JL, Terman D. Thalamocortical relay fidelity varies across subthalamic nucleus deep brain stimulation protocols in a data-driven computational model. Journal of neurophysiology. 2008 Mar;99(3):1477-92.

Hammond C, Bergman H, Brown P. Pathological synchronization in Parkinson's disease: networks, models and treatments. Trends in neurosciences. 2007 Jul 1;30(7):357-64.

Hand DJ, Yu K. Idiot's Bayes—not so stupid after all?. International statistical review. 2001 Dec;69(3):385-98.

Haslinger B, Kalteis K, Boecker H, Alesch F, Ceballos-Baumann AO. Frequency-correlated decreases of motor cortex activity associated with subthalamic nucleus stimulation in Parkinson's disease. Neuroimage. 2005 Nov 15;28(3):598-606.

Hausdorff JM, Schaafsma JD, Balash Y, Bartels AL, Gurevich T, Giladi N. Impaired regulation of stride variability in Parkinson's disease subjects with freezing of gait. Experimental brain research. 2003 Mar;149(2):187-94.

Heideman SG, Quinn AJ, Woolrich MW, van Ede F, Nobre AC. Dissecting beta-state changes during timed movement preparation in Parkinson's disease. Progress in neurobiology. 2020 Jan 1;184:101731.

Heremans E, Nieuwboer A, Vercruysse S. Freezing of gait in Parkinson's disease: where are we now?. Current neurology and neuroscience reports. 2013 Jun 1;13(6):350.

Herz DM, Little S, Pedrosa DJ, Tinkhauser G, Cheeran B, Foltynie T, Bogacz R, Brown P. Mechanisms underlying decision-making as revealed by deep-brain stimulation in patients with Parkinson's disease. Current Biology. 2018 Apr 23;28(8):1169-78.

Hirschmann J, Özkurt TE, Butz M, Homburger M, Elben S, Hartmann CJ, Vesper J, Wojtecki L, Schnitzler A. Distinct oscillatory STN-cortical loops

revealed by simultaneous MEG and local field potential recordings in patients with Parkinson's disease. Neuroimage. 2011 Apr 1;55(3):1159-68.

Hoerl AE, Kennard RW. Ridge regression: applications to nonorthogonal problems. Technometrics. 1970 Feb 1;12(1):69-82.

Hoerl AE, Kennard RW. Ridge regression: Biased estimation for nonorthogonal problems. Technometrics. 1970 Feb 1;12(1):55-67.

Högl B, Agostino PV, Peralta MC, Gershanik O, Golombek DA. Alterations in time estimation in multiple system atrophy. Basal Ganglia. 2014 Dec 1;4(3-4):95-9.

Holt AB, Kormann E, Gulberti A, Pötter-Nerger M, McNamara CG, Cagnan H, Baaske MK, Little S, Köppen JA, Buhmann C, Westphal M. Phase-dependent suppression of beta oscillations in Parkinson's disease patients. Journal of Neuroscience. 2019 Feb 6;39(6):1119-34.

Horn A, Li N, Dembek TA, Kappel A, Boulay C, Ewert S, Tietze A, Husch A, Perera T, Neumann WJ, Reisert M. Lead-DBS v2: Towards a comprehensive pipeline for deep brain stimulation imaging. Neuroimage. 2019 Jan 1;184:293-316.

Horn A, Neumann WJ, Degen K, Schneider GH, Kühn AA. Toward an electrophysiological “sweet spot” for deep brain stimulation in the subthalamic nucleus. Human brain mapping. 2017 Jul;38(7):3377-90.

Huebl J, Schoenecker T, Siegert S, Brücke C, Schneider GH, Kupsch A, Yarrow K, Kühn AA. Modulation of subthalamic alpha activity to emotional stimuli correlates with depressive symptoms in Parkinson's disease 1. Movement Disorders. 2011 Feb 15;26(3):477-83.

Houston BC, Thompson MC, Ojemann JG, Ko AL, Chizeck HJ. Classifier-based closed-loop deep brain stimulation for essential tremor. In2017 8th International IEEE/EMBS Conference on Neural Engineering (NER) 2017 May 25 (pp. 316-320). IEEE.

Husch A, Petersen MV, Gemmar P, Goncalves J, Hertel F. PaCER-A fully automated method for electrode trajectory and contact reconstruction in deep brain stimulation. NeuroImage: Clinical. 2018 Jan 1;17:80-9.

Hwang K, Ghuman AS, Manoach DS, Jones SR, Luna B. Cortical neurodynamics of inhibitory control. Journal of Neuroscience. 2014 Jul 16;34(29):9551-61.

Iturrate I, Martin S, Chavarriaga R, Orset B, Leeb R, Sobolewski A, Pralong E, Castro-Jiménez M, Benninger D, Bloch J, Millán JD. Beta-driven closed-loop deep brain stimulation can compromise human motor behavior in Parkinson's Disease. BioRxiv. 2019 Jan 1:696385.

Jana S, Hannah R, Muralidharan V, Aron AR. Temporal cascade of frontal, motor and muscle processes underlying human action-stopping. Elife. 2020 Mar 18;9:e50371.

Jankovic J. Parkinson's disease: clinical features and diagnosis. Journal of neurology, neurosurgery & psychiatry. 2008 Apr 1;79(4):368-76.

Johnson LA, Nebeck SD, Muralidharan A, Johnson MD, Baker KB, Vitek JL. Closed-loop deep brain stimulation effects on parkinsonian motor symptoms in a non-human primate–is beta enough?. Brain stimulation. 2016 Nov 1;9(6):892-6.

Jones CR, Jahanshahi M. Contributions of the basal ganglia to temporal processing: evidence from Parkinson's disease. Timing & Time Perception. 2014 Jan 1;2(1):87-127.

Kardous R, Joly H, Giordana B, Stefanini L, Mulliez A, Giordana C, Lemaire JJ, Fontaine D. Functional and dysfunctional impulsivities changes after subthalamic nucleus-deep brain stimulation in Parkinson disease. Neurochirurgie. 2021 Apr 9.

Kent AR, Grill WM. Recording evoked potentials during deep brain stimulation: development and validation of instrumentation to suppress the stimulus artefact. Journal of neural engineering. 2012 Apr 18;9(3):036004.

Khawaldeh S, Tinkhauser G, Shah SA, Peterman K, Debove I, Nguyen TK, Nowacki A, Lachenmayer ML, Schuepbach M, Pollo C, Krack P. Subthalamic nucleus activity dynamics and limb movement prediction in Parkinson's disease. Brain. 2020 Feb 1;143(2):582-96.

Khawaldeh S, Tinkhauser G, Torrecillos F, He S, Foltynie T, Limousin P, Zrinzo L, Oswal A, Quinn AJ, Vidaurre D, Tan H. Balance between competing spectral states in subthalamic nucleus is linked to motor impairment in Parkinson's disease. Brain. 2021 Jul 15.

Kim MK, Kim SP. Decoding movement information from cortical activity for invasive BMIs. In2018 6th International Conference on Brain-Computer Interface (BCI) 2018 Jan 15 (pp. 1-3). IEEE.

Kim J, Duchin Y, Shamir RR, Patriat R, Vitek J, Harel N, Sapiro G. Automatic localization of the subthalamic nucleus on patient-specific

clinical MRI by incorporating 7 T MRI and machine learning: Application in deep brain stimulation. Human brain mapping. 2019 Feb 1;40(2):679-98.

Kiss ZH. Bilateral pallidal neurostimulation—long-term motor and cognitive effects in primary generalized dystonia. Nature Clinical Practice Neurology. 2007 Sep;3(9):482-3.

Klostermann F, Nikulin VV, Kühn AA, Marzinzik F, Wahl M, Pogosyan A, Kupsch A, Schneider GH, Brown P, Curio G. Task-related differential dynamics of EEG alpha-and beta-band synchronization in cortico-basal motor structures. European Journal of Neuroscience. 2007 Mar;25(5):1604-15.

Koop MM, Andrzejewski A, Hill BC, Heit G, Bronte-Stewart HM. Improvement in a quantitative measure of bradykinesia after microelectrode recording in patients with Parkinson's disease during deep brain stimulation surgery. Movement disorders: official journal of the Movement Disorder Society. 2006 May;21(5):673-8.

Kubota KJ, Chen JA, Little MA. Machine learning for large-scale wearable sensor data in Parkinson's disease: Concepts, promises, pitfalls, and futures. Movement disorders. 2016 Sep;31(9):1314-26.

Kühn AA, Brücke C, Schneider GH, Trottenberg T, Kivi A, Kupsch A, Capelle HH, Krauss JK, Brown P. Increased beta activity in dystonia patients after drug-induced dopamine deficiency. Experimental neurology. 2008b Nov 1;214(1):140-3.

Kühn AA, Kempf F, Brücke C, Doyle LG, Martinez-Torres I, Pogosyan A, Trottenberg T, Kupsch A, Schneider GH, Hariz MI, Vandenberghe W. High-frequency stimulation of the subthalamic nucleus suppresses

oscillatory β activity in patients with Parkinson's disease in parallel with improvement in motor performance. Journal of Neuroscience. 2008a Jun 11;28(24):6165-73.

Kühn AA, Kupsch A, Schneider GH, Brown P. Reduction in subthalamic 8–35 Hz oscillatory activity correlates with clinical improvement in Parkinson's disease. European Journal of Neuroscience. 2006 Apr;23(7):1956-60.

Kühn AA, Trottenberg T, Kivi A, Kupsch A, Schneider GH, Brown P. The relationship between local field potential and neuronal discharge in the subthalamic nucleus of patients with Parkinson's disease. Experimental neurology. 2005 Jul 1;194(1):212-20.

Kühn AA, Tsui A, Aziz T, Ray N, Brücke C, Kupsch A, Schneider GH, Brown P. Pathological synchronisation in the subthalamic nucleus of patients with Parkinson's disease relates to both bradykinesia and rigidity. Experimental neurology. 2009 Feb 1;215(2):380-7.

Kühn AA, Tsui A, Aziz T, Ray N, Brücke C, Kupsch A, Schneider GH, Brown P. Pathological synchronisation in the subthalamic nucleus of patients with Parkinson's disease relates to both bradykinesia and rigidity. Experimental neurology. 2009 Feb 1;215(2):380-7.

Lanciego JL, Luquin N, Obeso JA. Functional neuroanatomy of the basal ganglia. Cold Spring Harbor perspectives in medicine. 2012 Dec 1;2(12):a009621.

Levy R, Ashby P, Hutchison WD, Lang AE, Lozano AM, Dostrovsky JO. Dependence of subthalamic nucleus oscillations on movement and dopamine in Parkinson’s disease. Brain. 2002a Jun 1;125(6):1196-209.

Levy R, Hutchison WD, Lozano AM, Dostrovsky JO. Synchronized neuronal discharge in the basal ganglia of parkinsonian patients is limited to oscillatory activity. Journal of Neuroscience. 2002b Apr 1;22(7):2855-61.

Lewis GN, Byblow WD, Walt SE. Stride length regulation in Parkinson's disease: the use of extrinsic, visual cues. Brain. 2000 Oct 1;123(10):2077-90.

Li MC, Cook MJ. Deep brain stimulation for drug-resistant epilepsy. Epilepsia. 2018 Feb;59(2):273-90.

Liker MA, Won DS, Rao VY, Hua SE. Deep brain stimulation: An evolving technology. Proceedings of the IEEE. 2008 Jun 17;96(7):1129-41.

Little S, Beudel M, Zrinzo L, Foltynie T, Limousin P, Hariz M, Neal S, Cheeran B, Cagnan H, Gratwicke J, Aziz TZ. Bilateral adaptive deep brain stimulation is effective in Parkinson's disease. Journal of Neurology, Neurosurgery & Psychiatry. 2016 Jul 1;87(7):717-21.

Little S, Brown P. Debugging adaptive deep brain stimulation for Parkinson's Disease. Movement Disorders. 2020 Apr;35(4):555-61.

Gilron R, Little S, Perrone R, Wilt R, de Hemptinne C, Yaroshinsky MS, Racine CA, Wang SS, Ostrem JL, Larson PS, Wang DD. Long-term wireless streaming of neural recordings for circuit discovery and adaptive stimulation in individuals with Parkinson’s disease. Nature Biotechnology. 2021 May 3.

Little S, Pogosyan A, Neal S, Zavala B, Zrinzo L, Hariz M, Foltynie T, Limousin P, Ashkan K, FitzGerald J, Green AL. Adaptive deep brain

stimulation in advanced Parkinson disease. Annals of neurology. 2013 Sep;74(3):449-57.

Little S, Tripoliti E, Beudel M, Pogosyan A, Cagnan H, Herz D, Bestmann S, Aziz T, Cheeran B, Zrinzo L, Hariz M. Adaptive deep brain stimulation for Parkinson's disease demonstrates reduced speech side effects compared to conventional stimulation in the acute setting. Journal of Neurology, Neurosurgery & Psychiatry. 2016 Dec 1;87(12):1388-9.

Litvak V, Eusebio A, Jha A, Oostenveld R, Barnes G, Foltynie T, Limousin P, Zrinzo L, Hariz MI, Friston K, Brown P. Movement-related changes in local and long-range synchronization in Parkinson's disease revealed by simultaneous magnetoencephalography and intracranial recordings. Journal of Neuroscience. 2012 Aug 1;32(31):10541-53.

Litvak V, Jha A, Eusebio A, Oostenveld R, Foltynie T, Limousin P, Zrinzo L, Hariz MI, Friston K, Brown P. Resting oscillatory cortico-subthalamic connectivity in patients with Parkinson’s disease. Brain. 2011 Feb 1;134(2):359-74.

Litvak V, Jha A, Eusebio A, Oostenveld R, Foltynie T, Limousin P, Zrinzo L, Hariz MI, Friston K, Brown P. Resting oscillatory cortico-subthalamic connectivity in patients with Parkinson’s disease. Brain. 2011 Feb 1;134(2):359-74.

Lofredi R, Neumann WJ, Bock A, Horn A, Huebl J, Siegert S, Schneider GH, Krauss JK, Kühn AA. Dopamine-dependent scaling of subthalamic gamma bursts with movement velocity in patients with Parkinson’s disease. Elife. 2018 Feb 1;7:e31895.

Lofredi R, Tan H, Neumann WJ, Yeh CH, Schneider GH, Kühn AA, Brown P. Beta bursts during continuous movements accompany the velocity decrement in Parkinson's disease patients. Neurobiology of disease. 2019 Jul 1;127:462-71.

López-Azcárate J, Tainta M, Rodríguez-Oroz MC, Valencia M, González R, Guridi J, Iriarte J, Obeso JA, Artieda J, Alegre M. Coupling between beta and high-frequency activity in the human subthalamic nucleus may be a pathophysiological mechanism in Parkinson's disease. Journal of Neuroscience. 2010 May 12;30(19):6667-77.

Lozano AM, Lipsman N, Bergman H, Brown P, Chabardes S, Chang JW, Matthews K, McIntyre CC, Schlaepfer TE, Schulder M, Temel Y. Deep brain stimulation: current challenges and future directions. Nature Reviews Neurology. 2019 Mar;15(3):148-60.

Mallet N, Pogosyan A, Sharott A, Csicsvari J, Bolam JP, Brown P, Magill PJ. Disrupted dopamine transmission and the emergence of exaggerated beta oscillations in subthalamic nucleus and cerebral cortex. Journal of Neuroscience. 2008 Apr 30;28(18):4795-806.

Mamun KA, Mace M, Lutman ME, Stein J, Liu X, Aziz T, Vaidyanathan R, Wang S. Movement decoding using neural synchronization and inter-hemispheric connectivity from deep brain local field potentials. Journal of neural engineering. 2015 Aug 26;12(5):056011.

Marceglia SA, Fiorio M, Foffani G, Mrakic-Sposta S, Tiriticco M, Locatelli M, Caputo E, Tinazzi M, Priori A. Modulation of beta oscillations in the subthalamic area during action observation in Parkinson's disease. Neuroscience. 2009 Jul 21;161(4):1027-36.

Marek K, Jennings D, Seibyl J. Do dopamine agonists or levodopa modify Parkinson's disease progression?. European journal of neurology. 2002 Nov;9:15-22.

Marmor O, Valsky D, Joshua M, Bick AS, Arkadir D, Tamir I, Bergman H, Israel Z, Eitan R. Local vs. volume conductance activity of field potentials in the human subthalamic nucleus. Journal of neurophysiology. 2017 Jun 1;117(6):2140-51.

Marquardt DW, Snee RD. Ridge regression in practice. The American Statistician. 1975 Feb 1;29(1):3-20.

Marquaridt DW. Generalized inverses, ridge regression, biased linear estimation, and nonlinear estimation. Technometrics. 1970 Aug 1;12(3):591-612.

Marreiros AC, Cagnan H, Moran RJ, Friston KJ, Brown P. Basal ganglia–cortical interactions in Parkinsonian patients. Neuroimage. 2013 Feb 1;66:301-10.

Marsden CD, Obeso JA. The functions of the basal ganglia and the paradox of stereotaxic surgery in Parkinson's disease. Brain. 1994 Aug 1;117(4):877-97.

McColl CD, Reardon KA, Shiff M, Kempster PA. Motor response to levodopa and the evolution of motor fluctuations in the first decade of treatment of Parkinson's disease. Movement disorders: official journal of the Movement Disorder Society. 2002 Nov;17(6):1227-34.

McIntyre CC, Anderson RW. Deep brain stimulation mechanisms: the control of network activity via neurochemistry modulation. Journal of Neurochemistry. 2016 Oct;139:338-45.

Meidahl AC, Moll CK, van Wijk BC, Gulberti A, Tinkhauser G, Westphal M, Engel AK, Hamel W, Brown P, Sharott A. Synchronised spiking activity underlies phase amplitude coupling in the subthalamic nucleus of Parkinson's disease patients. Neurobiology of disease. 2019 Jul 1;127:101-13.

Mei J, Desrosiers C, Frasnelli J. Machine learning for the diagnosis of parkinson's disease: A review of literature. Frontiers in aging neuroscience. 2021 May 6;13:184.

Merchant H, Luciana M, Hooper C, Majestic S, Tuite P. Interval timing and Parkinson’s disease: heterogeneity in temporal performance. Experimental Brain Research. 2008 Jan;184(2):233-48.

Milardi D, Gaeta M, Marino S, Arrigo A, Vaccarino G, Mormina E, Rizzo G, Milazzo C, Finocchio G, Baglieri A, Anastasi G. Basal ganglia network by constrained spherical deconvolution: a possible cortico-pallidal pathway?. Movement Disorders. 2015 Mar;30(3):342-9.

Mink JW. The basal ganglia: focused selection and inhibition of competing motor programs. Progress in neurobiology. 1996 Nov 1;50(4):381-425.

Moore ST, MacDougall HG, Ondo WG. Ambulatory monitoring of freezing of gait in Parkinson's disease. Journal of neuroscience methods. 2008 Jan 30;167(2):340-8.

Moran A, Bergman H, Israel Z, Bar-Gad I. Subthalamic nucleus functional organization revealed by parkinsonian neuronal oscillations and synchrony. Brain. 2008 Dec 1;131(12):3395-409.

Moran RJ, Mallet N, Litvak V, Dolan RJ, Magill PJ, Friston KJ, Brown P. Alterations in brain connectivity underlying beta oscillations in Parkinsonism. PLoS computational biology. 2011 Aug 11;7(8):e1002124.

Moro E, Esselink RJ, Xie J, Hommel M, Benabid AL, Pollak P. The impact on Parkinson's disease of electrical parameter settings in STN stimulation. Neurology. 2002 Sep 10;59(5):706-13.

Mosharov EV, Borgkvist A, Sulzer D. Presynaptic effects of levodopa and their possible role in dyskinesia. Movement Disorders. 2015 Jan;30(1):45-53.

Moshel S, Shamir RR, Raz A, de Noriega FR, Eitan R, Bergman H, Israel Z. Subthalamic nucleus long-range synchronization—an independent hallmark of human Parkinson's disease. Frontiers in systems neuroscience. 2013 Nov 19;7:79.

Mücke D, Hermes A, Roettger TB, Becker J, Niemann H, Dembek TA, Timmermann L, Visser-Vandewalle V, Fink GR, Grice M, Barbe MT. The effects of thalamic deep brain stimulation on speech dynamics in patients with essential tremor: An articulographic study. PLoS One. 2018 Jan 23;13(1):e0191359.

Müller EJ, Robinson PA. Quantitative theory of deep brain stimulation of the subthalamic nucleus for the suppression of pathological rhythms in

Parkinson’s disease. PLoS computational biology. 2018 May 29;14(5):e1006217.

Nambu A, Tokuno H, Takada M. Functional significance of the cortico–subthalamo–pallidal ‘hyperdirect’pathway. Neuroscience research. 2002 Jun 1;43(2):111-7.

Neumann WJ, Degen K, Schneider GH, Brücke C, Huebl J, Brown P, Kühn AA. Subthalamic synchronized oscillatory activity correlates with motor impairment in patients with Parkinson's disease. Movement Disorders. 2016 Nov;31(11):1748-51.

Neumann WJ, Kühn AA. Subthalamic beta power-Unified Parkinson’s disease rating scale III correlations require akinetic symptoms. Mov Disord. 2017 Jan 1;32(1):175-6.

Neumann WJ, Staub-Bartelt F, Horn A, Schanda J, Schneider GH, Brown P, Kühn AA. Long term correlation of subthalamic beta band activity with motor impairment in patients with Parkinson’s disease. Clinical Neurophysiology. 2017 Nov 1;128(11):2286-91.

Niktarash AH, Shahidi GA. Effects of the activity of the internal globus pallidus-pedunculopontine loop on the transmission of the subthalamic nucleus-external globus pallidus-pacemaker oscillatory activities to the cortex. Journal of computational neuroscience. 2004 Mar;16(2):113-27.

O’Connor WT. Functional neuroanatomy of the basal ganglia as studied by dual-probe microdialysis. Nuclear medicine and biology. 1998 Nov 1;25(8):743-6.

O'Suilleabhain PE, Frawley W, Giller C, Dewey RB. Tremor response to polarity, voltage, pulsewidth and frequency of thalamic stimulation. Neurology. 2003 Mar 11;60(5):786-90.

Obeso I, Wilkinson L, Jahanshahi M. Levodopa medication does not influence motor inhibition or conflict resolution in a conditional stop-signal task in Parkinson's disease. Experimental brain research. 2011 Sep 1;213(4):435.

Oostenveld R, Fries P, Maris E, Schoffelen JM. FieldTrip: open source software for advanced analysis of MEG, EEG, and invasive electrophysiological data. Computational intelligence and neuroscience. 2011 Oct;2011.

Oswal A, Beudel M, Zrinzo L, Limousin P, Hariz M, Foltynie T, Litvak V, Brown P. Deep brain stimulation modulates synchrony within spatially and spectrally distinct resting state networks in Parkinson's disease. Brain. 2016 May 1;139(5):1482-96.

Oswal A, Brown P, Litvak V. Movement related dynamics of subthalmo-cortical alpha connectivity in Parkinson's disease. Neuroimage. 2013 Apr 15;70:132-42.

Özkurt TE, Butz M, Homburger M, Elben S, Vesper J, Wojtecki L, Schnitzler A. High frequency oscillations in the subthalamic nucleus: a neurophysiological marker of the motor state in Parkinson's disease. Experimental neurology. 2011 Jun 1;229(2):324-31.

Pavlides A, Hogan SJ, Bogacz R. Computational models describing possible mechanisms for generation of excessive beta oscillations in

Parkinson's disease. PLoS computational biology. 2015 Dec;11(12):e1004609.

Peles O, Werner-Reiss U, Bergman H, Israel Z, Vaadia E. Phase-specific microstimulation differentially modulates beta oscillations and affects behavior. Cell reports. 2020 Feb 25;30(8):2555-66.

Perugini A, Ditterich J, Shaikh AG, Knowlton BJ, Basso MA. Paradoxical decision-making: a framework for understanding cognition in Parkinson's disease. Trends in neurosciences. 2018 Aug 1;41(8):512-25.

Pfurtscheller G, Andrew C. Event-related changes of band power and coherence: methodology and interpretation. Journal of clinical neurophysiology. 1999 Nov 1;16(6):512.

Pfurtscheller G, Da Silva FL. Event-related EEG/MEG synchronization and desynchronization: basic principles. Clinical neurophysiology. 1999 Nov 1;110(11):1842-57.

Pfurtscheller G. Central beta rhythm during sensorimotor activities in man. Electroencephalography and clinical neurophysiology. 1981 Mar 1;51(3):253-64.

Pham U, Solbakk AK, Skogseid IM, Toft M, Pripp AH, Konglund AE, Andersson S, Haraldsen IR, Aarsland D, Dietrichs E, Malt UF. Personality changes after deep brain stimulation in Parkinson's disease. Parkinson's Disease. 2015 Jan 29;2015.

Piña-Fuentes D, Beudel M, Little S, Brown P, Oterdoom DM, van Dijk JM. Adaptive deep brain stimulation as advanced Parkinson's disease

treatment (ADAPT study): protocol for a pseudo-randomised clinical study. BMJ open. 2019 Jun 1;9(6):e029652.

Piña-Fuentes D, van Dijk JM, van Zijl JC, Moes HR, van Laar T, Oterdoom DM, Little S, Brown P, Beudel M. Acute effects of adaptive deep brain stimulation in parkinson's disease. Brain stimulation. 2020 Nov 1;13(6):1507-16.

Poewe W, Seppi K, Tanner CM, Halliday GM, Brundin P, Volkmann J, Schrag AE, Lang AE. Parkinson disease. Nature reviews Disease primers. 2017 Mar 23;3(1):1-21.

Pollok B, Krause V, Martsch W, Wach C, Schnitzler A, Südmeyer M. Motor-cortical oscillations in early stages of Parkinson's disease. The Journal of physiology. 2012 Jul 1;590(13):3203-12.

Pollok B, Latz D, Krause V, Butz M, Schnitzler A. Changes of motor-cortical oscillations associated with motor learning. Neuroscience. 2014 Sep 5;275:47-53.

Ponsen MM, Daffertshofer A, van den Heuvel E, Wolters EC, Beek PJ, Berendse HW. Bimanual coordination dysfunction in early, untreated Parkinson's disease. Parkinsonism & Related Disorders. 2006 May 1;12(4):246-52.

Priori A, Foffani G, Pesenti A, Tamma F, Bianchi AM, Pellegrini M, Locatelli M, Moxon KA, Villani RM. Rhythm-specific pharmacological modulation of subthalamic activity in Parkinson's disease. Experimental neurology. 2004 Oct 1;189(2):369-79.

Priori A, Foffani G, Rossi L, Marceglia S. Adaptive deep brain stimulation (aDBS) controlled by local field potential oscillations. Experimental neurology. 2013 Jul 1;245:77-86.

Quinn AJ, van Ede F, Brookes MJ, Heideman SG, Nowak M, Seedat ZA, Vidaurre D, Zich C, Nobre AC, Woolrich MW. Unpacking transient event dynamics in electrophysiological power spectra. Brain topography. 2019 Nov;32(6):1020-34.

Quinn EJ, Blumenfeld Z, Velisar A, Koop MM, Shreve LA, Trager MH, Hill BC, Kilbane C, Henderson JM, Brontë-Stewart H. Beta oscillations in freely moving Parkinson's subjects are attenuated during deep brain stimulation. Movement Disorders. 2015 Nov;30(13):1750-8.

Rappel P, Marmor O, Bick AS, Arkadir D, Linetsky E, Castrioto A, Tamir I, Freedman SA, Mevorach T, Gilad M, Bergman H. Subthalamic theta activity: a novel human subcortical biomarker for obsessive compulsive disorder. Translational psychiatry. 2018 Jun 18;8(1):1-1.

Ray NJ, Jenkinson N, Wang S, Holland P, Brittain JS, Joint C, Stein JF, Aziz T. Local field potential beta activity in the subthalamic nucleus of patients with Parkinson's disease is associated with improvements in bradykinesia after dopamine and deep brain stimulation. Experimental neurology. 2008 Sep 1;213(1):108-13.

Redgrave P, Coizet V, Comoli E, McHaffie JG, Leriche Vazquez M, Vautrelle N, Hayes LM, Overton PG. Interactions between the midbrain superior colliculus and the basal ganglia. Frontiers in neuroanatomy. 2010 Sep 22;4:132.

Redgrave P, Prescott TJ, Gurney K. The basal ganglia: a vertebrate solution to the selection problem?. Neuroscience. 1999;89(4):1009-23.

Redgrave P. Basal ganglia. Scholarpedia. 2007 Jun 5;2(6):1825.

Rinvik E. Demonstration of nigrothalamic connections in the cat by retrograde axonal transport of horseradish peroxidase. Brain Research. 1975 Jun 13;90(2):313-8.

Rish I. An empirical study of the naive Bayes classifier. InIJCAI 2001 workshop on empirical methods in artificial intelligence 2001 Aug 4 (Vol. 3, No. 22, pp. 41-46).

Robnik-Šikonja M, Kononenko I. Theoretical and empirical analysis of ReliefF and RReliefF. Machine learning. 2003 Oct;53(1):23-69.

Rodriguez-Oroz MC, Lopez-Azcarate J, Garcia-Garcia D, Alegre M, Toledo J, Valencia M, Guridi J, Artieda J, Obeso JA. Involvement of the subthalamic nucleus in impulse control disorders associated with Parkinson’s disease. Brain. 2011 Jan 1;134(1):36-49.

Rodriguez-Oroz MC, Obeso JA, Lang AE, Houeto JL, Pollak P, Rehncrona S, Kulisevsky J, Albanese A, Volkmann J, Hariz MI, Quinn NP. Bilateral deep brain stimulation in Parkinson's disease: a multicentre study with 4 years follow-up. Brain. 2005 Oct 1;128(10):2240-9.

Rosa M, Arlotti M, Ardolino G, Cogiamanian F, Marceglia S, Di Fonzo A, Cortese F, Rampini PM, Priori A. Adaptive deep brain stimulation in a freely moving Parkinsonian patient. Movement Disorders. 2015 Jun;30(7):1003-5.

Rosa M, Fumagalli M, Giannicola G, Marceglia S, Lucchiari C, Servello D, Franzini A, Pacchetti C, Romito L, Albanese A, Porta M. Pathological gambling in Parkinson's disease: subthalamic oscillations during economics decisions. Movement Disorders. 2013 Oct;28(12):1644-52.

Rosa M, Arlotti M, Marceglia S, Cogiamanian F, Ardolino G, Fonzo AD, Lopiano L, Scelzo E, Merola A, Locatelli M, Rampini PM. A daptive deep brain stimulation controls levodopa-induced side effects in P arkinsonian patients. Movement Disorders. 2017 Apr;32(4):628-9.

Rosin B, Slovik M, Mitelman R, Rivlin-Etzion M, Haber SN, Israel Z, Vaadia E, Bergman H. Closed-loop deep brain stimulation is superior in ameliorating parkinsonism. Neuron. 2011 Oct 20;72(2):370-84.

Rossi L, Foffani G, Marceglia SA, Bracchi F, Barbieri S, Priori A. An electronic device for artefact suppression in human local field potential recordings during deep brain stimulation. Journal of neural engineering. 2007 Mar 13;4(2):96.

Salanova V, Witt T, Worth R, Henry TR, Gross RE, Nazzaro JM, Labar D, Sperling MR, Sharan A, Sandok E, Handforth A. Long-term efficacy and safety of thalamic stimulation for drug-resistant partial epilepsy. Neurology. 2015 Mar 10;84(10):1017-25.

Salinas E, Sejnowski TJ. Correlated neuronal activity and the flow of neural information. Nature reviews neuroscience. 2001;2(8):539.

Santos FJ, Costa RM, Tecuapetla F. Stimulation on demand: closing the loop on deep brain stimulation. Neuron. 2011 Oct 20;72(2):197-8.

Schmidt SL, Peters JJ, Turner DA, Grill WM. Continuous deep brain stimulation of the subthalamic nucleus may not modulate beta bursts in

patients with Parkinson's disease. Brain stimulation. 2020 Mar 1;13(2):433-43.

Schnitzler A, Gross J. Normal and pathological oscillatory communication in the brain. Nature reviews neuroscience. 2005 Apr;6(4):285-96.

Schor JS, Nelson AB. Multiple stimulation parameters influence efficacy of deep brain stimulation in parkinsonian mice. The Journal of clinical investigation. 2019 Sep 3;129(9):3833-8.

Schüpbach WM. Impulsivity, impulse control disorders, and subthalamic stimulation in Parkinson's disease. Basal Ganglia. 2012 Dec 1;2(4):205-9.

Shah SA, Tan H, Brown P. Continuous force decoding from deep brain local field potentials for Brain Computer Interfacing. In2017 8th International IEEE/EMBS Conference on Neural Engineering (NER) 2017 May 25 (pp. 371-374). IEEE.

Shah SA, Tinkhauser G, Chen CC, Little S, Brown P. Parkinsonian tremor detection from subthalamic nucleus local field potentials for closed-loop deep brain stimulation. In2018 40th Annual International Conference of the IEEE Engineering in Medicine and Biology Society (EMBC) 2018 Jul 18 (pp. 2320-2324). IEEE.

Shamir RR, Dolber T, Noecker AM, Walter BL, McIntyre CC. Machine learning approach to optimizing combined stimulation and medication therapies for Parkinson's disease. Brain stimulation. 2015 Nov 1;8(6):1025-32.

Sharott A, Gulberti A, Zittel S, Jones AA, Fickel U, Münchau A, Köppen JA, Gerloff C, Westphal M, Buhmann C, Hamel W. Activity parameters of subthalamic nucleus neurons selectively predict motor symptom severity

in Parkinson's disease. Journal of Neuroscience. 2014 Apr 30;34(18):6273-85.

Singh A, Levin J, Mehrkens JH, Bötzel K. Alpha frequency modulation in the human basal ganglia is dependent on motor task. European Journal of Neuroscience. 2011 Mar;33(5):960-7.

Skodda S. Effect of deep brain stimulation on speech performance in Parkinson's disease. Parkinson’s Disease. 2012 Oct;2012.

Smith Y, Bevan MD, Shink E, Bolam JP. Microcircuitry of the direct and indirect pathways of the basal ganglia. Neuroscience. 1998 Sep 1;86(2):353-87.

Spildooren J, Vercruysse S, Desloovere K, Vandenberghe W, Kerckhofs E, Nieuwboer A. Freezing of gait in Parkinson's disease: the impact of dual-tasking and turning. Movement Disorders. 2010 Nov 15;25(15):2563-70.

Steiner LA, Neumann WJ, Staub-Bartelt F, Herz DM, Tan H, Pogosyan A, Kuhn AA, Brown P. Subthalamic beta dynamics mirror Parkinsonian bradykinesia months after neurostimulator implantation. Movement Disorders. 2017 Aug;32(8):1183-90.

Sveinbjornsdottir S. The clinical symptoms of Parkinson's disease. Journal of neurochemistry. 2016 Oct;139:318-24.

Swann NC, de Hemptinne C, Miocinovic S, Qasim S, Wang SS, Ziman N, Ostrem JL, San Luciano M, Galifianakis NB, Starr PA. Gamma oscillations in the hyperkinetic state detected with chronic human brain recordings in

Parkinson's disease. Journal of Neuroscience. 2016 Jun 15;36(24):6445-58.

Swann NC, de Hemptinne C, Thompson MC, Miocinovic S, Miller AM, Ostrem JL, Chizeck HJ, Starr PA. Adaptive deep brain stimulation for Parkinson’s disease using motor cortex sensing. Journal of neural engineering. 2018 May 9;15(4):046006.

Tan H, Debarros J, He S, Pogosyan A, Aziz TZ, Huang Y, Wang S, Timmermann L, Visser-Vandewalle V, Pedrosa DJ, Green AL. Decoding voluntary movements and postural tremor based on thalamic LFPs as a basis for closed-loop stimulation for essential tremor. Brain stimulation. 2019 Jul 1;12(4):858-67.

Tan H, Pogosyan A, Anzak A, Ashkan K, Bogdanovic M, Green AL, Aziz T, Foltynie T, Limousin P, Zrinzo L, Brown P. Complementary roles of different oscillatory activities in the subthalamic nucleus in coding motor effort in Parkinsonism. Experimental neurology. 2013 Oct 1;248:187-95.

Tan H, Pogosyan A, Anzak A, Foltynie T, Limousin P, Zrinzo L, Ashkan K, Bogdanovic M, Green AL, Aziz T, Brown P. Frequency specific activity in subthalamic nucleus correlates with hand bradykinesia in Parkinson's disease. Experimental neurology. 2013 Feb 1;240:122-9.

Tan H, Pogosyan A, Ashkan K, Green AL, Aziz T, Foltynie T, Limousin P, Zrinzo L, Hariz M, Brown P. Decoding gripping force based on local field potentials recorded from subthalamic nucleus in humans. Elife. 2016 Nov 18;5:e19089.

Tinkhauser G, Pogosyan A, Little S, Beudel M, Herz DM, Tan H, Brown P. The modulatory effect of adaptive deep brain stimulation on beta bursts in Parkinson's disease. Brain. 2017a Apr 1;140(4):1053-67.

Tinkhauser G, Pogosyan A, Tan H, Herz DM, Kühn AA, Brown P. Beta burst dynamics in Parkinson's disease OFF and ON dopaminergic medication. Brain. 2017b Nov 1;140(11):2968-81.

Tinkhauser G, Shah SA, Fischer P, Peterman K, Debove I, Nygyuen K, Nowacki A, Torrecillos F, Khawaldeh S, Tan H, Pogosyan A. Electrophysiological differences between upper and lower limb movements in the human subthalamic nucleus. Clinical neurophysiology. 2019 May 1;130(5):727-38.

Tinkhauser G, Torrecillos F, Pogosyan A, Mostofi A, Bange M, Fischer P, Tan H, Hasegawa H, Glaser M, Muthuraman M, Groppa S. The cumulative effect of transient synchrony states on motor performance in Parkinson's disease. Journal of neuroscience. 2020 Feb 12;40(7):1571-80.

Tolosa E, Wenning G, Poewe W. The diagnosis of Parkinson's disease. The Lancet Neurology. 2006 Jan 1;5(1):75-86.

Toro C, Deuschl G, Thatcher R, Sato S, Kufta C, Hallett M. Event-related desynchronization and movement-related cortical potentials on the ECoG and EEG. Electroencephalography and Clinical Neurophysiology/Evoked Potentials Section. 1994 Oct 1;93(5):380-9.

Torrecillos F, Tinkhauser G, Fischer P, Green AL, Aziz TZ, Foltynie T, Limousin P, Zrinzo L, Ashkan K, Brown P, Tan H. Modulation of beta bursts in the subthalamic nucleus predicts motor performance. Journal of neuroscience. 2018 Oct 10;38(41):8905-17.

Trager MH, Koop MM, Velisar A, Blumenfeld Z, Nikolau JS, Quinn EJ, Martin T, Bronte-Stewart H. Subthalamic beta oscillations are attenuated after withdrawal of chronic high frequency neurostimulation in Parkinson's disease. Neurobiology of Disease. 2016 Dec 1;96:22-30.

Trottenberg T, Kupsch A, Schneider GH, Brown P, Kühn AA. Frequency-dependent distribution of local field potential activity within the subthalamic nucleus in Parkinson's disease. Experimental neurology. 2007 May 1;205(1):287-91.

Turner RS, Desmurget M. Basal ganglia contributions to motor control: a vigorous tutor. Current opinion in neurobiology. 2010 Dec 1;20(6):704-16.

van Albada SJ, Gray RT, Drysdale PM, Robinson PA. Mean-field modeling of the basal ganglia-thalamocortical system. II: dynamics of parkinsonian oscillations. Journal of theoretical biology. 2009 Apr 21;257(4):664-88.

van Wijk B, Beek PJ, Daffertshofer A. Neural synchrony within the motor system: what have we learned so far?. Frontiers in human neuroscience. 2012 Sep 4;6:252.

van Wijk BC, Beudel M, Jha A, Oswal A, Foltynie T, Hariz MI, Limousin P, Zrinzo L, Aziz TZ, Green AL, Brown P. Subthalamic nucleus phase–amplitude coupling correlates with motor impairment in Parkinson’s disease. Clinical Neurophysiology. 2016 Apr 1;127(4):2010-9.

Van Wijk BC, Pogosyan A, Hariz MI, Akram H, Foltynie T, Limousin P, Horn A, Ewert S, Brown P, Litvak V. Localization of beta and high-frequency oscillations within the subthalamic nucleus region. NeuroImage: Clinical. 2017 Jan 1;16:175-83.

Varela F, Lachaux JP, Rodriguez E, Martinerie J. The brainweb: phase synchronization and large-scale integration. Nature reviews neuroscience. 2001 Apr;2(4):229.

Velisar A, Syrkin-Nikolau J, Blumenfeld Z, Trager MH, Afzal MF, Prabhakar V, Bronte-Stewart H. Dual threshold neural closed loop deep brain stimulation in Parkinson disease patients. Brain stimulation. 2019 Jul 1;12(4):868-76.

Vercruysse S, Spildooren J, Heremans E, Vandenbossche J, Levin O, Wenderoth N, Swinnen SP, Janssens L, Vandenberghe W, Nieuwboer A. Freezing in Parkinson's disease: a spatiotemporal motor disorder beyond gait. Movement Disorders. 2012 Feb;27(2):254-63.

Vidaurre D, Hunt LT, Quinn AJ, Hunt BA, Brookes MJ, Nobre AC, Woolrich MW. Spontaneous cortical activity transiently organises into frequency specific phase-coupling networks. Nature communications. 2018 Jul 30;9(1):1-3.

Vidaurre D, Smith SM, Woolrich MW. Brain network dynamics are hierarchically organized in time. Proceedings of the National Academy of Sciences. 2017 Nov 28;114(48):12827-32.

Vidaurre D, Woolrich MW, Winkler AM, Karapanagiotidis T, Smallwood J, Nichols TE. Stable between-subject statistical inference from unstable within-subject functional connectivity estimates. Human brain mapping. 2019 Mar;40(4):1234-43.

Volkmann J, Mueller J, Deuschl G, Kühn AA, Krauss JK, Poewe W, Timmermann L, Falk D, Kupsch A, Kivi A, Schneider GH. Pallidal neurostimulation in patients with medication-refractory cervical dystonia: a

randomised, sham-controlled trial. The Lancet Neurology. 2014 Sep 1;13(9):875-84.

Weinberger M, Mahant N, Hutchison WD, Lozano AM, Moro E, Hodaie M, Lang AE, Dostrovsky JO. Beta oscillatory activity in the subthalamic nucleus and its relation to dopaminergic response in Parkinson's disease. Journal of neurophysiology. 2006 Dec;96(6):3248-56.

Wessel JR. β-bursts reveal the trial-to-trial dynamics of movement initiation and cancellation. Journal of Neuroscience. 2020 Jan 8;40(2):411-23.

Wiest C, Tinkhauser G, Pogosyan A, Bange M, Muthuraman M, Groppa S, Baig F, Mostofi A, Pereira EA, Tan H, Brown P. Local field potential activity dynamics in response to deep brain stimulation of the subthalamic nucleus in Parkinson's disease. Neurobiology of disease. 2020 Sep 1;143:105019.

Wiest C, Tinkhauser G, Pogosyan A, He S, Baig F, Morgante F, Mostofi A, Pereira EA, Tan H, Brown P, Torrecillos F. Subthalamic deep brain stimulation induces finely-tuned gamma oscillations in the absence of levodopa. Neurobiology of disease. 2021 May 1;152:105287.

Yagi S, Yoshikawa E, Futatsubashi M, Yokokura M, Yoshihara Y, Torizuka T, Ouchi Y. Progression from unilateral to bilateral parkinsonism in early Parkinson disease: implication of mesocortical dopamine dysfunction by PET. Journal of Nuclear Medicine. 2010 Aug 1;51(8):1250-7.

Yao L, Brown P, Shoaran M. Improved detection of Parkinsonian resting tremor with feature engineering and Kalman filtering. Clinical Neurophysiology. 2020 Jan 1;131(1):274-84.

Yeh CH, Al-Fatly B, Kühn AA, Meidahl AC, Tinkhauser G, Tan H, Brown P. Waveform changes with the evolution of beta bursts in the human subthalamic nucleus. Clinical neurophysiology. 2020 Sep 1;131(9):2086-99.

Yousif N, Liu X. Investigating the depth electrode–brain interface in deep brain stimulation using finite element models with graded complexity in structure and solution. Journal of neuroscience methods. 2009 Oct 30;184(1):142-51.

Yousif N, Liu X. Modeling the current distribution across the depth electrode–brain interface in deep brain stimulation. Expert review of medical devices. 2007 Sep 1;4(5):623-31.

Zaidel A, Spivak A, Grieb B, Bergman H, Israel Z. Subthalamic span of β oscillations predicts deep brain stimulation efficacy for patients with Parkinson's disease. Brain. 2010 Jul 1;133(7):2007-21.

Zanos S, Rembado I, Chen D, Fetz EE. Phase-locked stimulation during cortical beta oscillations produces bidirectional synaptic plasticity in awake monkeys. Current Biology. 2018 Aug 20;28(16):2515-26.

Zavala B, Brittain JS, Jenkinson N, Ashkan K, Foltynie T, Limousin P, Zrinzo L, Green AL, Aziz T, Zaghloul K, Brown P. Subthalamic nucleus local field potential activity during the Eriksen flanker task reveals a novel role for theta phase during conflict monitoring. Journal of Neuroscience. 2013 Sep 11;33(37):14758-66.

Zavala B, Damera S, Dong JW, Lungu C, Brown P, Zaghloul KA. Human subthalamic nucleus theta and beta oscillations entrain neuronal firing during sensorimotor conflict. Cerebral Cortex. 2017 Jan 1;27(1):496-508.

Zavala BA, Tan H, Little S, Ashkan K, Hariz M, Foltynie T, Zrinzo L, Zaghloul KA, Brown P. Midline frontal cortex low-frequency activity drives subthalamic nucleus oscillations during conflict. Journal of Neuroscience. 2014 May 21;34(21):7322-33.